THERMOPHYSICAL PROPERTIES OF BIOFUEL COMPONENTS DERIVED FROM BIOMASS

Submitted in fulfilment of the academic requirements of the degree of Master of Technology: Chemistry in the faculty of Applied Sciences at the Durban University of Technology, Chemistry Department, Durban, South Africa

MBALENHLE B. NDULI

2015

Supervisor:_____ Date: _____

PREFACE

The work described in this thesis was performed by the author under the supervision of Professor. N. Deenadayalu at Durban University of Technology, Durban, South Africa, from 2014 – 2015. The study presents original work by the author and has not been submitted in any form to another university. Where use is made of the work of others, it has been clearly stated in the text.

Signed: Date:

Mbalenhle B. Nduli

Signed: Date:

Prof. N. Deenadayalu (Supervisor)

ACKNOWLEDGEMENTS

First and foremost I thank God for blessings and guidance.

I would like to express my special appreciation and thanks to my supervisor Prof N. Deenadayalu, who has been abundantly helpful and offered invaluable assistance, support and guidance throughout the duration of this research project.

I would also like to thank the Durban University of Technology for giving me the opportunity to do my research and for financial support and the National Research Foundation (NRF) for a bursary and for funding the project.

A special thanks to my family and friends for their loving support and understanding throughout the duration of my studies.

I thank my fellow Thermodynamics lab mates for encouragement and insightful comments throughout the duration of this project.

Finally, I would like to dedicate this work to my late grandmother and to all my family.

ABSTRACT

The thermophysical properties of the binary mixtures containing biofuel components derived from biomass were determined. Experimental densities, speed of sound, and refractive indices for the binary mixtures (methanol or 1-ethyl-3-methylimidazolium acetate [EMIM][OAc] + furfural or furfuryl alcohol) were measured at T = (298.15, 303.15, 308.15, 313.15 and 318.15) K. From the experimental data, excess molar volume, $V_{\mathrm{m}}^{\mathrm{E}}$, isentropic compressibility, κ_s, molar refractions, R, and deviation in refractive index, Δn, were calculated. The excess molar volumes were found to be negative for all systems studied. The isentropic compressibility were found to be both positive for the whole composition and temperature range and increases slightly with increasing temperature.

The deviation in refractive index was positive over the whole composition range. The obtained values of excess molar volumes and changes of refractive index on mixing were satisfactorily correlated by the Redlich–Kister equation. The Lorentz–Lorenz equation was applied to predict the density and calculate the excess molar volume of the binary mixtures.

CONTENTS **Page**

List of Tables

List of Figures

Figure 6.4. Experimental density, ρ , of the binary mixture {[EMIM][OAc] (x_1) + furfuryl alcohol (x_2)} against mole fraction x_1 of methanol at 298.15 K;◊, T = 303.15 K;□ , T = 308.15 K;Δ , T = 313.15 K; × and , ∗, T = 318.15 K.

List of Symbols

ρ = density (g· cm^{-3}).

V_m^E = excess molar volume ($cm^3 \cdot mol^{-1}$).

T = temperature (K).

x_1 = mole fraction of the 1st component.

x_2 = mole fraction of the 2nd component.

σ = standard deviation.

M_1 = molar mass of the 1st component. ($g \cdot mol^{-1}$).

M_2 = molar mass of the 2nd component. ($g \cdot mol^{-1}$).

A_i = polynomial coefficient.

N = polynomial degree.

n = number of experimental points.

N_A = Avogadro's number (mol^{-1}).

k = number of coefficients used in the Redlich-Kister correlation.

u = speed of sound (m· s^{-1}).

κ_s = isentropic compressibility (Pa^{-1}).

Δn = refractive index deviation.

n^{id} = ideal refractive index.

R = molar refraction.

n = refractive index of mixture.

n_1 = refractive index of 1st component.

n_2 = refractive index of 2nd component.

CHAPTER 1

INTRODUCTION

1.1. FURFURAL FROM LIGNOCELLULOSIC FEEDSTOCKS

The energy crisis has caused great pressure on economic development and environmental sustainability worldwide, resulting in renewable energy, such as, solar, wind and biomass, receiving significant attention (Fang *et al* 2014). Within the last 10 years global energy demand had grown by approximately 26% and is projected to rise by 47% by 2035 (Gardezi *et al*. 2013). At present this demand is met mostly by fossil resources i.e. coal, natural gas and oil. While large reserves of coal are available, it contributes significantly to CO_2 gas emissions and it has to be transported from where it is plentiful to where it is required for power generation (Gardezi *et al.* 2013). The production of biofuels from lignocellulosic feedstocks, such as agricultural waste, wood or energy crops provides a means to meet this demand in a manner that reduces the emission of greenhouse gases (Doherty *et al.* 2010). Lignocellulosic biomass is a key resource because it is CO_2 neutral, generates lower greenhouse emissions, and can be produced in a sustainable manner, its global demand is expected to increase over the next 20 years due to reduced reliance on fossil liquid fuel (Shittu 2010; Gardezi *et al.* 2013). Lignocellulosic biomass refers to plant based material such as bagasse, wheat straw, rice straw, wood chips etc. Taken as a whole, with billions of tons of primary plant productivity of lignocellulosic material per-year world-wide, it is foreseeable that such quantities could become the main raw material for various renewable products such are biofuel, biodegradable plastics, biosurfactants, enzymes etc. (Gunny and Arbain 2013).

Biomass contains varying amounts of cellulose, hemicellulose, lignin and a small amount of other extractives. Woody plant species are typically characterised by slow growth and are composed of tightly bound fibres, giving a hard external surface, while herbaceous plants are usually perennial, with more loosely bound fibres, indicating a lower proportion of lignin, which binds together the cellulosic fibres: both materials are examples of polysaccharides; long-chain natural polymers. The relative proportions of cellulose and lignin is one of the determining factors in identifying the suitability of plant species for subsequent processing as energy crops. Cellulose is a polymer of glucose units linked via β-glycosidic bonds, imparting the structure with rigid crystallinity that impedes hydrolysis. Cellulose is typically isolated within the complex lignin/hemicellulose matrix, and it is largely inaccessible to hydrolysis in untreated biomass (McKendry 2002).

Hemicellulose is a mixture of polysaccharides, composed almost entirely of sugars such as glucose, mannose, xylose, arabinose and methylglucuronic and galaturonic acids, with an average molecular weight of <30,000. In contrast to cellulose, hemicellulose is a heterogeneous branched polysaccharide that binds tightly, but non-covalently, to the surface of each cellulose micro fibril. Hemicellulose differs from cellulose, in consisting primarily of xylose and other five-carbon monosaccharide's (McKendry 2002). Lignin can be regarded as a group of amorphous, high molecular-weight, chemically related compounds composed of methoxylated phenylpropane structures, such as coniferyl alcohol, sinapyl alcohol, and coumaryl alcohol (Huber *et al.* 2006) which provide plants with structural rigidity and a hydrophobic vascular system for the transportation of water and solutes. Lignin surrounds the hemicellulose and cellulose fractions, and one function of biomass retreatment is to de-polymerize the lignin seal such that the carbohydrate portions can be accessed (Alonso *et al.* 2010; McKendry2002).

There is a growing trend towards employing modern technologies and efficient bio-energy conversion for a range of biofuels, which are becoming competitive with fossil fuels. The term biofuel is referred to as liquid or gaseous fuels for the transport sector that are predominantly produced from biomass. A variety of fuels can be produced from biomass resources including liquid fuels, such as ethanol, methanol, biodiesel, Fischer-Tropsch diesel, and gaseous fuels, such as hydrogen and methane (Demirbas 2008; Demirbas 2009). Furfural is derived from biomass and is one of the key intermediates to connect the bio-resource to bio-fuels or chemical products (Tai *et al.* 2014) and was identified as one of the most promising chemicals for sustainable production of fuels and chemicals in the 21st century (Bozell *et al*. 2010). Furfural is a relatively inexpensive aldehyde and is considered as one of the most important intermediates for the synthesis of valuable chemicals and biofuels (Malinowski *et al.* 2012).

1.2. PRODUCTION OF FURFURAL

Industrial production of furfural commenced in about 1821 by Johann Wolfgang Döbereiner and officially reported in 1832 (Dunlop and Peters 1953). In 1840 John Stenhouse, a Scottish chemist, discovered that furfural could be produced by distilling food crop materials like corn and oats using sulphuric acid. He also determined the chemical formula and in the early years of the 20th century the chemical structure was elucidated. Its name was derived from the Latin word “furfur” meaning bran, an early source of the product. As early as 1922, the Quaker Oats Company started to produce furfural from oat hulls, based on a batch process using concentrated sulphuric acid (De Jong *et al*. 2010). Following the Quaker Oats process, other furfural production processes were developed in batch or in a continuous reactor including the Westpro-modified Huaxia Technology, Suprayield and Vedernikov's single step furfural production (Westpro 2004; Gravitis 2001; Vedernikovs 2010). However, these commercial processes often utilize mineral acids (e.g., H_2SO_4, HCl) in single phase operation, which

increases the difficulty in the recovery of furfural, and the operation or handling of the corrosive mineral acid. Recently, it was found that the ionic liquids-based process has offered an advantageous route from pentoses and pentosans to furfural (Lange 2007; Mc killip *et al.* 2001; Yan *et al.* 2014).

Furfural is a natural dehydration product of xylose, a monosaccharide often found in large quantities in the hemicellulose fraction of lignocellulosic biomass, from which it is almost exclusively produced. In theory, any material containing a large amount of the pentose (five carbon) sugars arabinose and xylose can serve as a raw material for furfural production (Cai *et al.* 2014). Today, over 280,000t of furfural is produced every year. The greatest amount was produced in China (200,000t), followed by the Dominican Republic (32,000t) and then South Africa (20,000t) (Zeitsch 2000) Together, these three nations account for ~90% of global furfural production (Yan *et al.* 2014).

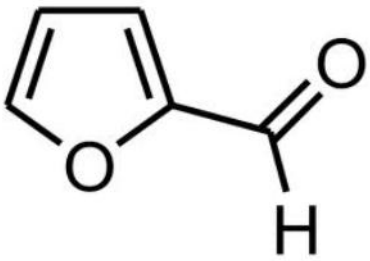

Figure 1.1. Structure of furfural

1.3. APPLICATIONS OF FURFURAL

Furfural is a widely used chemical for applications such as industrial solvent or precursor for high value-added products (Mamman *et al.* 2008). Furfural has found applications as a selective solvent in the refining of petroleum, lubricating oils, diesel fuels and vegetable oils. Furfural has conjugating double bonds and is susceptible to the phenomenon of 'intermolecular conjugation', whereby furfural interacts with other unsaturated compounds (double bonds only) to form enlarged conjugated systems, which allow for their separation from mixtures containing saturated compounds (Mandalika 2012). Furfural is one of the furan derivatives and is regaining attention as a bio-based alternative for the production of a range of products for example, plastics and paints (Yan *et al.* 2014). Furfural is an almond-scented, oily, colourless liquid that turns yellow to dark brown when exposed to air. The physical properties of furfural are listed in Table 1.1.

Table 1.1 General Properties of Furfural*

Molecular Weight (g/mol)	96.1
Freezing Point (°C)	-36.5
Boiling Point (°C)	161.7
Density at 25°C	1.16
Viscosity at 25°C	1.5
Critical Pressure (psi)	798.2
Critical Temperature (°C)	397.4
Heat of Combustion at 25°C (kcal/gm.mole)	-560.3
Heat of Formation (liquid at 25°C) (kcal/gm.mole)	-49.2
Heat of Fusion (kcal/gm.mole)	3.43
Heat of Vaporization at 433.8°K (kcal/gm.mole)	9.22

*(Shittu 2010)

The greatest application of furfural, however, is its conversion into derivatives such as furfuryl alcohol, furan, furoic acid and the potential applications for these chemicals.

1.4. FURFURYL ALCOHOL

Furfural is also a natural precursor of other range of furan-based chemicals and solvents (Cai *et al.* 2014). The most important furfural derivative is furfuryl alcohol, which consists of 62% of the total consumption of furfural produced each year (Kottke 2000) with tetrahydrofuran and tetrahydrofurfuryl alcohol being the other main two chemicals obtained from furfural (Wettstein *et al.* 2012). This amber liquid (at 20 ° C) is a very important feedstock for the polymer industry (Malinowski and Wardzińska 2012). Furfuryl alcohol is industrially produced through conversion of furfural derived from a selective dehydration of xylose. Polymeric furfuryl alcohol has been used for preparing corrosion-protective materials, adhesives, pastes, electrode materials, and acid-resistant materials (Kim *et al.* 2011).

The most common use of furfural is its conversion into furfuryl alcohol by hydrogenation over copper chromite catalysts (Figure 1.2). In the past, commercial production of furfuryl alcohol was carried out using 1-2% copper chromite catalyst at 1,000-1,500 psi by hydrogenating technical-grade furfural in 110-gallon autoclaves at T = 448 K. Wojcik (1948) has also reported that the hydrogenation reaction may be carried out in presence of other suitable catalysts, but that it was difficult to terminate the reaction once furfuryl alcohol was produced. Quantitative yields of 96-99% were reported for this reaction. Further hydrogenation of furfuryl alcohol (using copper chromite) at ~ T = 523 K and slightly higher pressures produces 2-methylfuran (36%), pentanol (36%), 1,5-pentanediol (15%) and 1,2- pentanediol (14%) as products of hydrogenolysis of the alcohol.

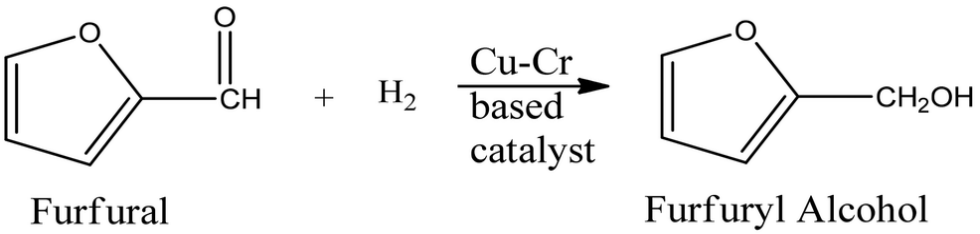

Furfural Furfuryl Alcohol

Figure. 1.2 Copper chromite catalyzed conversion of furfural into furfuryl alcohol (Wojcik 1948).

The major applications of furfuryl alcohol are the production of acid proof bricks, thermostatic resins, corrosion resistant polymer concrete, corrosion resistant fiber glass and liquid resins for galvanic bathtubs. Furfuryl alcohol is also an important intermediate chemical in the synthesis of vitamin C, lysine, lubricants, dispersing agents, plasticizer and tetrahydrofurfuryl alcohol (Li *et al.* 2004; Nagaraja *et al.* 2007).

1.5. IONIC LIQUIDS

1.5.1. HISTORY OF IONIC LIQUIDS

In 1888, Gabriel reported the discovery of the protic ionic liquid ethanolammonium nitrate with a melting point of 325.15–328.15 K (Gabriel and Weiner 1888). The first room temperature ionic liquids (ILs) introduced in 1914 by Paul Walden (Walden 1914) was ethylammonium nitrate with a melting point of 285.15 K; however, it was not until the first air and water stable ILs were introduced in 1992 that considerable research began (Wilkes and Zaworotko 1992). ILs are organic salts with melting points around or below the ambient temperature. ILs are composed of organic cations and either organic or inorganic anions. The most common ILs are divided into four groups according to their cations, which include the

following: quaternary ammonium ILs, N-alkyl-pyridinium ILs, N-alkyl-isoquinolinium ILs, and 1-alkyl-3-methyl-imidazolium ILs. ILs appear to be an environmentally attractive alternative to traditional volatile organic solvents because of their unique chemical and physical properties (Welton 1999).

1.5.2. IMPORTANCE OF IONIC LIQUIDS

Room temperature ionic liquids (RTILs) are salts that are liquids at room temperatures. ILs are composed only of ions, usually a combination of a larger organic cation and a smaller anion (Holm and Lassi 2011). ILs also offer other attractive properties such as low vapour pressures, good thermal stability, electro conductivity and unique solubility properties (FitzPatrick *et al.* 2010; Fort *et al.* 2007; Kiefer *et al.* 2008; Lee *et al.* 2008; Yang and Pan, 2005). ILs are seen as a promising ‘‘green’’ alternative for conventional organic solvents in industries (Sheldon 2005; Zhao *et al.* 2007). They offer a great opportunity (due to their unique properties) to be used in industrial processes namely reactions involving biocatalysts, separation processes, fuel cells, solvents for carbon dioxide absorption etc. (Yuan *et al.* 2007; Anouti *et al.* 2008; Kurnia *et al.* 2009). RTILs interesting and tenability properties make them of fundamental interest to all chemists, since both the thermodynamics and kinetics of reactions carried out in ionic liquids are different to those in conventional molecular solvents, Ionic liquids have no measurable vapour pressure, and hence can emit no volatile organic compounds (VOCs) (Earle and Seddon 2000).

1.5.3. PROPERTIES OF IONIC LIQUIDS

ILs is considered as green solvent due to these unique properties:

i) Non-volatility

ILs have very low vapour pressure at ambient temperatures. This feature makes ILs a potential alternative to highly volatile organic solvents, hence, reducing the amount of air pollution caused through solvent evaporation (Brennecke *et al.* 2011). ILs are also known to be inflammable in nature (Singh *et al.* 2010). However, there were few reports demonstrated the combustibility of several ionic liquids. Therefore, caution should be taken when working with or near a heat or ignition source (FitzPatrick 2011).

ii) Low toxicity

ILs can be tailored to be non-toxic or have a low toxic effect. Alkyl chain length on the ILs cation can be designed and tailored to affect the toxicity of ILs. It was found that the shorter the chain length of alkyl substituent, the lower the toxic effect of ILs (Romero 2008; Romero *et al.* 2008).

iii) Biodegradability

One of the green chemistry principles states that "a chemical compound should be designed so that at the end of its function, it does not persist in the environment, but degrades into harmless products" (Anastas and Warner 1998). Due to this reason, chemicals or products which have the ability to degrade naturally have received more attention in industries. Gathergood *et al*. (2006) found that there are few ionic liquids that are readily biodegradable while others show poor biodegradability. Pieraccini *et al*. (2007) reported that a higher level of biodegradability may be obtained by introducing an ester in the alkyl chain of ILs.

iv) Recyclable

In comparison with other organic solvents, one of the significant benefits of ILs is that they are easy to recycle and reuse. Effective recovery and large scale manufacture of ILs would minimize costs.

v) Non-corrosive

Most bio-refinery technologies are looking to replace the strong corrosive acids that they are using currently in order to optimise the high processing and maintenance cost. ILs such as 1-ethyl-3-methylimidazolium acetate [EMIM][OAc] is non-corrosive (Francisco *et al.* 2012). This will eliminate the use of dangerous solvents and provide a safer workplace.

1.5.4. APPLICATIONS FOR IONIC LIQUIDS

ILs have been used in many applications such as reactions and separation technologies (Wasserscheid and Welton 2003). They act as solvents in many reactions, including hydrogenation, hydro formulation, alkylation and Diels-Alder reactions (Holbrey and Seddon 1999). Due to their good conductivity, ILs have been used in batteries and solar cells (Rogers *et al*. 2002). ILs has been applied in a wide variety of fields such as electrochemistry, extraction, organic synthesis, polymer chemistry, and biocatalysis, especially as alternatives to organic solvents in non-aqueous reaction system (Wang *et al.* 2012). The application of ILs as both solvents and catalyst for cellulose processing (Dutta and Pal 2014) has been emerging since Swatloski *et al.* (2002) reported the use of ILs for cellulose dissolution in high concentrations without derivatization.

In addition, the highly crystalline structure of lignocellulose could be fractionated by ILs for recovery of all three major biopolymers: lignin, hemicellulose, and cellulose (Wyman *et al.* 2009). ILs have been investigated as lubricants and heat transfer fluids. Additionally, the investigation for ILs as liquid-in-glass thermometers have yielded a positive outcome. (Brennecke et al. 2001; Zhao 2006; Rodriguez et al. 2008; Ficke 2010)

ILs can be used as solvents for synthesis e.g. Diels-Alder cycloaddition reactions, Friedel- Craft acylation and alkylation, hydrogenation and oxidation reactions and Heck reactions; as biphasis system in combination with an organic solvent or water in extraction and separation technologies; as catalyst immobilizers for easy recycling of homogeneous catalysts; as electrolytes in electrochemistry (Zhong and Wang 2007).

Several groups have reported using ILs as mobile phase modifiers to improve liquid chromatography separations. The first time ILs were used as mobile phase additives was to study the chromatographic behavior of ephedrines and catecholamines (He *et al.* 2003). The addition of 2.0–50.0 mM IL to the aqueous mobile phases improved the basic compound peak shapes, but these improvements were associated with the changes in the retention factors (Han and Row 2010).

Most work on applications of RTILs in gas chromatography (GC) to date has been conducted by Armstrong (1999). As one of the early reports of the use of RTILs as stationary phase in GC, this group has examined the behavior of two common RTILs, 1-butyl-3-methylimidazolium hexafluorophosphate ([BMIM][PF_6]) and 1-butyl-3-methylimidazolium chloride [BMIM][Cl] when coated onto fused silica capillary. It was observed that the wetting

ability and the viscosity of RTILs make them ideal coating stationary phases in various GC applications (Pandey 2006; Armstrong 1999).

Some ILs are suitable for conventional liquid-liquid extraction because of their immiscibility with water (which allows formation of biphasic systems) as well as the high solubility of the organic species in ILs. The design of safe and environmentally benign separation processes plays an increasingly important role in the development of extraction technology (Han and Row 2010).

Excellent reviews detail the applications of ionic liquids to electrochemical device such as super capacitors, lithium ion batteries, polymer-electrolyte fuel cells and dye-sentisized solar cells (Tsuda *et al.* 2007; Singh *et al*. 2012; Debbie 2011; Mythri *et al*. 2014; Park *et al*. 2013; Armand *et al*. 2009). In an electrochemical device, an ionic liquid acts as an electrolyte (Khupse and Kumar 2010).

Table 1.2. lists the properties of ILs.

Table 1.2. Properties of Ionic Liquids*

Property	Value
Freezing point	< 373.15 K
Liquidus range	298.15 - 473.15 K
Thermal stability	High
Viscosity	< 100 Cp
Dielectric constant	< 30 ($F \cdot m^{-1}$)
Polarity	47 – 49
Specific conductivity	< 10 $mS \cdot cm^{-1}$
Molar conductivity	< 10 $Scm^2 \cdot mol^{-1}$
Electrochemical window	2V- 4.5 V
Solvent and / or catalyst	Excellent for many organic reactions
Vapour pressure	Usually negligible

*Singh 2013

The IL used in this work is 1-ethyl-3-methymidazolium acetate ([EMIM][OAc]). This IL is also used in biomass processing. Figure 1.3 is the structure of the IL.

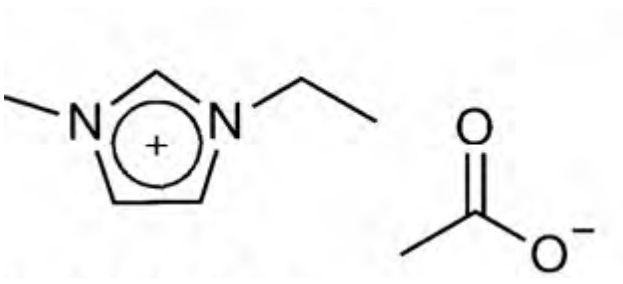

Figure 1.3 Structure of ionic liquid used in this work, 1-ethyl-3-methymidazolium acetate [EMIM][OAc].

1.6. IMPORTANCE OF THERMOPHYSICAL PROPERTIES

The thermodynamic properties: excess molar volumes, change of refractive indices, and change of isentropic compressibilities are of great interest for the adequate design of industrial processes and for theoretical purposes (Iglesias *et al.* 1999).

Accurate information on the green solvents at a wide range of pressures and temperatures is needed to carry out cost-effective and reliable process design in order to use these green compounds in any chemical process. The thermodynamic data of mixtures gives information on their intermolecular interactions (Lomba *et al.* 2011). Studies on the refractive index, viscosity and density of binary mixtures along with other thermodynamic properties are being increasingly used as tools for the investigation of the properties of pure components and the nature of intermolecular interactions between liquid mixture constituents (Yang *et al.* 2004).

The experimental values of thermophysical properties: density, sound velocity, refractive index, viscosity; and the thermodynamic properties: heat capacity, Gibbs energy, excess molar volume, excess molar enthalpy allow for new correlations and/or predictive models to be developed. These properties also provide information about the intermolecular interactions that can occur in binary or ternary systems especially where hydrogen bonding occurs (Bahadur *et al.* 2014).

Physical properties are very important for the design or simulation of processes in industries. Although physical properties for many ILs have recently been measured, these properties still remain scarce for most ILs and even more so when these data are concentration dependent, such as in binary or ternary mixtures (Quijada-Maldonado *et al.* 2012).

The physical and chemical properties of pure ILs and mixtures containing (IL + solvents) are studied consistently worldwide because accurate knowledge is essential for economic and efficient use of ILs in industries (Malek *et al.* 2014). The thermophysical characterization of binary mixtures of ionic liquids is fundamental in order to obtain information about molecular interactions and structural changes involved in the mixing process. This information is relevant for the design of processes and products involving ionic liquids (García-Mardones *et al.* 2013).

Ionic liquids are relatively new substances and detailed knowledge of their physical properties is required to a better understanding of the behavior of these substances, pure or mixed with other solvents, to find new applications or to design new technological processes (González *et al.* 2012). In this way, the density is necessary for developing equations of state and required for the design of different equipment, while the excess molar volume is of great importance when studying the nature of the molecular interactions present in mixtures. On the other hand, refractive index can be used as a measure of the electronic polarizability of a molecule and can provide useful information when studying the forces between molecules or their behavior in solution (González *et al.* 2012).

Understanding basic thermophysical properties of ILs is vital for design and evaluation. For instance, melting points, glass-transition temperatures, and thermal decomposition temperatures are needed to set the feasible temperature operating range for a particular fluid. Density (as a function of temperature) is needed for equipment sizing. Heat capacities are needed to estimate heating and cooling requirements as well as heat-storage capacity (Fredlake *et al.* 2004).

1.7. THERMODYNAMIC PROPERTIES INVESTIGATED IN THIS STUDY

In this work, solvents derived from biomass namely, furfural and one of its most important derivative furfuryl alcohol were used. The chosen ionic liquid was 1-ethyl-3-methylimidazolium acetate ([EMIM][OAc]). [EMIM][OAc] is used mainly in the dissolution and further processing of lignocellulosic biomass. ILs are an important class of solvents because of their properties, such as very low vapour pressure at normal temperature and pressure conditions, low melting point, ability to dissolve organic, inorganic, and polymeric materials, good thermal stability, and their wide liquid range. These novel solvents can also be used as replacement solvents for traditional volatile organic solvents (VOCs). They are easy to recycle and, in general, non-flammable. In order to fully exploit the potential of ionic liquids as solvent and recovery medium in various applications, it would be essential to investigate certain binary systems of green solvents. The organic alcohol chosen in this work; methanol is one of the most versatile solvent used in various chemical and technological processes and is relatively cheap.

Experimental densities, speed of sound, and refractive indices for the binary mixtures (methanol or 1-ethyl-3-methylimidazolium acetate [EMIM][OAc] + furfural) and (methanol or 1-ethyl-3-methylimidazolium acetate [EMIM][OAc] + furfuryl alcohol) were measured at T = (298.15, 303.15, 308.15, 313.15 and 318.15) K. From the experimental data, excess molar volume, isentropic compressibility, molar refraction, R, and deviation in refractive index were calculated.

The Redlich-Kister smoothing equation was applied successfully for the correlation of $V_{\mathrm{m}}^{\mathrm{E}}$ and Δn. The Lorentz-Lorenz equation was also used to correlate the volumetric property and

predict the refractive index or density of the binary mixtures. The Lorentz–Lorenz equation was applied to predict the density and calculate the excess molar volume of the binary mixtures. The thermodynamic properties have been discussed in terms of intermolecular interactions between the components of the binary mixtures.

CHAPTER **2**

LITERATURE REVIEW

A survey of the literature shows that the thermophysical properties of furfural derivatives are limited (Lomba *et al.* 2014).

The availability of thermodynamic property data for furfural and its derivatives is limited in the literature whereas the number of other compounds produced in furfural production and within further upgrading of furfural are numerous (Zaitseva *et al.* 2014).

Naorem *et al.* (1989) determined experimental densities, speeds of sound for the binary mixtures of furfural with methanol, ethanol, 1 -propanol, 2-propanol, 1-butanol, and 2-butanol and calculated the excess molar volume and deviation in isentropic compressibility at T = 308.15 K. The $V^{E}_{m,\,min}$ for (furfural + methanol) at T = 308 K was estimated to be 0.21 $cm^3 \cdot mol^{-1}$.

The excess molar volumes at equimolar concentration, $V^{E}_{0.5}$ were found to increase in the order: methanol < ethanol < 1-propanol < 1-butanol < 2-propanol < 2-butanol. Experimentally determined V^{E} values were all negative and they reveal that the unlike interactions between the aliphatic alcohols and furfural are fairly strong.

Bendiaf *et al.* (2015) measured the densities, and sound velocities for the binary systems (furfural + ethanol, or 1-butanol, or 2-butanol) over the entire composition range and at T = (283.15, 293.15, 303.15 and 313.15) K and at p = 1 x10^5 Pa. The V_m^E values are negative for the systems (furfural + ethanol or 1-butanol) and both positive and negative for the system

(furfural + 2-butanol). The density and sound velocity data decrease linearly with temperatures and increase with the concentration of furfural.

Naorem *et al.* (1989) also reported the densities and excess molar volumes at T = 298.15 K for the binary systems tetrahydrofuran, furan, furfural, and furfuryl alcohol with benzene, chlorobenzene, and bromobenzene. The V^E values for mixtures containing tetrahydrofuran or furan (except for the binary mixtures of furan and benzene) were negative and those containing furfural or furfuryl alcohol (except for the mixtures containing benzene) were found to be positive over the entire composition range.

Saba *et al*. (2014) determined the density, refractive index, conductivity and viscosity for the binary mixtures of 1-ethyl-3-methylimidazolium acetate ([EMIM][OAc]), 1-ethyl-3-methylimidazolium formate ([EMIM][COOH]) and 1-ethyl-3-methylimidazolium methyl phosphate ([EMIM][$PO_2(CH_3)H$]) with ethanol at T = 298.15K. The excess molar volumes were all negative. The relationship of refractive index with mole fraction has shown a gradual increase with increasing mole fraction for all the ILs + ethanol systems.

Bendiaf and Negadi (2013) investigated the densities and speed of sound for three binary mixtures containing solvents derived from biomass: (furfuryl alcohol + ethanol), (furfuryl alcohol + toluene), or (ethanol + 1, 3-propanediol). The measurements were performed for different compositions including the pure compounds at seven temperatures from T = 283.15 K to 343.15 K and atmospheric pressure. Excess molar volumes and deviations in isentropic compressibility for the binary systems at the above-mentioned temperatures were calculated. These results were fitted by the Redlich−Kister equation to determine the fitting parameters and the root-mean-square deviations

Zaoui-Djelloul- Daouadji *et al.* (2015) measured the density and speed of sound for binary mixtures of (furfural or furfuryl alcohol + toluene) and (furfuryl alcohol + ethanol) at T =

(283.15, 293.15, 303.15, and 313.15) K under atmospheric pressure. From these measurements, excess molar volume and deviation in isentropic compressibility at the above-mentioned temperatures as a function of concentration were calculated. The $V_{\mathrm{m}}^{\mathrm{E}}$ values were negative for the (furfural + toluene) and (furfuryl alcohol + ethanol) binary systems and sinusoidal shape for the (furfuryl alcohol + toluene) binary system with both negative and positive $V_{\mathrm{m}}^{\mathrm{E}}$ values.

CHAPTER **3**

INSTRUMENTATION AND THEORETICAL FRAMEWORK

A. INSTRUMENTATION AND THEORY

3.1. INSTRUMENTS TO MEASURE DENSITY

The excess molar volume is the difference between the actual molar volume and the ideal molar volume of a mixture (Shana'a et al. 1968) and is given by equation (3.1):

$$V_m^E = V_{mixture} - \sum_{i=1}^{N} x_i V_i^0 \qquad (3.1)$$

where $V_{\mathrm{m}}^{\mathrm{E}}$ is the excess molar volume , x_{i} is the mole fraction of component and V_i^0 is the molar volume of the pure component *i* at the same temperature and pressure as the mixture. For a binary mixture the excess molar volume is given by equation (3.2):

$$V_m^E = V_{mixture} - (x_1 V_1^0 + x_2 V_2^0) \qquad (3.2)$$

The volume change on mixing of binary liquid mixtures, $V_{\mathrm{m}}^{\mathrm{E}}$, at constant pressure, is of interest to chemical thermodynamicists for two main reasons (Battino 1971):

(i) they serve as an accurate and sensitive indicator to the measure of the theories of solution.

(ii) relatively easy to obtain experimentally.

V_m^E of a binary liquid mixture can arise out of a number of factors (Handa and Benson 1976) :

(a) difference in size and/or shape of the component molecules,

(b) changes in molecular orientations,

(c) difference in intermolecular interaction energies between like and unlike molecules,

(d) formation of products in solution.

From these factors, it can be seen that V_m^E is a complex property (Mercer-Chalmers1992).

Ideal binary liquid mixture formation is accompanied with no volume change. But due to molecular interactions between components of binary liquid mixtures in a real liquid mixture causes an increase or decrease of volume. This increase or decrease in the volume on mixing the liquids can be taken as a criterion and measure of molecular interaction. This volume change for the binary mixture is calculated by using equation 3.1 (Patill *et al*. 2011).

3.2. MEASUREMENT OF DENSITY

Volume changes for binary mixtures, V_m^E, can be determined in one of two ways:

(i) indirectly by means of density measurements, or

(ii) directly, by measuring the resultant volume change upon mixing of the two components.

3.2.1. DIRECT METHOD

The direct method measures the volume change that occurs when the liquids are mixed. Direct methods of measurement of, V_m^E, include batch dilatometer and continuous dilution dilatometer. Batch dilatometer is characterized by the determination of a single data point per

loading of the apparatus and continuous dilatometer is characterized by the determination of many data points per loading of the apparatus. Apparatus for the direct measurement of volume change were designed along two fundamental lines: (a) one composition per loading of the apparatus at a single temperature or batch dilatometers; and (b) a number of compositions per loading at a single temperature or continuous dilution dilatometers (Mercer-Chalmers 1992; Handa and Benson 1979; Nevines 1997; Redhi 2003).

(i) Batch dilatometer

An example of a batch dilatometer is shown in Figure 3.1. The dilatometer is filled with known masses of pure liquids, which are separated by mercury. The height of mercury in the calibrated graduated column is noted. The liquids are mixed by rotating the dilatometer and the volume change on mixing is indicated by the change in the height of the mercury in the calibrated capillary. The, V_m^E, is determined from the volume change and the masses of the components. It was reported that a precision of ± 0.003 $cm^3 \cdot mol^{-1}$ in V_m^E, could be achieved over the temperature range of (280 to 350) K using this technique. A disadvantage of this apparatus is that it is difficult to fill the dilatometer and this is usually accomplished using a narrow needle. A major source of error in this method is the determination of the composition as is it necessary to weigh the dilatometer as it contains mercury. This results in large errors in the measured mass. The error associated with taking a difference in large masses is usually quiet significant (Keyes and Hildebrand 1917; Nevines 1997; Redhi 2003).

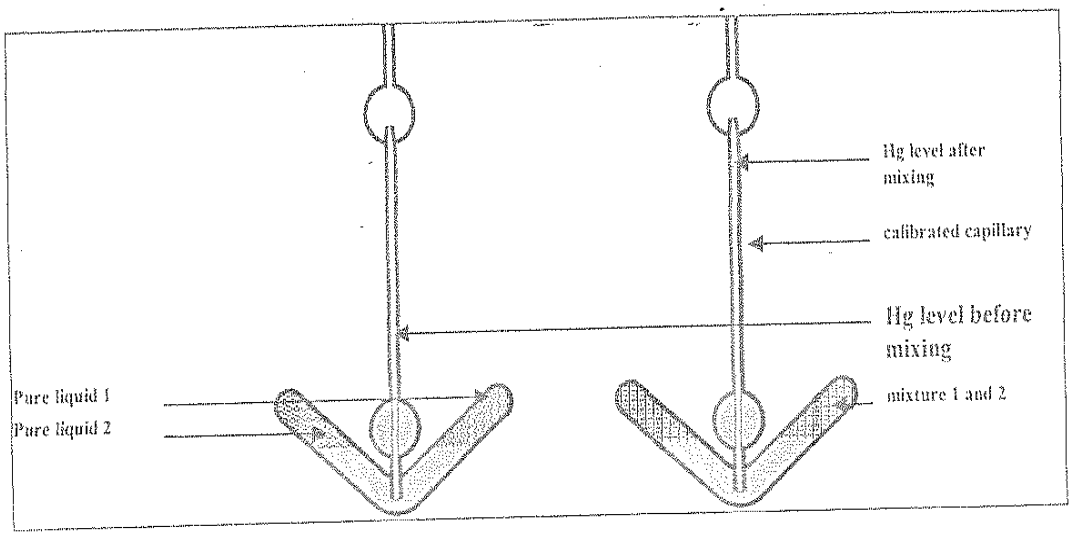

Figure 3.1 Schematic representation of a typical batch dilatometer.

(Nevines, 1997; Redhi, 2003; Sibiya, 2008)

(ii) Continuous dilatometer

This technique has become more popular than the batch technique because it is less time consuming and more data is generated per loading. The mode of operation involves the successive addition of one liquid into the reservoir, which contains the other liquid and detecting the volume change that accompanies the addition. The instrument of Kumaran and McGlashan (1977) is considered an improvement on the one developed by Bottomly and Scott (1974) because it is easier to load. Kumaran and McGlashan (1977) reported a precision of 0.0003 $cm^3 \cdot mol^{-1}$ in V_m^E, for their apparatus.

Figure 3.2. represents a schematic representation of a continuous dilatometer. A measurement is made by filling the burette (e) with one of the pure liquids and the bulb (d) with the other pure liquid. As the dilatometer is tilted some of the mercury is displaced into the burette through a capillary (c) and collects at the bottom of the burette. This displaced mercury forces some of

the pure liquid from the burette into the bulb through the higher capillary (b). After mixing the change in volume is registered as a change in the level of the mercury in the calibrated capillary (a). The amount of pure liquid that is displaced is determined from the height of the mercury in the burette. Because mercury is used, a capillary pressure effect is possible and the compressibility of mercury has to be considered when determining the excess molar volume.

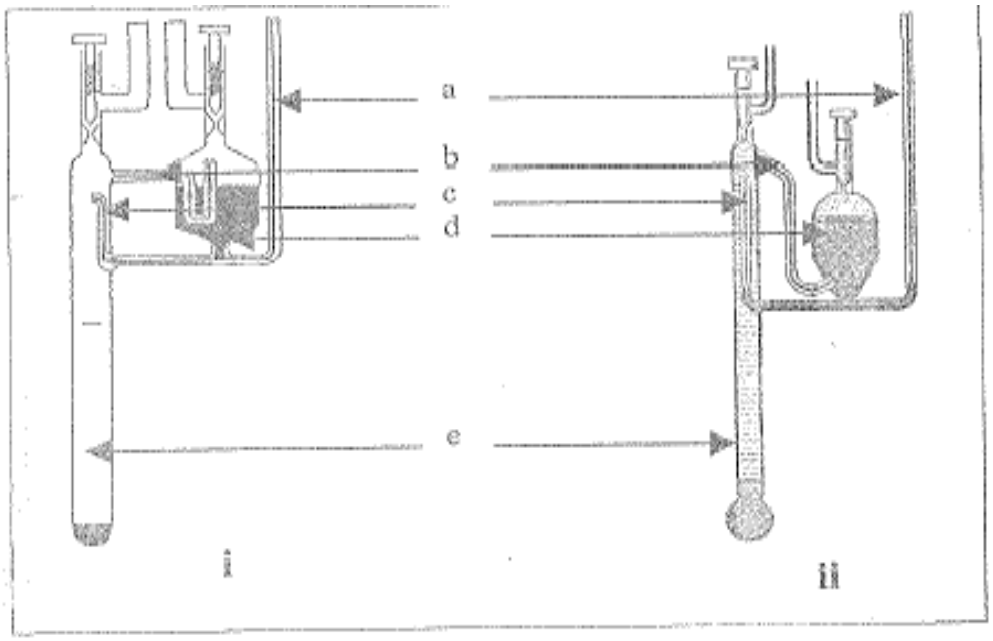

Figure 3.2. Schematic representation of a continuous dilatometer (i) design of Bottomly and Scott (1974) (ii) Kumaran and McGlashan (1977) a; calibrated capillary from which the volume change is determined, b; liquid capillary, c; mercury capillary, d; bulb that contains mercury, e; burette liquid 2.

(Bottomly and Scott, 1974; Kumaran and McGlashan, 1977; Sibiya, 2008; Singh, 2013)

3.2.2. INDIRECT MEASUREMENTS

There are many different methods used to determine densities of liquids namely, pycnometry, magnetic float and mechanical oscillating densitometers.

(i) Pycnometers

A variety of pycnometers with varying characteristics are made use of in the measurement of densities. A single-arm pycnometer, showed in Figure 3.3, can be used to obtain 0.00001 $g \cdot cm^{-3}$ precision in density measurements. The bulb has an 11 cm^3 capacity and the 1 mm internal diameter precision capillary has 11 lines lightly etched around the stems, and spaced 1 mm apart. The bulb is filled using a hypodermic syringe and cannula. Corrections for buoyancy and vapour space are feasibly applied.

When determining densities by means of this technique, it is important to be able to also determine the composition of the mixtures with precision. Many workers weighed the two components into the pycnometer. This also brings to the fore the problems of adequate mixing, evaporation, and vapour space composition. However, careful measurements using this method can provide very precise density values. The pycnometer based on the design of (Wood and Brusie 1943) is shown in Figure 3.2.

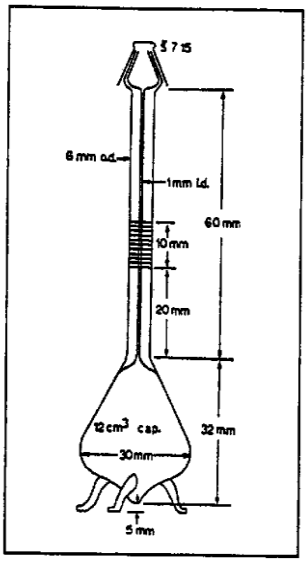

Figure 3.3. Schematic representation of a pycnometer based on the design of Wood and Brusie (1943).

(ii) Magnetic float densimeters

The mode of operation of a magnetic float densimeter is based on the determination of the height of a magnetic float in a liquid mixture. The height of this magnetic float in the presence of a known magnetic field is a function of the buoyancy of the liquid. The buoyancy of the liquid is related to the density of the liquid. An instrument with a precision 3×10^{-6} g·cm^{-3} has been reported and this translates to a precision of 0.0008 cm^{3}·mol^{-1} (Franks and Smith 1967) and is shown in Figure 3.4.

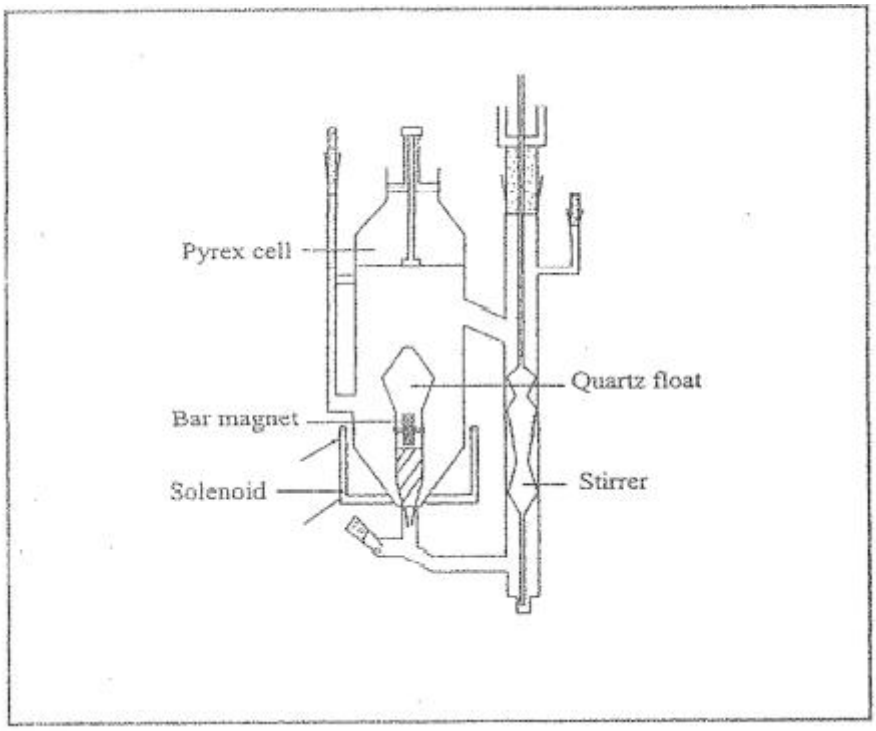

Figure 3.4. Schematic representation of a magnetic float densimeter (Franks and Smith 1967).

(iii) Mechanical oscillating densitometer

Mechanical oscillating (vibrating tube) densimeters linked to digital output displays are widely used in the chemical industry and in research laboratories to measure densities of pure liquids and liquid mixtures. The frequency of the vibrating tube containing a liquid that is subjected to a constant electric stimulation is related to the density of the liquid. According to Handa and Benson (1979), the frequency of vibration of an undamped oscillator (e.g. tube containing a liquid) connected by a spring with a constant elasticity, *c*, is related to the mass of the oscillator and the liquid, *M*, by the following equation:

$$2\pi\nu = \left[\frac{c}{M}\right]^{\frac{1}{2}} \qquad (3.3)$$

where M is the mass of the contents in the tube and, c, is the constant elasticity. Since the oscillator is a hollow tube if a liquid with a density, ρ, fills the hollow tube occupying a volume V, then:

$$M = M_0 + \rho V \tag{3.4}$$

M_0 is the mass of the empty oscillator.

Substitution of equation (3.3) into equation (3.4) and solving for ρ, :

$$\rho = -\frac{M_0}{V} + \left[\frac{c}{4\pi^2}\right]\left[\frac{1}{V^2}\right] \tag{3.5}$$

Where $A = -\frac{M_0}{V}$ and $B = \left[\frac{c}{4\pi^2}\right]$ are constants. Therefore the following equation is valid:

$$\rho = A + B\left(\frac{1}{v}\right)^2 \tag{3.6}$$

The constants A and B are characteristics of the oscillator, τ is the period and density is given by the symbol ρ, hence:

$$\rho = A + B\tau^2 \tag{3.7}$$

where A and B are determined by calibration. This involves determining the period for two pure substances of known density.

Since densities are measured relative to a reference material:

$$\rho - \rho_0 = B\left(\tau - \tau_0^2\right) \tag{3.8}$$

Commercially available vibrating tube densimeters with a precision of 0.001 % are available. This implies a precision of 0.003 $cm^3 \cdot mol^{-1}$ in the measurement of V_m^E (Nevines 1997; Singh, 2013).

In this work an Anton Paar DSA 5000 M instrument was used to measure the density and speed of sound the densities of mixtures at different temperatures.

The density, ρ, of a sample is defined as the mass, (m) divided by the volume, (v):

$$\rho = \frac{m}{v} \tag{3.9}$$

Density is used to calculate excess molar volume.

3.3. SPEED OF SOUND AND ISENTROPIC COMPRESSIBILITY

3.3.1. INSTRUMENTATION

The speed of sound is an important property in chemistry and physics which is usually used in the development of an equation of state that describes the fluid and consequently can be used to derive several thermophysical properties, such as the reduced isobaric thermal expansion coefficient, isentropic and isothermal compressibility, bulk modulus, thermal pressure coefficient, isobaric and isochoric heat capacities, and the Joule–Thomson coefficient method (Sattarib *et al*, 2014; Sattarib *et al.* 2014).

Measurement of the speed of sound, *u*, in liquids is a powerful source of information (e.g. to detect small changes in gas composition or the effects of small concentrations changes) about the thermophysical properties of chemical substances and their mixtures (Azevedo and Szydlowski 2004).

Speed of sound and density, are used to calculate isentropic compressibility by means of the Newton-Laplace equation (3.9):

$$\kappa_s = \frac{1}{\rho u^2} \tag{3.9}$$

3.3.1.1. Ultrasonic interferometer

An ultrasonic interferometer is a simple and direct device to determine the ultrasonic velocity in liquids with a high degree of accuracy, it consists of the following:

(i) high frequency generator, which is designed to excite the quartz plate fixed at the bottom of the measuring cell at its resonant frequency to generate ultrasonic waves in the experimental liquid in the measuring cell.

(ii) a macro-ammeter to observe the changes in the current and two controls for the purpose of sensitivity regulation and initial adjustments of micro-ammeter are provided on the high frequency generator.

(iii) measuring cell, which is a specially designed double walled cell for maintaining the temperature of the liquid constant during the experiment. A fine micrometer screw is provided at the top, which can lower or raise the reflector plate in the cell through a known distance. It has a quartz plate fixed at the bottom.

A diagram showing the ultrasonic interferometer is shown in Figure 3.5.

Figure 3.5 Diagram of an Ultrasonic interferometer M-81G.

(Taken from Instruction Manual of Mittal Enterprises Ultrasonic Interferometer for Liquids)

The principle used in the measurement of velocity, (u), is based on the accurate determination of the wavelength, (λ), in the medium. Ultrasonic waves of known frequency (v) are produced by a quartz plate cell. A movable plate kept parallel to the quartz plate reflects the waves. If the separation between these plates is exactly a whole multiple of the sound wavelength, standing waves are formed in the medium. The acoustic resonance give rise to an electrical reaction on the generator driving the quartz plate and the anode current of the generator becomes a maximum. If the distance between the reflector and crystal is increased or decreased and the variation is exactly one half wavelength, $(\lambda / 2)$ or multiple of it, the anode current again becomes maximum. From the knowledge of wavelength, (λ) , the velocity, (u), can be obtained by the relation:

Velocity =Wavelength × frequency

3.4. REFRACTIVE INDICES AND MOLAR REFRACTION

3.4.1. Theory

The refractive index, *n*, is a constant for a pure solvent. It can be defined as:

$$n = \frac{\text{speed of light in material 2}}{\text{speed of light in material 1}} \tag{3.10}$$

This is usually written $n_{1,2}$ and is the refractive index in material 2 relative to material 1. The incident light is in material 1 and the refracted light is in material 2. If the incident light is in a vacuum this value is called the absolute refractive index of material 2. By definition the refractive index in a vacuum is 1. In practice, air makes little difference to the refraction of light with an absolute refractive index of 1.0008, so the value of the absolute refractive index can be used assuming the incident light is in air.

The refractive index is also defined as the ratio of the speed of a wave either light or sound in a reference medium to a second medium. It is most commonly used in the context of the speed of the wave of light with a vacuum as a reference medium, although historically other reference media (e.g. air at a standardized pressure and temperature) have been used.

Another common definition of the refractive index is the ratio of the sine of the angle of incidence (medium1) θ_1 and the angle of refraction of (medium 2) θ_2 and is given by (Iglesias-Otero *et al.* 2008):

$$n = \frac{sin\theta_1}{sin\theta_2} \tag{3.11}$$

The angles are measured to the normal of the surface. This definition is based on Snell's law

(Iglesias-Otero *et al.* 2008) and is equivalent to the definition above if the light enters from the reference medium (a vacuum).

3.4.2. Instruments used for the determination of refractive index

(i) ATAGO RX 5000 Refractometer

The RX-5000 digital refractometer gives quick and accurate measurements. The RX-5000 measures sample for refractive index with an accuracy and resolutions of ± 0.00004 and 0.00001/0.01 in four seconds the instrument ranges from 132700-1.5800. All data, including date, time, current temperature, measurement result and measurement temperature are electronically displayed. It is used for testing and developing medicines, or chemical products, or processed foods, by checking the refractive index and concentration of materials as an auxiliary means of analysis. Figure 3.6 shows the photograph of an ATAGO RX 5000 Refractometer.

Figure 3.6. Photograph of an ATAGO RX 5000 Refractometer

(ii) Abbemat Digital Refractometer

Abbemat digital refractometers allows for fast but less accurate refractive index measurements. They are factory calibrated with official standards from the Physikalisch-Technische Bundesanstalt (PTB, National Metrology Institute of Germany). Refractive index results from an Abbemat 300/350 are accurate to ± 0.0001 n_D and for an Abbemat 500/550 ± 0.00002. Abbemat 350/550 refractometers are set up conveniently with touchscreen. The instrument has a coloured LCD screen and membrane keys which are resistant to spillage and dirt. Instrument generates automatic warning if the sample is not large enough. There is a quick wipe system which cleans the prism after each measurement. Abbemat 350/550 measures turbid, coloured or opaque samples and all samples from liquids to pastes and polymers to solids. There is no influence from humidity, temperature or vibrations. A wide range of scales are stored in the Abbemat for converting refractive index into concentrations.

Figure 3.7 is the photograph of an Abbemat Digital Refractometer 350/550

Figure 3.7 Photograph of an Abbemat Digital Refractometer 350/550.

In this work for the measurement of refractive index the instrument Anton Paar refractive index analyzer RXA 156 was used. The description of the instrument is given in chapter 4, section 4.2.

B. CORRELATION

3.5. REDLICH-KISTER POLYNOMIAL

The V_m^E and Δn data were fitted by the Redlich–Kister polynomial (Redlich and Kister, 1948) at the temperatures T = (298.15, 303.15, 308.15, 313.15 and 318.15) K. The Redlich–Kister equation for binary mixtures is given below:

$$Z = x_1 x_2 \sum_{i=0}^{N} A_i (2x-1)^i, \tag{3.12}$$

Where Z is the V_m^E or Δn; x_1 is the mole fraction of the methanol, or [EMIM][OAc] x_2 is the mole fraction of furfural or furfuryl alcohol; N is the degree of the polynomial expansion; and A_i is the Redlich–Kister parameters obtained for the system. The standard deviation, σ, was calculated using equation (3.13) below:

$$\sigma = \left(\frac{\sum_{i}^{n} (Z_{\exp} - Z_{cal})}{N-k} \right)^{1/2} \tag{3.13}$$

where Z_{exp}, Z_{cal}, are the values of the experimental and calculated V_m^E or Δn and N is the number of experimental data points and k is the number of coefficients used in the Redlich-Kister correlation, respectively.

3.6. LORENTZ-LORENZ EQUATION

The Lorentz-Lorenz relationship between the refractive index at zero frequency and mean molecular polarizability, α, of a nonpolar, nonmagnetic material results in the following definition (Brocos *et al*. 2003) of molar refraction *R*,

$$R = \left(\frac{n^2 - 1}{n^2 + 2} \right) V_m \tag{3.14}$$

Where V_m is the molar volume and n is the refractive index of the mixture.

The molar refraction is also given by:

$$R = \frac{N_A \alpha}{3\varepsilon_0} \tag{3.15}$$

where N_A is the Avogadro constant and ε_o is the permittivity of free space.

3.6.1. Prediction of density by the Lorentz-Lorenz (L-L) approximation

The Lorentz–Lorenz equation is used for predicting the density ρ , which is related to the refractive index n, by:

$$\rho = \frac{\left(\frac{n^2 - 1}{n^2 + 2} \right) \left(x_1 M_1 + x_2 M_2 \right)}{\left(\frac{n_1^2 - 1}{n_1^2 + 2} \right) x_1 \frac{M_1}{\rho_1} + x_2 \left(\frac{n_2^2 - 1}{n_2^2 + 2} \right) \frac{M_2}{\rho_2}} \tag{3.16}$$

Equation (3.26) was used to predict the density of the binary mixture, ρ, hence, if ρ_i and n_i for the pure components, and n for the mixture, are known, the density of the mixture can be estimated.

3.6.2. Correlation of *n* by the Lorentz-Lorenz approximation

From equation (3.17) can be obtained and allows one to obtain the inverse prediction i.e., to predict n from the pure solvent density and refractive index data and from the experimental density of the mixture. The Lorentz-Lorenz equation for the prediction of n is given below:

$$n = \left(\frac{2\left[\left(\frac{n_1^2 - 1}{n_2^2 - 1} \right) x_1 \rho \frac{M_1}{M_1} + x_2 \left(\frac{n_1^2 - 1}{n_2^2 - 1} \right) \rho \frac{M_2}{M_2} \right] + \left[x_1 M_1 + x_2 M_2 \right]}{\left[x_1 M_1 + x_2 M_2 \right] - \left[\left(\frac{n_1^2 - 1}{n_2^2 - 1} \right) x_1 \rho \frac{M_1}{\rho_1} + x_2 \left(\frac{n_1^2 - 1}{n_2^2 - 1} \right) \rho \frac{M_2}{\rho_2} \right]} \right)^{1/2} \tag{3.17}$$

On simplifying equation (3.16) equation (3.17) is obtained. The derivation is given below:

$$\rho = \frac{\left(\frac{n^2 - 1}{n^2 + 2} \right) \left(x_1 M_1 + x_2 M_2 \right)}{\left(\frac{n_1^2 - 1}{n_1^2 + 2} \right) x_1 \frac{M_1}{\rho_1} + \mathrm{x}_2 \left(\frac{n_2^2 - 1}{n_2^2 + 2} \right) \frac{M_2}{\rho_2}} \tag{3.18}$$

$$1 = \frac{\left(\frac{n^2 - 1}{n^2 + 2} \right) \left(x_1 M_1 + x_2 M_2 \right)}{\left(\frac{n_1^2 - 1}{n_1^2 + 2} \right) x_1 \rho \frac{M_1}{\rho_1} + x_2 \rho \left(\frac{n_2^2 - 1}{n_2^2 + 2} \right) \frac{M_2}{\rho_2}} \tag{3.19}$$

Assume:

$a = x_1M_1 + x_2M_2$ and (3.20)

$$b = \left(\frac{n_1^2 - 1}{n_1^2 + 2} \right) x_1 \frac{M_1}{\rho_1} + x_2 \left(\frac{n_2^2 - 1}{n_2^2 + 2} \right) \frac{M_2}{\rho_2} \quad (3.21)$$

Equation (3.19) becomes

$$1 = \frac{\left(\frac{n^2 - 1}{n^2 + 2} \right) a}{b} \quad (3.22)$$

$$\frac{b}{a} = \left(\frac{n^2 - 1}{n^2 + 2} \right) \quad (3.23)$$

$B\,(n^2+2) = a\,(n^2-1)$ (3.24)

$$n^2 = \frac{2b + a}{a - b} \quad (3.25)$$

$$n = \sqrt{\frac{2b + a}{a - b}} \quad (3.26)$$

After substituting the values of *a* and *b* from equations (3.20) and (3.21) in equation (3.26) the Lorentz- Lorenz predictive equation (3.17) for *n* is obtained.

3.6.3. Correlation of excess molar volume by the Lorentz-Lorenz approximation

Correlation of the excess molar volume can be obtained using the refractive index obtained for the binary mixtures by the Lorentz-Lorenz approximation. Within the framework of the Lorentz-Lorenz approximation, $V_{\mathrm{m}}^{\mathrm{E}}$ can be correlated via the change in reduced free volume, namely:

$$\Delta\left(\frac{V_{\mathrm{m,f}}}{R}\right)=\frac{V_{\mathrm{m,f}}}{R}-\left(\frac{V_{\mathrm{m,f}}}{R}\right)^{\mathrm{id}} \tag{3.27}$$

Application of the Lorentz-Lorenz equation allows this expression to be reduced to:

$$\Delta\left(\frac{V_{\mathrm{m,f}}}{R}\right)=\frac{3}{n^2-1}-\frac{3}{\left(n^{\mathrm{id}}\right)^2-1} \tag{3.28}$$

The assumption $R = R^{\mathrm{id}}$, is most often a highly accurate approximation. The following expression can then be obtained from equation (3.28).

$$\Delta\left(\frac{V_{\mathrm{m,f}}}{R}\right)=\frac{V_M^E}{R} \tag{3.29}$$

Where $V_{\mathrm{m}}^{\mathrm{f}}-V_{\mathrm{m,f}}^{\mathrm{id}}=V_{\mathrm{m,f}}=V_M^E$ (3.30)

Therefore,

$$V_M^E=(-n)\frac{3R(n^{\mathrm{id}}+n)}{\left(n^2-1\right)\left(\left(n^{\mathrm{id}}\right)^2-1\right)} \tag{3.31}$$

CHAPTER **4**

EXPERIMENTAL

A. EXCESS MOLAR VOLUME AND ISENTROPIC COMPRESSIBILITY

4.1. EXPERIMENTAL APPARATUS AND TECHNIQUE

The, $V_{\mathrm{m}}^{\mathrm{E}}$, for a binary mixture is determined from density measurements using the following equation:

$$V_m^E = \frac{x_1 M_1 + x_2 M_2}{\rho} - \frac{x_1 M_1}{\rho_1} - \frac{x_2 M_2}{\rho_2} \tag{4.1}$$

where x_1 and x_2 are mole fractions, M_1 and M_2 are the molecular masses, ρ_1 and ρ_2 are the densities of pure components 1 and 2, respectively (Govender 1996; Nevines 1997; Redhi 2003).

In this work ρ and u were determined using the Anton Paar oscillating U-tube DSA 5000 M.

This device simultaneously determines two independent physical properties using one sample. The two in one instrument is equipped with a density cell and a sound velocity cell thus combining the Anton Paar oscillating U-tube method with a highly accurate instrument for the measurement of sound velocity. Both cells are temperature-controlled by a built-in Peltier thermostat. The temperature is controlled to ± 0.02 K.

The sample is introduced into a U-shaped borosilicate glass tube that is excited to vibrate at its characteristic frequency electronically. The characteristic frequency changes depending on the density of the sample. Through a precise determination of the characteristic frequency and a mathematical conversion, the density of the sample can be measured. This method is based on

the law of harmonic oscillation in which a U-tube filled with sample to be analyzed is subjected to an electromagnetic force. By measuring the frequency and period of vibration of the sample the density of the sample is determined. This method gives highly accurate measurements for the density. For measurements of the speed of sound, the equipment has a stainless steel cell and uses the technique of pulse-echo, which refers to the transmission of a short pulse of ultrasound through the middle of the sample. The sound velocity was measured at a frequency of approximately 3 MHz (Fortin *et al.* 2013).When an obstacle is encountered, part of the pulse is reflected and the other part is transmitted. Thus, the equipment stores the time between the emission of the pulse and receiving the echo, converting it into distance (Cunha 2013).

The density, ρ, is calculated from the quotient of the period of oscillation of the U-tube and the reference oscillator:

$$\rho = \mathrm{KA} \times Q^2 \times f_1 - \mathrm{KB} \times f_2 \qquad (4.2)$$

KA, KB are the apparatus constants

Q is the quotient of the period of oscillation of the U-tube divided by the period of oscillation of the reference oscillator

f_1, f_2 are the correction terms for temperature, viscosity and non-linearity

The value of the density is displayed on the LCD screen. The DSA 5000 M is coupled with a computer which is loaded with software that stores all the measured density values. A photograph of the Density and Sound Velocity Meter (DSA 5000 M) is given in Figure 4.1. below.

Figure 4.1. Photograph of the Density and Sound Velocity Meter (DSA 5000 M)

(Taken from Instruction Manual of Anton Paar DSA 5000 M)

For the measurement of the sound velocity, the sample is introduced into the sound velocity measuring cell that is bordered by an ultrasonic transmitter on one side, and a receiver on the other side. The transmitter sends sound waves of a known period through the sample. The velocity of sound, *u*, can be calculated by using the period of the sound waves and the distance between the transmitter and receiver.

$$u = \frac{l \text{ x } (1 + 1.6 \text{ x } 10^{-5} \text{ x } \Delta T)}{\frac{Ps}{512} - A \text{ x } f_3} \qquad (4.3)$$

where l is the original path length of the sound waves, ΔT is the temperature deviation to 278.15 K, P_S is the oscillation period of the received sound waves, A is apparatus constant for sound velocity, and f_3 is the correction term for temperature. The frequency of the measurement was done at 3 MHz (Fortin *et al.* 2013).

Due to the high temperature dependency of the density and velocity of sound, the measuring cells are thermostated precisely, using the Peltier elements.

The key features of the DSA 5000M is the high accuracy of the density measurements. The DSA 5000 M instrument is equipped with the world's most advanced digital density and sound velocity measurement technology where:

(i) the period of oscillation of the U-tube is measured by optical pickups.

(ii) two integrated Pt 100 platinum thermometers together with the Peltier elements provide an extremely precise thermostatting of the sample.

(iii) there is a thermo balance which is an additional reference oscillator that provides long-term stability and enables precise measurements over the whole temperature range of the instrument with only one adjustment at T = 293.15 K.

(iv) viscosity- related errors are automatically corrected over the full viscosity range by measuring the damping effect of the viscous sample followed by a mathematical correction for the density value.

(v) special adjustments with standards of high viscosity and high density lead to an enhanced precision when samples with high viscosity and high density are used.

A major source of measuring errors when using a density and sound velocity meter are gas bubbles in the measuring cells. To reduce the formation of gas bubbles Anton Paar introduced two new features:

(i) Filling Check: The instrument automatically detects gas bubbles in the density measuring cell by an advanced analysis of its oscillation pattern and generates a warning message.

(ii) U-View: Using a real-time camera with zoom function the U-tube can be visually inspected for gas bubbles in the density measuring cell.

The specifications for the DSA 5000 M are given in Table 4.1

Table 4.1. Specifications of the DSA 5000 M

Measuring range density	0 to 3 g/cm^3
Measuring range sound velocity	1000 to 2000 m/s
Measuring range temperature	273.15 to 343.15 K (32 to 158 °F)
Pressure range	0 to 3 bar (0 to 44 psi)
Repeatability density	0.000001 g/cm^3
Repeatability sound velocity	0.1 m/s
Repeatability temperatures	273.151 K (0.002 °F)
Measuring time per sample	1 to 4 minutes
Sample volume	approx. 3 ml
Ambient air pressure sensor	yes
Reference oscillator	yes
Automatic bubble detection	yes
Visual check of the density measuring cell	camera

B. REFRACTIVE INDEX

4.2. EXPERIMENTAL APPARATUS

In this work Δn was determined using the Anton Paar refractive index analyzer RXA 156. The DSA 5000 M was coupled with the RXA 156 and Xsample 452. A photograph of the DSA 5000 M and the RXA 156 and Xsample 452 is given in Figure 4.2.

Figure 4.2. Photograph of the DSA 5000 M and the RXA 156 and Xsample 452

(Taken from Instruction Manual of Anton Paar DSA 5000 M)

An overview of Anton Paar refractive index analyzer RXA 156 is given briefly in the description below.

The RXA 156 and RXA 170 modules are equipped with a micro flow cell and an integrated Peltier thermostat ensuring accurate and automatic temperature control. Fast and non-destructive measurements, requiring only small sample volume, are required to obtain the refractive index (RI). Both RXA types can be used as a module in measuring systems.

In this work the RXA 156 module was used.

The Anton Paar refractive index analyzer RXA 156 consists of the following features:

(i) it can be combined with a DMA 4100/4500/5000 M, DSA 5000 M or Soft Drink Analyzer M.

(ii) RXA 156/170 instruments can be used separately.

(iii) for pasty or expensive samples, manual filling of the refractometer is possible.

(iv) simple adjustment of the DSA 5000 M and RXA 156/170 using air and water in one procedure.

(v) automatic filling and cleaning of the DSA 5000 M and RXA 156/170 sample changer. One measuring cycle, three sample parameters

(vi) save time by simultaneously determining the density, sound velocity, and refractive index.

(vii) fast and reliable results. Reliable measuring methods

(viii) established U-tube method for measuring density.

(ix) highly accurate measurement of the angle of total reflection for determining the refractive index.

Table 4.2. lists the specifications of the refractometer RXA 156.

Table 4.2. Specifications of the refractometer RXA 156

Refractive index	
Measuring range	1.32 – 1.56 n_D
Resolution	0.000001
Accuracy	0.00002
Temperature	
Measuring temperature	283.15 - 343.15 K
Resolution	273.16 K
Accuracy	273.18 K
Stability	273.152 K
Speed of temperature change from ambient temperature to 293.15 K	20 s

C. BINARY MIXTURES

4.3. CHEMICALS

Furfural was supplied by Merck with a quoted mass fraction purity >0.98. Methanol, furfuryl alcohol, heptane, ethanol and 1-ethyl-3-methylimidazolium acetate [EMIM][OAc] were supplied by Sigma Aldrich with mass fraction purity >0.98, >0.999, >0.999, >0.998 and >0.97, respectively. The samples were analyzed by Karl Fisher titration (831 Metrohm), the mass percentage water content was found to be 0.0002 for methanol, 0.0080 for furfural, 0.0010 for furfuryl alcohol, 0.0020 for heptane, 0.0009 for ethanol and 0.0076 for [EMIM][OAc]. A summary of the chemicals, used in this work and their suppliers are given in Table 4.3. The purities of the chemicals were checked by comparing the experimental density, speed of sound and refractive index values of the pure chemicals at various temperatures with those reported

in literature and showed excellent correlation. These results are given in Table 4. 4. No further purification was performed.

Table 4.3. Chemicals, suppliers, mass % purity and CAS number

Chemical	**Supplier**	**Mass fraction purity**	**CAS No.**
Methanol	Sigma Aldrich	>0.999	67-56-1
Heptane	Sigma Aldrich	>0.99	142-82-5
Ethanol	Sigma Aldrich	>0.998	64-17-5
Furfural	Merck	>0.98	98-01-1
Furfuryl alcohol	Sigma Aldrich	>0.98	98-00-0
1-ethyl-3-ethylimidazolium acetate	Sigma Aldrich	>0.971	143314-17-4

Table 4.4.Comparison of experimental and literature density, ρ, speed of sound, u, and refractive index, n, of pure components at T = (298.15, 303.15, 308.15, 313.15 and 318.15) K

Component	T/K	ρ/(g·cm^{-3})		u/(m·s^{-1})		n	
		Exp.	Lit.	Exp.	Lit.	Exp.	Lit.
Furfural	298.15	1.154314	1.154805[a]	1440.45	1440.19[c]	1.523107	1.523577[c]
			1.15493[a]				1.5235[d]
			1.1546[b]				
			1.15525[b]				
	303.15	1.148987	1.149478[c]	1422.73	1422.05[c]	1.520455	1.520969[c]
			1.149766[e]		1422.5[f]		1.5206[e]
			1.14869[f]				
	308.15	1.143643	1.14414[c]	1404.70	1403.96[c]	1.517839	1.518355[c]
	313.15	1.138290	1.138793[c]	1386.70	1385.97[c]	1.515167	1.51574[c]
			1.13801[f]		1386.5[f]		
	318.15	1.132928	1.133433[c]	1368.65	1368.06[c]	1.512565	1.513114[c]
			1.133829[e]				
Methanol	298.15	0.787104	0.78710[g]	1107.73	1101.9[i]	1.327042	1.32652[h]
			0.78664[h]		1102.00[i]		1.32645[j]
			0.786710[i]		1102.98[i]		1.3265[k]
			0.78650[j]		1104[l]		1.32685[l]
			0.78666[k]		1108.30[n]		1.32676[o]
			0.78741[l]				1.32720[l]
			0.78720[m]				1.32649[g]
	303.15	0.782382	0.781808[p]	1092.29	1085.8[h]	1.325480	1.32410[h]
			0.7818[h]		1086.46[p]		1.3247[t]
			0.7844[q]		1086.0[r]		
			0.7822[r]		1080.8[r]		
			0.78203[r]		1087.0[r]		
			0.78184[r]		1088.56[s]		

Table 4.4 continued

			0.78165[r]				
			0.78196[r]				
			0.782686[s]				
	308.15	0.777639	0.7771[h]	1077.90	1068.9[h]	1.323720	1.32223[h]
			0.777941[s]		1072.04[s]		
	313.15	0.772866	0.7724[h]	1065.03	1053.2[h]	1.321952	1.32018[h]
			0.77226[p]		1053.97[p]		
			0.7748[q]		1052.0[r]		
			0.77232[q]		1055.91[s]		
			0.77247[r]				
			0.7726[r]				
			0.7727[r]				
			0.773168[s]				
	318.15	0.768059	0.7676[h]	1055.53	1037.3[h]	1.320300	1.31759[h]
[EMIM][OAc]	298.15	1.097553	1.0993[u]	1734.76		1.499707	1.4771[w]
			1.1020[u]				1.49[z]
			1.0997[u]				
			1.0974[v]				
			1.0270[w]				
			1.09968[x]				
			1.09778[y]				
			1.135[z]				
	303.15	1.094449	1.09472[u]	1722.42		1.498325	1.4981[x]
			1.09460[v]				
			1.09664[x]				
	308.15	1.091362	1.09167[u]	1710.12		1.496928	
			1.09160[v]				
			1.09360[x]				
	313.15	1.088295	1.08862[u]	1697.95		1.495511	1.4950[x]
			1.08860[v]				
			1.09057[x]				

Table 4.4 continued

	318.15	1.085247	1.08558[u]	1685.90		1.494127	
			1.08550[v]				
Furfuryl Alcohol	298.15	1.126912	1.130269[a]	1447.25	1449.80[a]	1.484546	1.486003[a]
			1.12499[e]				1.4837[e]
			1.1260 [b]				1.4841[e]
	303.15	1.122258	1.125616[a]	1430.78	1433.65[a]	1.482494	1.483885[a]
			1.12247[e]				
			1.1238[e]				
	308.15	1.117584	1.120942[aa]	1413.04	1417.62[aa]	1.480353	1.481786a[a]
			1.11990 [e]				
			1.14550[bb]				
	313.15	1.112890	1.116244[aa]	1394.33	1401.71[aa]	1.478149	1.479637[aa]
	318.15	1.108176	1.111518[aa]	1374.98	1385.85[aa]	1.475959	1.477501[aa]

Standard uncertainties u are $u(T) = \pm 0.01$ K and the combined expanded uncertainty Uc in density ,speed of sound and refractive index measurements were less than $U_c(\rho) = \pm 5 \times 10^{-5}$ g ·cm^{-3}, $U_c(u) = \pm 1$ m·s^{-1} and $U_c(n) = 5 \times 10^{-5}$, respectively (0.95 level of confidence)

[a] (Zhang 2013) [b] (Rilo *et al.* 2012) [c] (Lomba *et al.* 2013) [d] (Tai *et al.* 2014) [e] (Laura *et al*. 2011)[f] (Mohammed *et al.* 2007) [g] (de Almeida *et al.* 2012) [h] (Bendiaf *et al.* 2015)

[i] (Requejo *et al.* 2014) [j] (Orge *et al.* 1999) [k] (Alvarez *et al.* 2011) [l] (Orge *et al.* 1997)

[m] (González *et al.* 2014) [n] (Singh *et al.* 2013)[o] (Gonza´lez *et al.* 2004) [p] (Iglesias *et al.* 1996)

[q] (Zafarani-Moattar *et al.* 2006) [r] (García-Mardones *et al.* 2012) [s] (Dikio *et al.* 2012)

[t] (Pereira *et al.* 2003) [u] (Singh *et al.* 2013) [v] (García-Mardones *et al.* 2013)

[w] (Quijada-Maldonado *et al.* 2012) [x] (Anantharaj *et al.* 2012) [y] (Shah *et al.* 2013)

[z] (Fröba *et al.* 2010) [aa] (Zaitseva *et al*.2014) [bb] (Naorem and Suri 1993)

4.4. PREPARATION OF BINARY MIXTURES

The binary mixtures were prepared by mass, using an OHAUS (Pine Brook, USA) mass balance with a precision of ± 0.0001 g. The binary mixtures were prepared by injecting known masses of pure components into bottles and stoppered to diminish evaporation losses. Each mixture was shaken in order to ensure complete homogeneity of the two compounds. The binary composition was calculated using an EXCEL spreadsheet to ensure that the whole mole fraction range was covered.

4.5. EXPERIMENTAL PROCEDURE FOR INSTRUMENT

4.5.1. DENSITY AND SPEED OF SOUND

Densities and speeds of sound of the pure liquid and the binary mixtures were simultaneously and automatically measured using an Anton-Paar DSA 5000M digital vibrating tube densimeter with an accuracy of ± 0.02 K for temperature, ±0.000005 $g \cdot cm^{-3}$ for density, and ± 0.01 $m \cdot s^{-1}$ for speed of sound.

Prior to each experimental run, the cell was first cleaned with ethanol (liquid 1) and then dried with acetone (liquid 2) using a fully automatic Xsample 452 Module. Xsample 452 performs a cleaning routine after each measurement. Rinsing ethanol (liquid 1) dissolves sample residues in the measuring cell of the DSA 5000 M. Rinsing acetone (liquid 2) is highly volatile and soluble in rinsing liquid 1. Acetone removes cleaning liquid 1 and is easily evaporated by a stream of dry air in order to accelerate drying of the cell. Acetone is a good solvent for removing ethanol. After rinsing and cleaning the instrument was calibrated by ultra-pure water and ambient air. The goal of a calibration is to validate the accuracy of the density measurement. Each binary mixture is placed in a vial and sealed with a cap. Each vial is placed onto the Xsample 452 with a 48-position magazine. The DSA 5000 M automatically detects

the connected Xsample 452. The sample changer automatically fills the binary solutions from each sample vial into the measuring cell of the DSA 5000 M. The binary mixtures are filled easily and safely without evaporation losses or the formation of bubbles. The instrument automatically detects gas bubbles in the measuring cell by an advanced analysis of its oscillations pattern and generates a warning message. The instrument software also allows visual inspection for one of the gas bubbles on an external PC using a real time camera with zoom function. After each measurement, the measuring cell is automatically rinsed and cleaned with two rinsing liquids and subsequently dried. Density and speed of sound results are shown together on the LED display, and the computer using the pre-installed software. The estimated error in temperature, density and sound velocity was less than ± 0.02 K, ± 5 x10^{-5} g ·cm^{-3} and ± 1 m·s^{-1}, respectively. The estimated error in excess molar volume, isentropic compressibility and deviation in refractive index was ± 0.004 cm^3·mol^{-1}, ± 0.1 x 10^{12} Pa^{-1} and ± 3. 8 x10^{-4}, respectively

4.5.2. REFRACTIVE INDEX

Measurement of the refractive index of pure components and binary mixtures were obtained by a digital automatic refractometer (Anton Paar RXA 156) with an accuracy of ±0.03 K in temperature. The estimated error in refractive index was less than ± 5 x 10^{-5}. The RXA 156 measuring module is operated in combination with the density and sound velocity analyzer DSA 5000 M. The measuring results of the RXA 156 are transmitted to the DSA 5000 M instrument where refractive indices are displayed, saved and can be exported or printed. The LED screen displays the result of all three properties namely, density, speed of sound and refractive index. The instrument was calibrated by measuring the refractive index of ultra-pure water before each series of measurements according to the procedure in the instruction manual.

4.5.3. VALIDATION OF EXPERIMENTAL TECHNIQUE

The experimental technique was assessed by determining the excess molar volume, isentropic compressibility and change in refractive index on mixing for the test system (ethanol + heptane) at T = 303.15 K and comparing it with literature data (Orge *et al*. 1999). The maximum difference between the experimental and literature values for the excess molar volume, deviation in isentropic compressibility and deviation in refractive index was ± 0.029 $cm^3 \cdot mol^{-1}$, ± 0.01 x 10^{12} Pa^{-1}, and ± 0.00062, respectively for the test system.

The table for the literature and experimental data for V_m^E, κ_s and Δn for the test system {ethanol(x_1) + heptane (x_2)} at T = 303 K is given below in Table 4.5.

Table 4.5. The literature and experimental data for V_m^E, κ_s and Δn for the test system {ethanol(x_1) + heptane (x_2)} at T = 303 K

x_1	ρ / (g ·cm^{-3})	V_m^E / (cm^3·mol^{-1})	Δn	κ_s / (10^{12} Pa^{-1})
		Experimental		
		T = 303.15 K		
0.0000	0.67543	0.000	0.00000	1201.6
0.0529	0.67679	0.202	0.00024	1212.6
0.1415	0.68019	0.356	0.00105	1216.6
0.2074	0.68311	0.445	0.00172	1210.8
0.3038	0.68847	0.473	0.00246	1212.2
0.3948	0.69425	0.504	0.00308	1205.3
0.4682	0.69966	0.511	0.00345	1197.5
0.5400	0.70573	0.505	0.00368	1187.5
0.6356	0.71530	0.475	0.00372	1169.8
0.7653	0.73207	0.378	0.00309	1134.1
0.8296	0.74234	0.329	0.00263	1109.5
0.9584	0.77005	0.113	0.00082	1036.3
		Literature		
0.1191	0.67830	0.280	0.00056	1217.6
0.2042	0.68260	0.411	0.00123	1219.3
0.3024	0.68850	0.476	0.00203	1215.0
0.4031	0.69480	0.507	0.00274	1207.8
0.4887	0.70260	0.500	0.00317	1196.1
0.5972	0.71090	0.483	0.00335	1182.0
0.7027	0.72410	0.436	0.00308	1155.8
0.7956	0.73260	0.373	0.00250	1129.0
0.8890	0.75490	0.222	0.00145	1082.7

The graphs of the literature and experimental data for V_m^E, κ_s and Δn are given in Figures 4.3, 4.4 and 4.5, respectively.

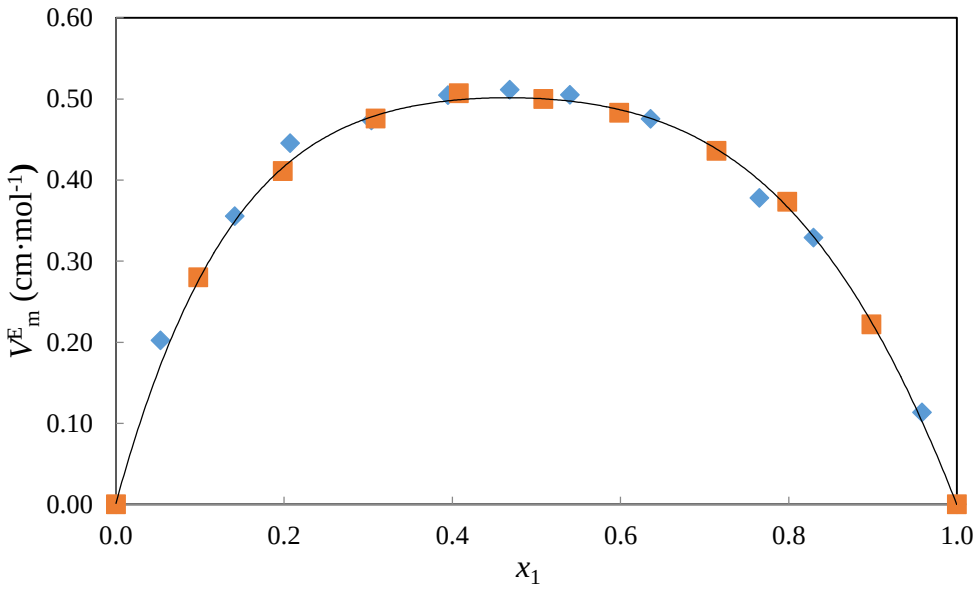

Figure 4.3. Comparison of the calculated V_m^E from this work with the literature data for the binary mixture (ethanol + heptane) at T = 303.15 K, □, literature data (Orge *et al*. 1999); ◊, this work.

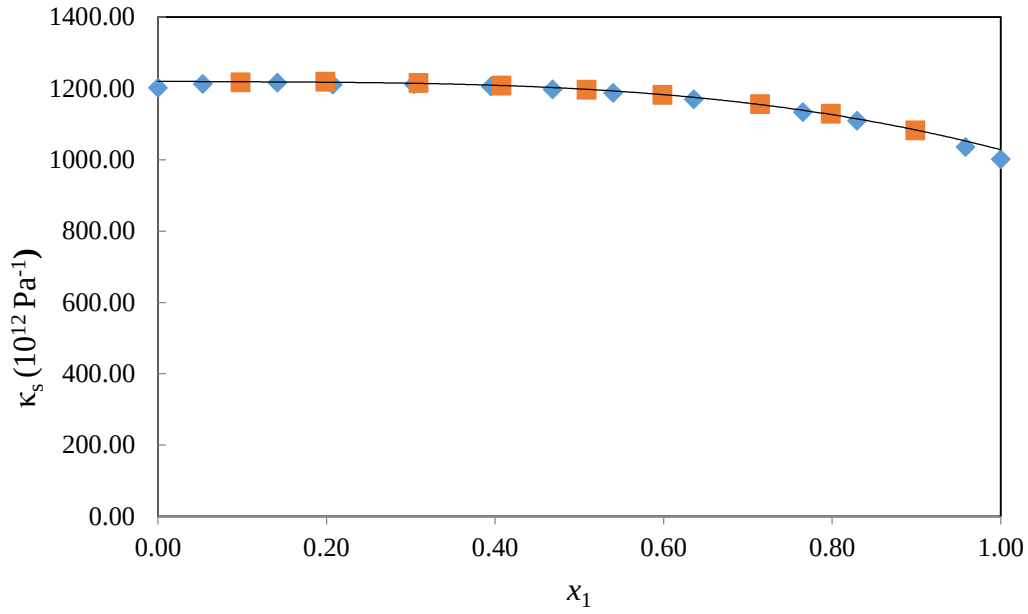

Figure 4.4. Comparison of the calculated κ_s from this work with the literature data for the binary mixture (ethanol + heptane) at $T = 303.15$ K, □, literature data (Orge *et al*. 1999); ◊, this work.

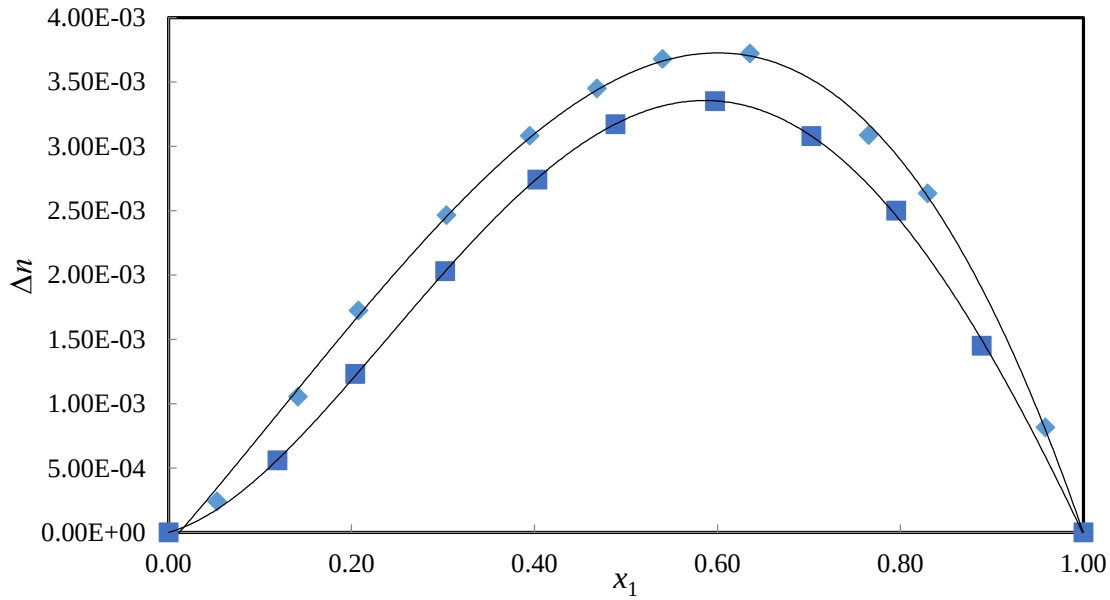

Figure 4.4. Comparison of the calculated Δn from this work with the literature data for the binary mixture (ethanol + heptane) at $T = 303.15$ K, □, literature data (Orge *et al*. 1999); ◊, this work.

CHAPTER **5**

RESULTS

5.1. EXCESS MOLAR VOLUME, V_m^E, ISENTROPIC COMPRESSIBILITY, κ_s, DEVIATION IN REFRACTIVE INDEX, Δn AND MOLAR REFRACTION, R

The results of excess molar volume, isentropic compressibility, deviation in refractive index, and molar refraction, for all binary systems at the five temperatures are given in this chapter.

The V_m^E, for binary mixtures {methanol (x_1) or [EMIM][OAc] (x_1) + furfural (x_2)} and {methanol (x_1) or [EMIM][OAc] (x_1) + furfuryl alcohol (x_2)} over the entire composition range was calculated from density data at temperatures between 298.15 K and 318.15 K in 5 K intervals using the following equation:

$$V_m^E = \frac{x_1 M_1 + x_2 M_2}{\rho} - \frac{x_1 M_1}{\rho_1} - \frac{x_2 M_2}{\rho_2} \tag{5.1}$$

where x_1 and x_2 are mole fractions, M_1 and M_2 are the molecular masses, ρ_1 and ρ_2 are the densities of pure components 1 and 2, respectively, where '1' refers to methanol, or [EMIM][OAc] and '2' to furfural or furfuryl alcohol. ρ, is the density of the mixture.

The results for density, ρ, and excess molar volume, V_m^E, for the binary systems {methanol (x_1) or [EMIM][OAc] (x_1) + furfural (x_2)} and { methanol (x_1) or [EMIM][OAc] (x_1) + furfuryl alcohol (x_2)} at T = (298.15, 303.15, 308.15, 313.15 and 318.15) K are presented in Tables 5.1, 5.2, 5.3 and 5.4.

The isentropic compressibilities, κ_s, were calculated from the Newton–Laplace equation given below:

$$\kappa_s = \frac{1}{\rho u^2} \tag{5.2}$$

Where ρ, is the density and u is the speed of sound of the binary mixtures.

The results of speed of sound, u, and isentropic compressibility, κ_s, for the binary systems {methanol (x_1) or [EMIM][OAc] (x_1) + furfural (x_2)} and { methanol (x_1) or [EMIM][OAc] (x_1) + furfuryl alcohol (x_2)} at T = (298.15, 303.15, 308.15, 313.15 and 318.15) K are also presented in Tables 5.1, 5.2, 5.3 and 5.4.

The deviation in refractive index, Δn, was calculated using equation (5.3):

$$\Delta n = n - x_1 n_1 - x_2 n_2 \tag{5.3}$$

where n_1 and n_2 are the refractive index of pure components and n is the refractive index of the mixtures. The results for deviation in refractive index, Δn, for the binary systems {methanol (x_1) or [EMIM][OAc] (x_1) + furfural (x_2)} and { methanol (x_1) or [EMIM][OAc] (x_1) + furfuryl alcohol (x_2)} at T = (298.15, 303.15, 308.15, 313.15 and 318.15) K are given in Tables 5.5, 5.6, 5.7 and 5.8.

The molar refraction, R, was calculated by the Lorentz–Lorenz equation given below:

$$R = \left(\frac{n^2 - 1}{n^2 + 2} \right) V_m \tag{5.4}$$

where V_m is the molar volume and n is the refractive index of the mixture. The results for molar refraction, R, for the binary systems {methanol (x_1) or [EMIM][OAc] (x_1) + furfural (x_2)} and {methanol (x_1) or [EMIM][OAc] (x_1) + furfuryl alcohol (x_2)} at T = (298.15, 303.15, 308.15, 313.15 and 318.15) K are also given in tables 5.5, 5.6, 5.7 and 5.8.

Table 5.1 Density, ρ, excess molar volume, V_m^E, speed of sound, *u*, and isentropic compressibility, κ_s, for the binary mixture {methanol (x_1) + furfural (x_2)} at *T* = (298.15, 303.15, 308.15, 313.15 and 318.15) K.

x_1	ρ / (g ·cm^{-3})	V_m^E / (cm^3·mol^{-1})	*u* / (m·s^{-1})	κ_s / (10^{12} Pa^{-1})
		T = 298.15 K		
0.0000	1.15431	0.000	1440	417.5
0.0713	1.14307	-0.143	1431	427.4
0.1608	1.12710	-0.288	1416	442.7
0.2650	1.10552	-0.407	1394	465.2
0.3742	1.07933	-0.505	1367	494.5
0.6054	1.00677	-0.562	1300	587.3
0.7510	0.94458	-0.494	1245	683.4
0.8333	0.90184	-0.430	1208	759.9
0.8990	0.86125	-0.289	1172	846.5
0.9367	0.83562	-0.204	1148	907.6
0.9685	0.81273	-0.142	1129	966.1
1.0000	0.78710	0.000	1108	1035.4
		T = 303.15 K		
0.0000	1.14899	0.000	1423	430.0
0.0713	1.13772	-0.142	1413	440.2
0.1608	1.12172	-0.286	1398	456.0
0.2650	1.10013	-0.404	1377	479.2
0.3742	1.07397	-0.505	1352	509.6
0.6054	1.00156	-0.568	1284	605.6

Table 5.1 continued

0.7510	0.93949	-0.499	1228	705.4
0.8333	0.89684	-0.435	1192	784.5
0.8990	0.85631	-0.291	1155	875.6
0.9367	0.83071	-0.203	1132	939.5
0.9685	0.80791	-0.143	1113	1000.0
1.0000	0.78238	0.000	1092	1071.3
		T = 308.15 K		
0.0000	1.14364	0.000	1405	443.1
0.0713	1.13236	-0.142	1395	453.7
0.1608	1.11632	-0.285	1380	470.1
0.2650	1.09467	-0.400	1360	493.9
0.3742	1.06849	-0.499	1333	526.4
0.6054	0.99625	-0.568	1267	625.0
0.7510	0.93428	-0.499	1212	728.6
0.8333	0.89171	-0.435	1177	809.8
0.8990	0.85128	-0.289	1139	906.1
0.9367	0.82576	-0.202	1116	972.7
0.9685	0.80307	-0.143	1097	1035.6
1.0000	0.77764	0.000	1078	1106.8
		T = 313.15 K		
0.0000	1.13829	0.000	1387	456.9
0.0713	1.12700	-0.143	1377	467.7
0.1608	1.11093	-0.285	1363	484.6
0.2650	1.08922	-0.396	1343	509.1

Table 5.1 continued

0.3742	1.06299	-0.492	1313	545.7
0.6054	0.99080	-0.561	1249	647.5
0.7510	0.92897	-0.495	1196	753.0
0.8333	0.88651	-0.432	1163	834.1
0.8990	0.84621	-0.287	1122	938.0
0.9367	0.82080	-0.201	1099	1007.0
0.9685	0.79820	-0.143	1081	1072.1
1.0000	0.77287	0.000	1065	1140.7
		T = 318.15 K		
0.0000	1.13293	0.000	1369	471.2
0.0713	1.12165	-0.145	1360	482.3
0.1608	1.10555	-0.286	1345	500.0
0.2650	1.08378	-0.394	1326	524.6
0.3742	1.05750	-0.487	1290	568.4
0.6054	0.98529	-0.553	1224	677.9
0.7510	0.92362	-0.490	1179	778.3
0.8333	0.88129	-0.429	1153	854.2
0.8990	0.84112	-0.285	1107	970.8
0.9367	0.81581	-0.200	1085	1041.0
0.9685	0.79330	-0.143	1066	1109.0
1.0000	0.76806	0.000	1056	1168.6

Standard uncertainties u are $u(T)$ = ±0.01 K and the combined expanded uncertainty Uc in density and speed of sound measurements were less than $U_c(\rho) = \pm 5 \times 10^{-5}$ g ·cm^{-3}, and $U_c(u) = \pm 1$ m·s^{-1} , respectively (0.95 level of confidence)

Table 5.2 Density, ρ, excess molar volume, V_m^E, speed of sound, *u*, and isentropic compressibility, κ_s, for the binary mixture {[EMIM][OAc] (x_1) + furfural (x_2)} at *T* = (298.15, 303.15, 308.15, 313.15 and 318.15) K.

x_1	ρ / (g ·cm^{-3})	V_m^E / (cm^3·mol^{-1})	*u* / (m·s^{-1})	κ_s / (10^{12} Pa^{-1})
		T = 298.15 K		
0.0000	1.15431	0.000	1440	417.5
0.0520	1.16852	-1.449	1473	394.2
0.1009	1.18714	-3.250	1510	369.7
0.1513	1.20953	-5.397	1557	341.0
0.3506	1.21352	-7.833	1742	271.6
0.4459	1.18837	-6.606	1736	279.2
0.5515	1.16593	-5.388	1730	286.8
0.6515	1.14985	-4.483	1723	292.8
0.7515	1.13584	-3.592	1720	297.7
0.8504	1.12093	-2.380	1723	300.5
0.8957	1.11302	-1.608	1728	301.1
0.9510	1.10517	-0.835	1732	301.7
1.0000	1.09755	0.000	1735	302.8
		T = 303.15 K		
0.0000	1.14899	0.000	1423	430.0
0.0520	1.16362	-1.478	1457	405.1
0.1009	1.18259	-3.306	1493	379.5
0.1513	1.20508	-5.463	1541	349.7
0.3506	1.20964	-7.915	1710	282.8
0.4459	1.18438	-6.650	1710	288.9
0.5515	1.16223	-5.430	1705	295.9
0.6515	1.14652	-4.539	1703	300.6
0.7515	1.13264	-3.641	1704	304.0
0.8504	1.11780	-2.413	1710	306.0

0.8957	1.10989	-1.631	1715	306.4

Table 5.2 continued

0.9510	1.10205	-0.845	1719	307.1
1.0000	1.09445	0.000	1722	308.0
		T = 308.15 K		
0.0000	1.14364	0.000	1405	443.1
0.0520	1.15867	-1.504	1444	416.3
0.1009	1.17794	-3.356	1476	389.5
0.1513	1.20050	-5.522	1524	358.5
0.3506	1.20593	-8.012	1686	291.8
0.4459	1.18064	-6.717	1687	297.7
0.5515	1.15869	-5.487	1685	303.9
0.6515	1.14326	-4.602	1687	307.4
0.7515	1.12943	-3.688	1690	310.1
0.8504	1.11465	-2.445	1697	311.6
0.8957	1.10676	-1.652	1702	311.9
0.9510	1.09894	-0.855	1707	312.4
1.0000	1.09136	0.000	1710	313.3
		T = 313.15 K		
0.0000	1.13829	0.000	1387	456.9
0.0520	1.15379	-1.536	1423	428.1
0.1009	1.17343	-3.418	1460	399.9
0.1513	1.19603	-5.590	1508	367.5
0.3506	1.20222	-8.111	1666	299.8
0.4459	1.17692	-6.786	1666	306.2
0.5515	1.15530	-5.560	1669	310.6
0.6515	1.14001	-4.667	1672	314.0
0.7515	1.12623	-3.734	1676	316.1
0.8504	1.11150	-2.473	1684	317.2
0.8957	1.10364	-1.672	1690	317.4
0.9510	1.09585	-0.865	1695	317.8
1.0000	1.08830	0.000	1698	318.7
		T = 318.15 K		

0.0000	1.13293	0.000	1369	471.2

Table 5.2 continued

0.0520	1.14905	-1.581	1406	440.2
0.1009	1.16924	-3.505	1444	410.2
0.1513	1.19186	-5.681	1493	376.5
0.3506	1.19844	-8.204	1648	307.1
0.4459	1.17342	-6.876	1649	313.3
0.5515	1.15196	-5.637	1654	317.3
0.6515	1.13677	-4.731	1657	320.5
0.7515	1.12299	-3.775	1663	322.2
0.8504	1.10834	-2.498	1672	322.9
0.8957	1.10053	-1.690	1677	322.9
0.9510	1.09278	-0.875	1682	323.3
1.0000	1.08525	0.000	1686	324.2

Standard uncertainties u are $u(T) = \pm 0.01$ K and the combined expanded uncertainty Uc in density and speed of sound measurements were less than $U_c(\rho) = \pm 5 \times 10^{-5}$ g ·cm^{-3}, and $U_c(u) = \pm 1$ m·s^{-1} , respectively (0.95 level of confidence)

Table 5.3 Density, ρ, excess molar volume, V_m^E, speed of sound, *u*, and isentropic compressibility, κ_s, for the binary mixture {methanol (x_1) + furfuryl alcohol (x_2)} at *T* = (298.15, 303.15, 308.15, 313.15 and 318.15) K.

x_1	ρ / (g ·cm^{-3})	V_m^E / (cm^3·mol^{-1})	*u* / (m· s^{-1})	κ_s / (10^{12} Pa^{-1})
		T = 298.15 K		
0.0000	1.12691	0.000	1447	423.7
0.0738	1.11629	-0.118	1435	434.8
0.1312	1.10735	-0.209	1427	443.5
0.2322	1.08957	-0.333	1411	460.7
0.3799	1.05803	-0.446	1380	496.1
0.5048	1.02554	-0.516	1347	537.6
0.6437	0.98056	-0.539	1300	603.2
0.7669	0.92968	-0.483	1248	691.1
0.8432	0.89098	-0.389	1208	769.4
0.8898	0.86425	-0.318	1182	828.2
0.9199	0.84528	-0.254	1163	874.4
0.9383	0.83277	-0.198	1148	910.5
0.9547	0.82124	-0.149	1137	942.6
1.0000	0.78710	0.000	1108	1035.4
		T = 303.15 K		
0.0000	1.12226	0.000	1431	435.3
0.0738	1.11165	-0.122	1420	446.2

Table 5.3 continued

0.1312	1.10271	-0.215	1411	455.3
0.2322	1.08493	-0.342	1394	474.2
0.3799	1.05340	-0.459	1364	510.6
0.5048	1.02090	-0.532	1330	553.6
0.6437	0.97591	-0.556	1284	621.8
0.7669	0.92501	-0.498	1231	713.1
0.8432	0.88629	-0.401	1192	794.1
0.8898	0.85956	-0.328	1166	855.2
0.9199	0.84058	-0.262	1152	896.3
0.9383	0.82807	-0.204	1133	940.3
0.9547	0.81653	-0.154	1121	974.2
1.0000	0.78238	0.000	1092.	1071.3
		T = 308.15 K		
0.0000	1.11758	0.000	1413	448.1
0.0738	1.10698	-0.126	1404	458.3
0.1312	1.09806	-0.222	1396	467.6
0.2322	1.08027	-0.352	1375	489.4
0.3799	1.04874	-0.473	1345	527.2
0.5048	1.01624	-0.549	1312	571.8
0.6437	0.97124	-0.573	1266	642.7
0.7669	0.92031	-0.513	1214	736.9
0.8432	0.88159	-0.414	1177	819.4
0.8898	0.85485	-0.339	1152	882.1

Table 5.3 continued

0.9199	0.83585	-0.270	1148	908.2
0.9383	0.82334	-0.210	1120	968.5
0.9547	0.81180	-0.159	1107	1005.5
1.0000	0.77764	0.000	1078	1106.8
		T = 313.15 K		
0.0000	1.11289	0.000	1394	462.2
0.0738	1.10230	-0.130	1388	470.6
0.1312	1.09338	-0.228	1380	480.2
0.2322	1.07560	-0.362	1356	506.0
0.3799	1.04406	-0.487	1325	545.9
0.5048	1.01156	-0.565	1292	592.5
0.6437	0.96654	-0.591	1246	666.7
0.7669	0.91560	-0.529	1197	762.7
0.8432	0.87687	-0.427	1161	845.7
0.8898	0.85011	-0.350	1138	907.5
0.9199	0.83110	-0.278	1080	992.1
0.9383	0.81859	-0.217	1110	1032.3
0.9547	0.80704	-0.164	1094	1035.7
1.0000	0.77287	0.000	1065	1140.7
		T = 318.15 K		
0.0000	1.10818	0.000	1375	477.3
0.0738	1.09759	-0.133	1373	483.3
0.1312	1.08867	-0.234	1365	493.2

Table 5.3 continued

0.2322	1.07090	-0.373	1334	525.0
0.3799	1.03937	-0.503	1303	567.0
0.5048	1.00686	-0.583	1269	616.3
0.6437	0.96182	-0.609	1224	694.1
0.7669	0.91086	-0.546	1178	790.6
0.8432	0.87211	-0.441	1146	872.8
0.8898	0.84534	-0.361	1127	930.8
0.9199	0.82632	-0.287	1080	1038.2
0.9383	0.81380	-0.224	1104	1009.1
0.9547	0.80225	-0.169	1083	1062.4
1.0000	0.76806	0.000	1066	1145.4

Standard uncertainties u are $u(T) = \pm 0.01$ K and the combined expanded uncertainty Uc in density and speed of sound measurements were less than $U_c(\rho) = \pm 5 \times 10^{-5}$ g ·cm^{-3}, and $U_c(u) = \pm 1$ m·s^{-1} , respectively (0.95 level of confidence)

Table 5.4 Density, ρ, excess molar volume, V_m^E, speed of sound, *u*, and isentropic compressibility, κ_s, for the binary mixture {[EMIM][OAc] (x_1) + furfuryl alcohol (x_2)} at *T* = (298.15, 303.15, 308.15, 313.15 and 318.15) K.

x_1	ρ / (g ·cm^{-3})	V_m^E / (cm^3·mol^{-1})	*u* / (m· s^{-1})	κ_s / (10^{12} Pa^{-1})
		T = 298.15 K		
0.0000	1.12691	0.000	1447	423.7
0.0572	1.12934	-0.426	1487	400.6
0.1058	1.12962	-0.653	1522	382.1
0.1534	1.12901	-0.800	1548	369.8
0.2087	1.12781	-0.924	1573	358.6
0.3068	1.12489	-1.047	1608	343.7
0.4080	1.12103	-1.054	1637	332.8
0.5063	1.11686	-0.971	1660	324.8
0.5513	1.11495	-0.915	1670	321.7
0.6031	1.11274	-0.837	1680	318.5
0.7053	1.10852	-0.657	1696	313.7
0.8045	1.10454	-0.445	1711	309.3
0.8441	1.10308	-0.362	1716	307.8
0.9020	1.10094	-0.230	1723	305.8
1.0000	1.09755	0.000	1735	302.8
		T = 303.15 K		
0.0000	1.12226	0.000	1431	435.3
0.0572	1.12499	-0.442	1471	411.2
0.1058	1.12550	-0.680	1506	391.8
0.1534	1.12503	-0.831	1532	378.7
0.2087	1.12397	-0.957	1557	366.8
0.3068	1.12120	-1.081	1594	351.1
0.4080	1.11748	-1.086	1623	339.6
0.5063	1.11342	-0.999	1647	331.2

0.5513	1.11155	-0.941	1656	328.0

Table 5.4 continued

0.6031	1.10939	-0.861	1666	324.6
0.7053	1.10524	-0.674	1683	319.5
0.8045	1.10133	-0.457	1698	314.8
0.8441	1.09989	-0.372	1704	313.3
0.9020	1.09779	-0.236	1711	311.2
1.0000	1.09445	0.000	1722	308.0
		T = 308.15 K		
0.0000	1.11758	0.000	1413	448.1
0.0572	1.12064	-0.459	1452	423.3
0.1058	1.12139	-0.708	1487	403.0
0.1534	1.12106	-0.864	1514	389.4
0.2087	1.12012	-0.992	1540	376.4
0.3068	1.11752	-1.117	1577	360.0
0.4080	1.11393	-1.119	1609	346.7
0.5063	1.10999	-1.028	1633	337.8
0.5513	1.10817	-0.969	1643	334.4
0.6031	1.10605	-0.886	1653	330.8
0.7053	1.10198	-0.694	1670	325.5
0.8045	1.09814	-0.471	1685	320.5
0.8441	1.09672	-0.383	1691	318.9
0.9020	1.09465	-0.243	1699	316.6
1.0000	1.09136	0.000	1710	313.3
		T = 313.15 K		
0.0000	1.11289	0.000	1394	462.2
0.0572	1.11627	-0.476	1430	438.2
0.1058	1.11726	-0.737	1465	417.0
0.1534	1.11708	-0.898	1490	403.2
0.2087	1.11628	-1.030	1519	388.1
0.3068	1.11386	-1.154	1558	370.1
0.4080	1.11041	-1.154	1595	354.0
0.5063	1.10657	-1.059	1620	344.5

0.5513	1.10479	-0.998	1629	341.0

Table 5.4 continued

0.6031	1.10273	-0.912	1640	337.2
0.7053	1.09873	-0.713	1657	331.5
0.8045	1.09497	-0.485	1673	326.3
0.8441	1.09357	-0.394	1678	324.6
0.9020	1.09154	-0.250	1686	322.2
1.0000	1.08830	0.000	1698	318.7
		T = 318.15 K		
0.0000	1.10818	0.000	1375	477.3
0.0572	1.11189	-0.494	1402	457.9
0.1058	1.11314	-0.769	1433	437.4
0.1534	1.11312	-0.935	1460	421.7
0.2087	1.11245	-1.069	1495	402.3
0.3068	1.11021	-1.194	1534	382.7
0.4080	1.10688	-1.189	1578	363.0
0.5063	1.10317	-1.092	1606	351.4
0.5513	1.10144	-1.028	1616	347.6
0.6031	1.09942	-0.940	1627	343.7
0.7053	1.09550	-0.734	1644	337.7
0.8045	1.09181	-0.499	1660	332.2
0.8441	1.09044	-0.406	1666	330.4
0.9020	1.08844	-0.257	1674	327.9
1.0000	1.08525	0.000	1686	324.2

Standard uncertainties u are $u(T)$ = ±0.01 K and the combined expanded uncertainty Uc in density and speed of sound measurements were less than $U_c(\rho) = \pm 5 \times 10^{-5}$ g ·cm^{-3}, and $U_c(u) = \pm 1$ m·s^{-1} , respectively (0.95 level of confidence)

Table 5.5 Refractive index, *n*, deviation in refractive index, Δn, molar refraction, *R*, for the binary mixture {methanol (x_1) + furfural (x_2)} at *T* = (298.15, 303.15, 308.15, 313.15 and 318.15) K.

x_1	n	Δn	R /($cm^3 \cdot mol^{-1}$)
		T = 298.15 K	
0.0000	1.52311	0.00000	25.43
0.0713	1.51695	0.00094	24.22
0.1608	1.50829	0.00199	22.70
0.2650	1.49675	0.00303	20.93
0.3742	1.48254	0.00379	19.07
0.6054	1.44349	0.00443	15.11
0.7510	1.41059	0.00432	12.60
0.8333	1.38835	0.00439	11.19
0.8990	1.36658	0.00290	10.03
0.9367	1.35329	0.00244	9.37
0.9685	1.34005	0.00079	8.78
1.0000	1.32704	0.00000	8.24
		T = 303.15 K	
0.0000	1.52046	0.00000	25.44
0.0713	1.51437	0.00098	24.23
0.1608	1.50578	0.00206	22.71
0.2650	1.49426	0.00306	20.94
0.3742	1.48001	0.00371	19.08
0.6054	1.44107	0.00425	15.11
0.7510	1.40836	0.00416	12.61
0.8333	1.38666	0.00462	11.20
0.8990	1.36483	0.00296	10.04
0.9367	1.35130	0.00218	9.38
0.9685	1.33800	0.00039	8.79
1.0000	1.32548	0.00000	8.25
		T = 308.15 K	
0.0000	1.51784	0.00000	25.45

Table 5.5 continued

0.0713	1.51175	0.00095	24.24
0.1608	1.50316	0.00200	22.72
0.2650	1.49167	0.00300	20.95
0.3742	1.47745	0.00362	19.09
0.6054	1.43860	0.00409	15.12
0.7510	1.40613	0.00410	12.62
0.8333	1.38465	0.00468	11.22
0.8990	1.36289	0.00298	10.06
0.9367	1.34932	0.00209	9.39
0.9685	1.33598	0.00020	8.79
1.0000	1.32372	0.00000	8.26
		T = 313.15 K	
0.0000	1.51517	0.00000	25.46
0.0713	1.50911	0.00096	24.25
0.1608	1.50049	0.00195	22.73
0.2650	1.48905	0.00295	20.96
0.3742	1.47481	0.00350	19.09
0.6054	1.43612	0.00397	15.13
0.7510	1.40388	0.00405	12.63
0.8333	1.38267	0.00479	11.23
0.8990	1.36102	0.00309	10.07
0.9367	1.34732	0.00199	9.40
0.9685	1.33390	-0.00004	8.80
1.0000	1.32195	0.00000	8.27
		T = 318.15 K	
0.0000	1.51257	0.00000	25.47
0.0713	1.50647	0.00090	24.26
0.1608	1.49790	0.00190	22.74
0.2650	1.48645	0.00285	20.97
0.3742	1.47221	0.00334	19.10
0.6054	1.43362	0.00374	15.14
0.7510	1.40164	0.00392	12.64

Table 5.5 continued

0.8333	1.38070	0.00481	11.25
0.8990	1.35916	0.00311	10.08
0.9367	1.34535	0.00183	9.41
0.9685	1.33179	-0.00042	8.80
1.0000	1.32030	0.00000	8.28

Standard uncertainties u are $u(T)$ = ±0.01 K and the combined expanded uncertainty Uc in refractive index measurements were less than $U_c(n)= 5 \times 10^{-5}$, respectively (0.95 level of confidence)

Table 5.6 Refractive index, *n*, deviation in refractive index, Δn, molar refraction, *R*, for the binary mixture {[EMIM][OAc] (x_1) + furfural (x_2)} at *T* = (298.15, 303.15, 308.15, 313.15 and 318.15) K.

x_1	n	Δn	R /($cm^3.mol^{-1}$)
		T = 298.15 K	
0.0000	1.52311	0.00000	25.43
0.0520	1.52707	0.00613	26.30
0.1009	1.53221	0.01315	27.04
0.1513	1.53812	0.02084	27.75
0.3506	1.54083	0.02946	31.60
0.4459	1.53551	0.02644	33.86
0.5515	1.52790	0.02108	36.17
0.6515	1.52088	0.01595	38.22
0.7515	1.51288	0.00964	40.16
0.8504	1.50712	0.00539	42.25
0.8957	1.50491	0.00383	43.29
0.9510	1.50183	0.00149	44.47
1.0000	1.49971	0.00000	45.59
		T = 303.15 K	
0.0000	1.52046	0.00000	25.44
0.0520	1.52461	0.00620	26.30
0.1009	1.53005	0.01342	27.05
0.1513	1.53609	0.02114	27.77
0.3506	1.53885	0.02948	31.61
0.4459	1.53402	0.02683	33.89
0.5515	1.52673	0.02167	36.21
0.6515	1.51904	0.01577	38.22
0.7515	1.51051	0.00884	40.11
0.8504	1.50572	0.00548	42.27
0.8957	1.50349	0.00386	43.31
0.9510	1.50043	0.00151	44.49
1.0000	1.49833	0.00000	45.61

Table 5.6 continued

		T = 308.15 K	
0.0000	1.51784	0.00000	25.45
0.0520	1.52220	0.00629	26.31
0.1009	1.52775	0.01351	27.06
0.1513	1.53404	0.02140	27.78
0.3506	1.53704	0.02967	31.61
0.4459	1.53194	0.02663	33.89
0.5515	1.52500	0.02170	36.23
0.6515	1.51751	0.01590	38.24
0.7515	1.50925	0.00916	40.14
0.8504	1.50426	0.00552	42.29
0.8957	1.50205	0.00389	43.33
0.9510	1.49904	0.00154	44.51
1.0000	1.49693	0.00000	45.63
		T = 313.15 K	
0.0000	1.51517	0.00000	25.46
0.0520	1.51978	0.00642	26.32
0.1009	1.52555	0.01376	27.07
0.1513	1.53188	0.02159	27.79
0.3506	1.53555	0.03021	31.64
0.4459	1.53046	0.02706	33.92
0.5515	1.52342	0.02192	36.24
0.6515	1.51587	0.01595	38.24
0.7515	1.50814	0.00965	40.18
0.8504	1.50285	0.00564	42.31
0.8957	1.50062	0.00395	43.35
0.9510	1.49764	0.00159	44.53
1.0000	1.49551	0.00000	45.65
		T = 318.15 K	
0.0000	1.51257	0.00000	25.47
0.0520	1.51739	0.00652	26.33
0.1009	1.52338	0.01398	27.07

Table 5.6 continued

0.1513	1.52976	0.02177	27.80
0.3506	1.53395	0.03060	31.66
0.4459	1.52852	0.02698	33.91
0.5515	1.52200	0.02225	36.26
0.6515	1.51424	0.01597	38.25
0.7515	1.50698	0.01005	40.22
0.8504	1.50140	0.00567	42.33
0.8957	1.49927	0.00405	43.37
0.9510	1.49621	0.00158	44.54
1.0000	1.49413	0.00000	45.67

Standard uncertainties u are $u(T)$ = ±0.01 K and the combined expanded uncertainty Uc irefractive index measurements were less than $U_c(n)= 5 \times 10^{-5}$, respectively (0.95 level of confidence)

Table 5.7. Refractive index, *n*, deviation in refractive index, Δn, molar refraction, *R*, for the binary mixture {methanol (x_1) + furfuryl alcohol (x_2)} at *T* = (298.15, 303.15, 308.15, 313.15 and 318.15) K.

x_1	n	Δn	R /($cm^3 \cdot mol^{-1}$)
		T = 298.15 K	
0.0000	1.48455	0.00000	24.93
0.0738	1.47974	0.00085	23.71
0.1312	1.47552	0.00136	22.76
0.2322	1.46697	0.00194	21.08
0.3799	1.45214	0.00267	18.62
0.5048	1.43701	0.00330	16.54
0.6437	1.41602	0.00359	14.22
0.7669	1.39244	0.00336	12.16
0.8432	1.37461	0.00277	10.88
0.8898	1.36237	0.00235	10.10
0.9199	1.35325	0.00149	9.58
0.9383	1.34770	0.00124	9.28
0.9547	1.34234	0.00080	9.00
1.0000	1.32704	0.00000	8.24
		T = 303.15 K	
0.0000	1.48249	0.00000	24.94
0.0738	1.47769	0.00085	23.73
0.1312	1.47346	0.00134	22.77
0.2322	1.46488	0.00187	21.08
0.3799	1.45006	0.00258	18.63
0.5048	1.43491	0.00316	16.55
0.6437	1.41396	0.00343	14.23
0.7669	1.39044	0.00318	12.17
0.8432	1.37269	0.00261	10.89
0.8898	1.36075	0.00245	10.11
0.9199	1.35137	0.00128	9.59
0.9383	1.34579	0.00099	9.28

Table 5.7 continued

0.9547	1.34042	0.00051	9.00
1.0000	1.32548	0.00000	8.25
		T = 308.15 K	
0.0000	1.48035	0.00000	24.95
0.0738	1.47557	0.00086	23.74
0.1312	1.47136	0.00138	22.78
0.2322	1.46272	0.00184	21.09
0.3799	1.44792	0.00254	18.63
0.5048	1.43280	0.00314	16.55
0.6437	1.41187	0.00338	14.24
0.7669	1.38845	0.00317	12.18
0.8432	1.37084	0.00269	10.90
0.8898	1.35883	0.00241	10.12
0.9199	1.34945	0.00122	9.60
0.9383	1.34380	0.00083	9.29
0.9547	1.33841	0.00032	9.01
1.0000	1.32372	0.00000	8.26
		T = 313.15 K	
0.0000	1.47815	0.00000	24.96
0.0738	1.47344	0.00093	23.74
0.1312	1.46920	0.00141	22.79
0.2322	1.46058	0.00188	21.10
0.3799	1.44578	0.00257	18.64
0.5048	1.43067	0.00314	16.56
0.6437	1.40979	0.00339	14.24
0.7669	1.38646	0.00319	12.18
0.8432	1.36887	0.00267	10.91
0.8898	1.35694	0.00243	10.13
0.9199	1.34751	0.00116	9.60
0.9383	1.34179	0.00068	9.29
0.9547	1.33642	0.00016	9.01
1.0000	1.32195	0.00000	8.27

Table 5.7 continued

		T = 318.15 K	
0.0000	1.47596	0.00000	24.97
0.0738	1.47131	0.00057	23.75
0.1312	1.46706	0.00068	22.80
0.2322	1.45841	0.00043	21.10
0.3799	1.44364	-0.00002	18.64
0.5048	1.42854	-0.00064	16.56
0.6437	1.40772	-0.00195	14.25
0.7669	1.38450	-0.00382	12.19
0.8432	1.36689	-0.00569	10.91
0.8898	1.35511	-0.00668	10.14
0.9199	1.34561	-0.00867	9.61
0.9383	1.33981	-0.00964	9.30
0.9547	1.33442	-0.01056	9.02
1.0000	1.33179	0.00000	8.55

Standard uncertainties u are $u(T)$ = ±0.01 K and the combined expanded uncertainty Uc in refractive index measurements were less than $U_c(n)$= 5 x 10^{-5} , respectively (0.95 level of confidence)

Table 5.8 Refractive index, *n*, deviation in refractive index, Δn, molar refraction, *R*, for the binary mixture {[EMIM][OAc] (x_1) + furfuryl alcohol (x_2)} at *T* = (298.15, 303.15, 308.15, 313.15 and 318.15) K.

x_1	n	Δn	R /($cm^3 \cdot mol^{-1}$)
		T = 298.15 K	
0.0000	1.48455	0.00000	24.93
0.0572	1.48755	0.00152	26.06
0.1058	1.48962	0.00244	27.04
0.1534	1.49097	0.00272	28.00
0.2087	1.49238	0.00299	29.13
0.3068	1.49445	0.00322	31.14
0.4080	1.49604	0.00314	33.23
0.5063	1.49719	0.00285	35.28
0.5513	1.49759	0.00264	36.22
0.6031	1.49799	0.00237	37.30
0.7053	1.49874	0.00191	39.44
0.8045	1.49918	0.00129	41.51
0.8441	1.49933	0.00104	42.34
0.9020	1.49949	0.00066	43.55
1.0000	1.49971	0.00000	45.59
		T = 303.15 K	
0.0000	1.48249	0.00000	24.94
0.0572	1.48564	0.00161	26.07
0.1058	1.48782	0.00257	27.06
0.1534	1.48922	0.00287	28.02
0.2087	1.49069	0.00314	29.14
0.3068	1.49282	0.00335	31.15
0.4080	1.49445	0.00324	33.25
0.5063	1.49562	0.00290	35.29
0.5513	1.49604	0.00268	36.23
0.6031	1.49646	0.00241	37.31
0.7053	1.49726	0.00195	39.46

Table 5.8 continued

0.8045	1.49776	0.00133	41.53
0.8441	1.49790	0.00107	42.36
0.9020	1.49808	0.00066	43.57
1.0000	1.49833	0.00000	45.61
		T = 308.15 K	
0.0000	1.48035	0.00000	24.95
0.0572	1.48362	0.00165	26.08
0.1058	1.48596	0.00273	27.07
0.1534	1.48745	0.00306	28.03
0.2087	1.48897	0.00333	29.15
0.3068	1.49117	0.00352	31.17
0.4080	1.49289	0.00341	33.26
0.5063	1.49409	0.00304	35.31
0.5513	1.49452	0.00280	36.25
0.6031	1.49494	0.00249	37.33
0.7053	1.49575	0.00198	39.47
0.8045	1.49629	0.00136	41.55
0.8441	1.49645	0.00108	42.38
0.9020	1.49664	0.00067	43.59
1.0000	1.49693	0.00000	45.63
		T = 313.15 K	
0.0000	1.47815	0.00000	24.96
0.0572	1.48161	0.00177	26.09
0.1058	1.48402	0.00286	27.08
0.1534	1.48560	0.00323	28.04
0.2087	1.48717	0.00348	29.16
0.3068	1.48949	0.00371	31.18
0.4080	1.49129	0.00359	33.28
0.5063	1.49256	0.00320	35.33
0.5513	1.49303	0.00297	36.26
0.6031	1.49347	0.00265	37.35
0.7053	1.49429	0.00209	39.49

Table 5.8 continued

0.8045	1.49483	0.00141	41.56
0.8441	1.49500	0.00112	42.39
0.9020	1.49521	0.00070	43.60
1.0000	1.49551	0.00000	45.65
		T = 318.15 K	
0.0000	1.47596	0.00000	24.97
0.0572	1.47956	0.00184	26.10
0.1058	1.48218	0.00307	27.09
0.1534	1.48374	0.00336	28.04
0.2087	1.48539	0.00365	29.17
0.3068	1.48773	0.00379	31.18
0.4080	1.48963	0.00368	33.29
0.5063	1.49097	0.00329	35.34
0.5513	1.49147	0.00306	36.28
0.6031	1.49195	0.00274	37.36
0.7053	1.49284	0.00218	39.51
0.8045	1.49339	0.00146	41.58
0.8441	1.49359	0.00118	42.41
0.9020	1.49382	0.00074	43.62
1.0000	1.49413	0.00000	45.67

Standard uncertainties u are $u(T)$ = ±0.01 K and the combined expanded uncertainty Uc in refractive index measurements were less than $U_c(n)$= 5 x 10^{-5} , respectively (0.95 level of confidence)

The graphs of excess molar volume versus mole fraction for all the binary systems studied at T = (298.15, 303.15, 308.15, 313.15 and 318.15) K are presented in Figures 5.1 to 5.4.

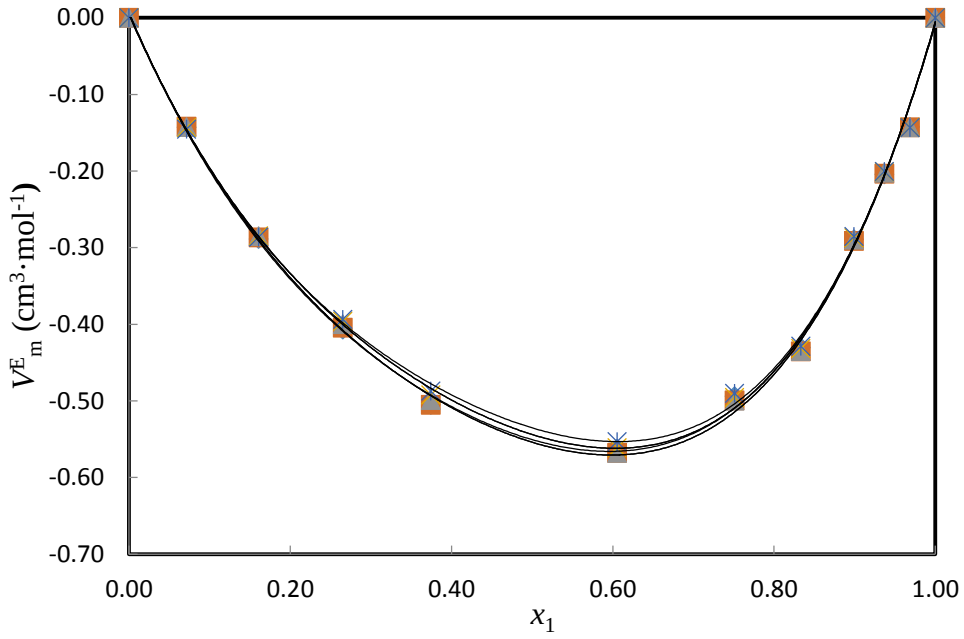

Figure 5.1 Plot of excess molar volumes, V_m^E, of the binary mixture of {methanol (x_1) + furfural (x_2)} against mole fraction x_1 of methanol at T = 298.15 K;◊, T = 303.15 K;□ , T = 308.15 K;Δ , T = 313.15 K; X and , ∗ T = 318.15 K. The solid lines were generated using the Redlich-Kister smoothing polynomial.

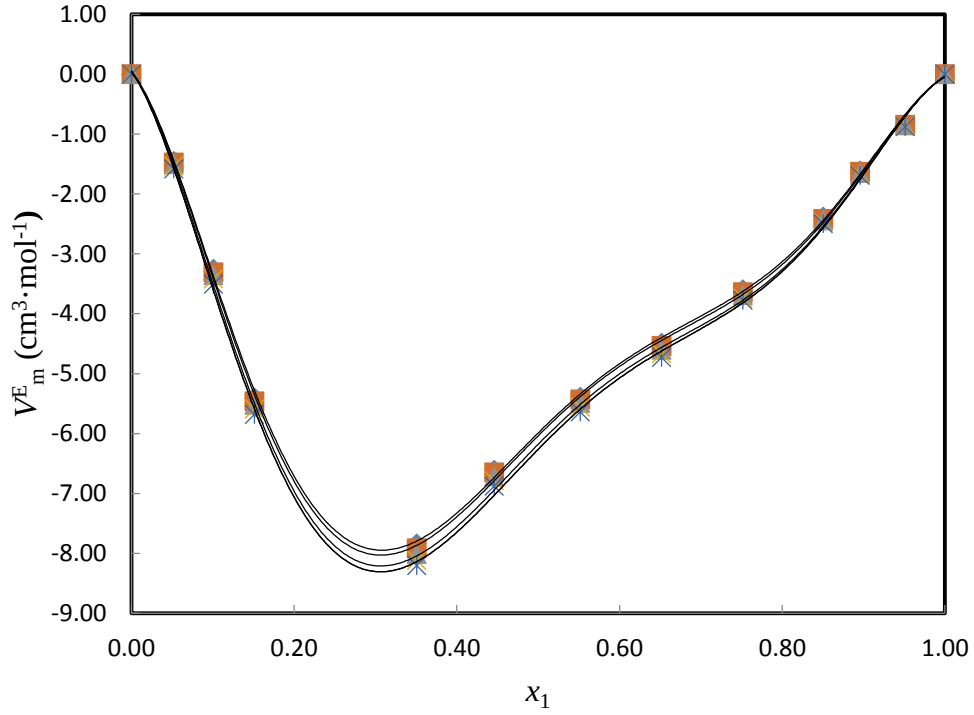

Figure 5.2 Plot of excess molar volumes, V^E_m, of the binary mixture of {[EMIM][OAc] (x_1) + furfural (x_2)} against mole fraction x_1 of [EMIM][OAc] at T = 298.15 K;◊, T = 303.15 K;□ , T = 308.15 K;Δ , T = 313.15 K; X and , ∗ T = 318.15 K. The solid lines were generated using the Redlich-Kister smoothing polynomial.

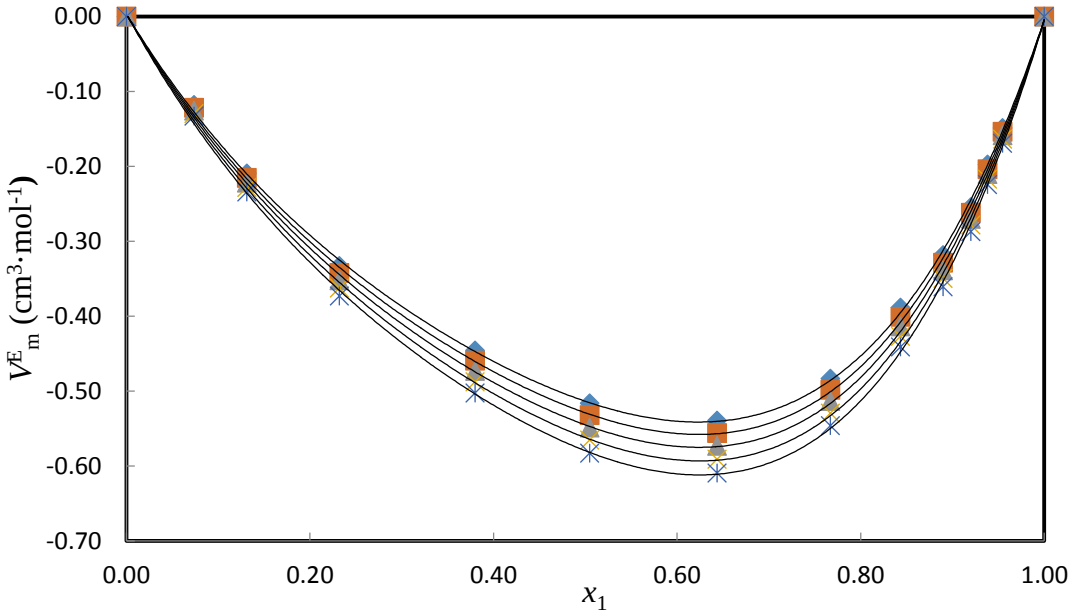

Figure 5.3 Plot of excess molar volumes, V_m^E, of the binary mixture of {methanol (x_1) + furfuryl alcohol (x_2)} against mole fraction x_1 of methanol at T = 298.15 K;◊, T = 303.15 K;□ , T = 308.15 K;Δ , T = 313.15 K; X and , ∗ T = 318.15 K. The solid lines were generated using the Redlich-Kister smoothing polynomial.

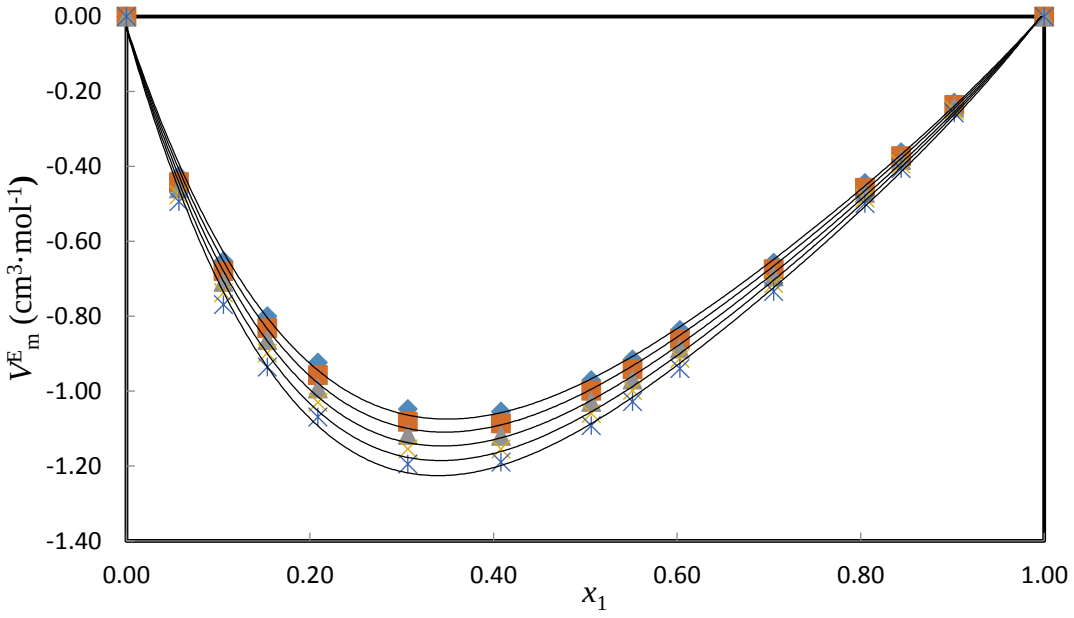

Figure 5.4 Plot of excess molar volumes, V_m^E, of the binary mixture of {[EMIM][OAc] (x_1) + furfuryl alcohol (x_2)} against mole fraction x_1 of [EMIM][OAc] at T = 298.15 K;◊, T = 303.15 K;□ , T = 308.15 K;Δ , T = 313.15 K; X and , ∗ T = 318.15 K. The solid lines were generated using the Redlich-Kister smoothing polynomial.

The graphs of isentropic compressibility versus mole fraction for all the binary systems studied at T = (298.15, 303.15, 308.15, 313.15 and 318.15) K are presented in Figures 5.5 to 5.8.

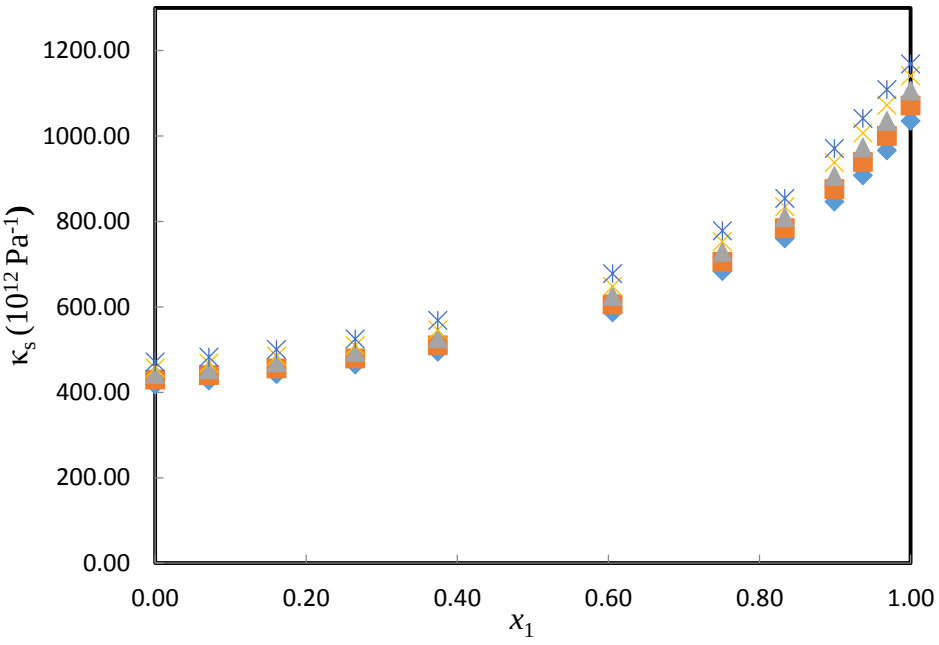

Figure 5.5 Plot of isentropic compressibility, κ_s, of the binary mixture of {methanol (x_1) + furfural (x_2)} against mole fraction x_1 of methanol at T = 298.15 K;◊, T = 303.15 K;□ , T = 308.15 K;Δ , T = 313.15 K; X and , ∗ T = 318.15 K.

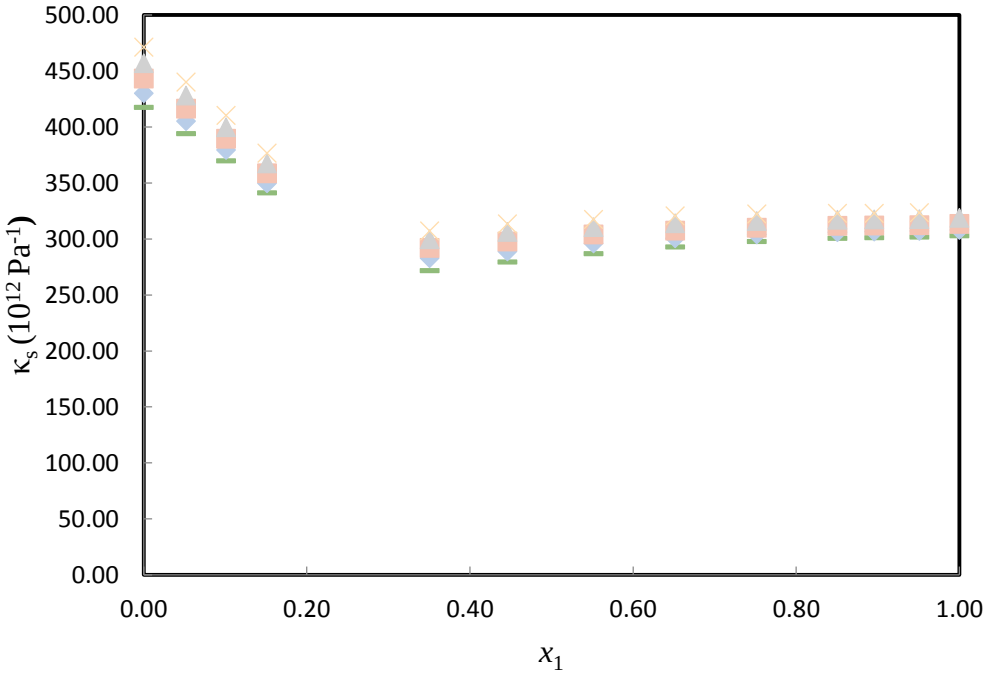

Figure 5.6 Plot of isentropic compressibility, κ_s, of the binary mixture of {[EMIM][OAc] (x_1) + furfural (x_2)} against mole fraction x_1 of [EMIM][OAc] at T = 298.15 K;◊, T = 303.15 K;□ , T = 308.15 K;Δ , T = 313.15 K; X and , ∗ T = 318.15 K.

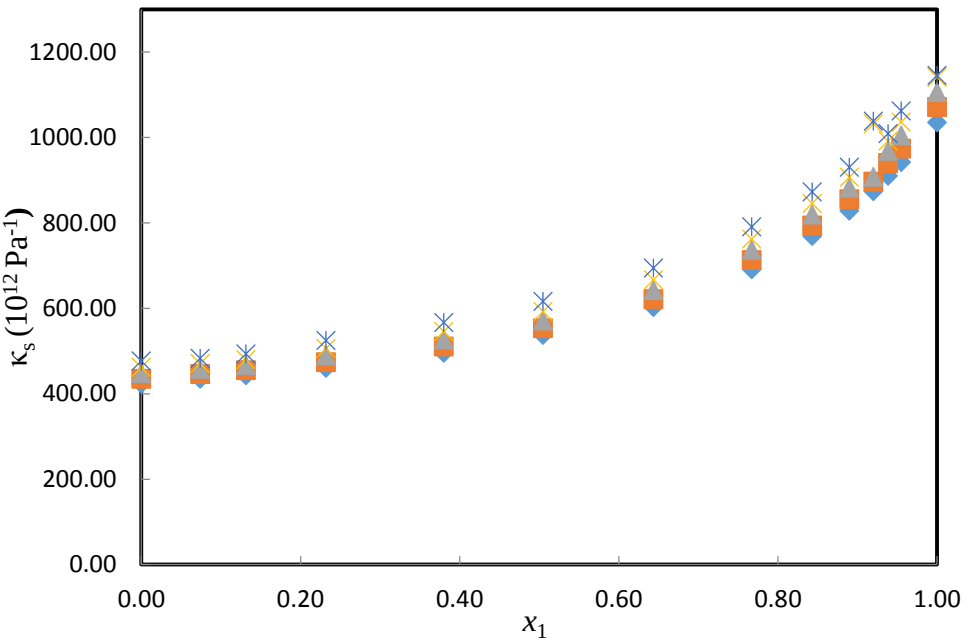

Figure 5.7 Plot of isentropic compressibility, κ_s, of the binary mixture of {methanol (x_1) + furfuryl alcohol (x_2)} against mole fraction x_1 of methanol at T = 298.15 K;◊, T = 303.15 K;□ , T = 308.15 K;Δ , T = 313.15 K; X and , ∗ T = 318.15 K.

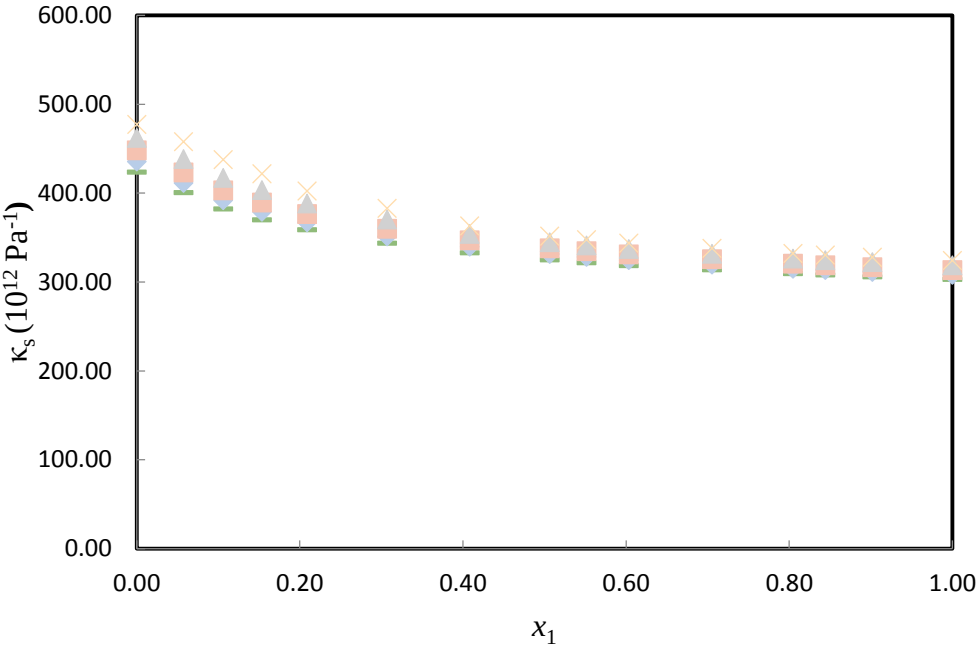

Figure 5.8 Plot of isentropic compressibility, κ_s , of the binary mixture of {[EMIM][OAc] (x_1) + furfuryl alcohol (x_2)} against mole fraction x_1 of [EMIM][OAc] at T = 298.15 K;◊, T = 303.15 K;□ , T = 308.15 K;△ , T = 313.15 K; X and , ∗ T = 318.15 K.

The graphs of deviation in refractive index versus mole fraction for all the binary systems studied at T = (298.15, 303.15, 308.15, 313.15 and 318.15) K are presented in Figure 5.9 to 5.12.

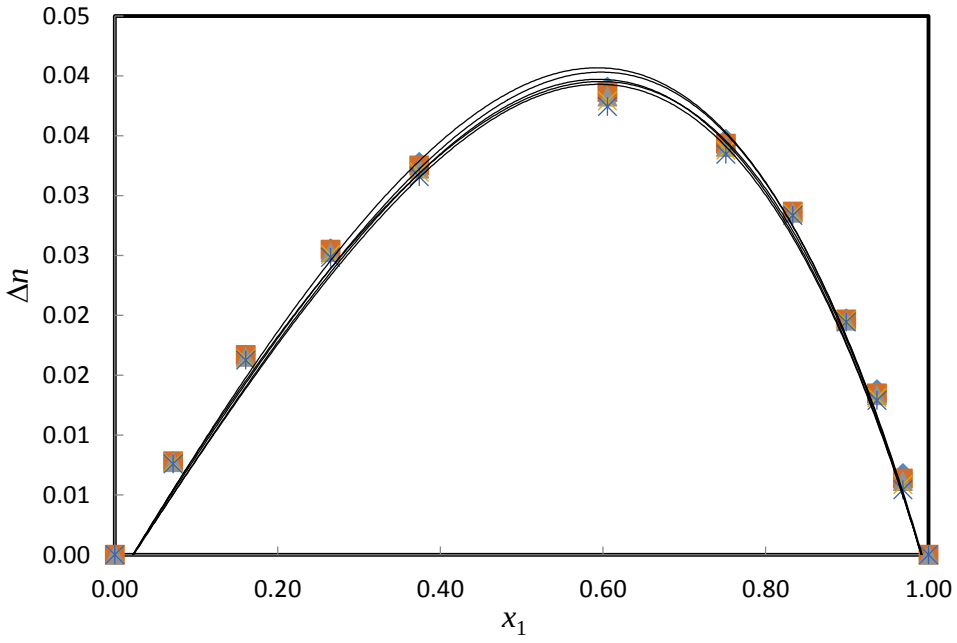

Figure 5.9 Plot of deviation in refractive index, Δn, of the binary mixture of {methanol (x_1) + furfural (x_2)} against mole fraction x_1 of methanol at T = 298.15 K;◊, T = 303.15 K;□ , T = 308.15 K;Δ , T = 313.15 K; X and , ∗ T = 318.15 K. The solid lines were generated using the Redlich-Kister smoothing polynomial.

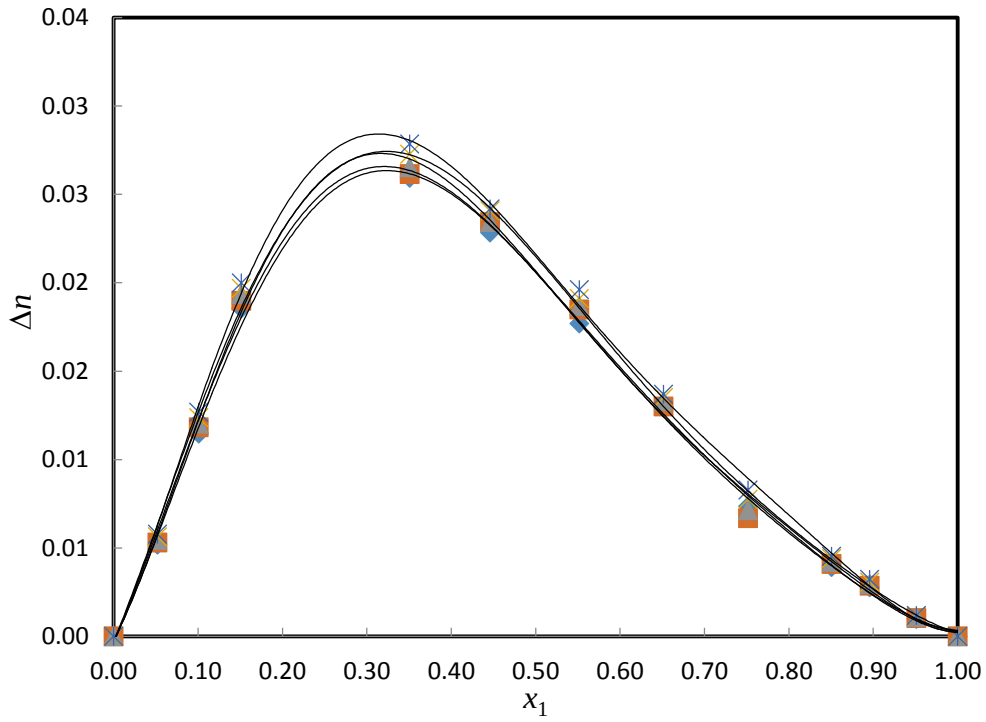

Figure 5.10 Plot of deviation in refractive index, Δn, of the binary mixture of {[EMIM][OAc] (x_1) + furfural (x_2)} against mole fraction x_1 of [EMIM][OAc] at T = 298.15 K;◊, T = 303.15 K;□ , T = 308.15 K;Δ , T = 313.15 K; X and , ∗ T = 318.15 K. The solid lines were generated using the Redlich-Kister smoothing polynomial.

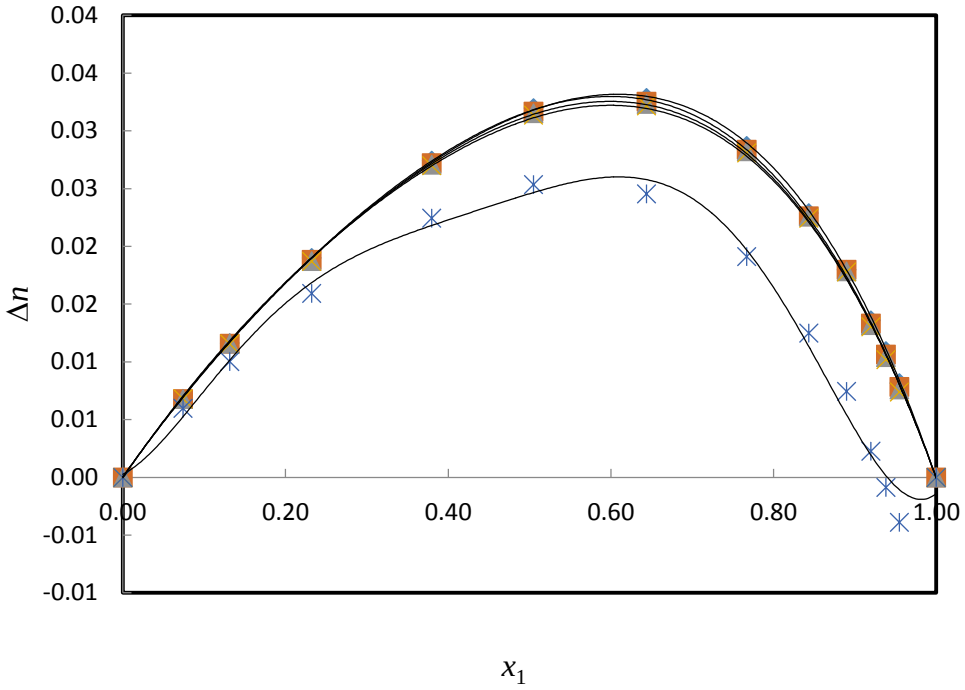

Figure 5.11 Plot of deviation in refractive index, Δn, of the binary mixture of {methanol (x_1) + furfuryl alcohol (x_2)} against mole fraction x_1 of methanol at T = 298.15 K;◊, T = 303.15 K;□ , T = 308.15 K;Δ , T = 313.15 K; X and , ✳ T = 318.15 K. The solid lines were generated using the Redlich-Kister smoothing polynomial.

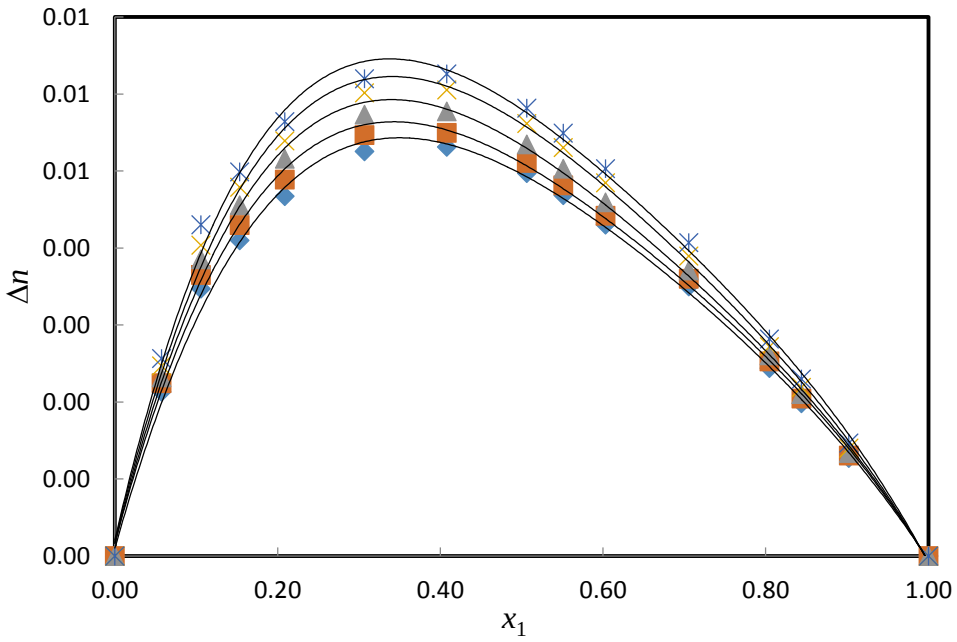

Figure 5.12 Plot of deviation in refractive index, Δn, of the binary mixture of {[EMIM][OAc] (x_1) + furfuryl alcohol (x_2)} against mole fraction x_1 of [EMIM][OAc] at T = 298.15 K;◊, T = 303.15 K;□ , T = 308.15 K;Δ , T = 313.15 K; X and , ∗ T = 318.15 K. The solid lines were generated using the Redlich-Kister smoothing polynomial.

The Redlich- Kister fitting parameters were calculated from equation (3.12):

$$Z = x_1 x_2 \sum_{i=0}^{N} A_i (2x-1)^i , \tag{3.12}$$

where Z is the V_m^E or Δn; x_1 is the mole fraction of the methanol, or [EMIM][OAc] ; x_2 is the mole fraction of furfural or furfuryl alcohol; N is the degree of the polynomial expansion; and A_i is the Redlich–Kister parameters obtained for the system.

and the root mean square deviation was calculated from equation (3.13)

$$\sigma = \left(\frac{\sum_{i}^{n} (Z_{\text{exp}} - Z_{cal})}{n-k} \right)^{1/2} \tag{3.13}$$

where Z_{exp}, Z_{cal}, are the values of the experimental and calculated V_m^E or Δn and n is the number of experimental data points and k is the number of coefficients used in the Redlich-Kister correlation, respectively.

The Redlich-Kister parameters and the root mean square deviation for all binary systems are given in Table 5.9.

Table 5.9 Redlich- Kister fitting parameters and root-mean-square deviation, σ, for the binary mixtures at T = (298.15, 303.15, 308.15, 313.15 and 318.15) K.

	T/K	A_0	A_1	A_2	A_3	A_4	A_5	σ
				{methanol (x_1) + furfural (x_2)}				
V_m^E/(cm^3·mol^{-1})	298.15	-2.204	0.430	-0.818	0.529			0.013
	303.15	-2.217	0.487	-0.802	0.470			0.013
	308.15	-2.204	0.538	-0.809	0.376			0.014
	313.15	-2.175	0.541	-0.847	0.342			0.014
	318.15	-2.142	0.521	-0.904	0.336			0.014
Δn	298.15	0.151	-0.052	0.029	-0.016			0.00023
	303.15	0.150	-0.052	0.030	-0.014			0.00039
	308.15	0.149	-0.052	0.030	-0.013			0.00046
	313.15	0.147	-0.052	0.030	-0.012			0.00055
	318.15	0.146	-0.052	0.030	-0.010			0.00069
				{[EMIM][OAc] (x_1) + furfural (x_2)}				
V_m^E (cm^3·mol^{-1})	298.15	-23.933	-24.974	-37.356	7.155	49.88	20.585	0.083
	303.15	-24.119	-25.135	-38.338	6.985	50.869	20.734	0.086
	308.15	-24.387	-25.400	-38.887	7.293	51.477	20.467	0.090
	313.15	-24.687	-25.581	-39.246	7.062	51.752	20.637	0.092
	318.15	-25.023	-25.752	-39.339	6.409	51.409	21.033	0.089
Δn	298.15	0.081	0.095	0.056	0.028	-0.095	-0.119	0.00032
	303.15	0.084	0.097	0.038	0.041	-0.066	-0.137	0.00050
	308.15	0.084	0.096	0.048	0.047	-0.079	-0.143	0.00045
	313.15	0.086	0.100	0.052	0.029	-0.085	-0.124	0.00035
	318.15	0.087	0.101	0.059	0.027	-0.093	-0.120	0.00034

Table 5.9 continued

		{methanol (x_1) + furfuryl alcohol (x_2)}						
V_m^E/(cm^3·mol^{-1})	298.15	-2.055	0.740	-0.750	0.252			0.005
	303.15	-2.118	0.767	-0.774	0.256			0.005
	308.15	-2.182	0.795	-0.798	0.262			0.005
	313.15	-2.249	0.823	-0.824	0.270			0.005
	318.15	-2.319	0.850	-0.845	0.289			0.005
Δn	298.15	0.127	-0.05	0.023	-0.0016			0.00011
	303.15	0.126	-0.05	0.022	-0.0006			0.00021
	308.15	0.126	-0.051	0.022	-0.0032			0.00026
	313.15	0.125	-0.051	0.021	-0.0055			0.00031
	318.15	0.106	-0.054	-0.050	0.1330			0.00021
		{[EMIM] [OAc] (x_1) + furfuryl alcohol (x_2)}						
V_m^E/(cm^3·mol^{-1})	298.15	-3.931	-2.282	-0.512	0.602	-1.268	-2.101	0.004
	303.15	-4.044	-2.356	-0.587	0.463	-1.304	-2.013	0.004
	308.15	-4.163	-2.431	-0.661	0.333	-1.356	-1.953	0.004
	313.15	-4.287	-2.519	-0.745	0.210	-1.395	-1.886	0.004
	318.15	-4.415	-2.598	-0.853	0.0044	-1.417	-1.732	0.004
Δn	298.15	0.02	0.0099	0.0043	-0.0001	0.0062	0.0092	0.00005
	303.15	0.021	0.011	0.0056	-0.0012	0.0053	0.011	0.00005
	308.15	0.021	0.011	0.0057	0.0011	0.0059	0.0081	0.00006
	313.15	0.023	0.012	0.0051	0.0018	0.0076	0.0085	0.00006
	318.15	0.023	0.012	0.0059	0.0049	0.0081	0.0060	0.00008

Standard uncertainties u are $u(T)$ = ±0.01 K and the combined expanded uncertainty Uc in density and refractive index measurements were less than $U_c(\rho)$ = ± 5 x 10^{-5} g ·cm^{-3} and $U_c(n)$= 5 x 10^{-5} , respectively (0.95 level of confidence)

5.2. CORRELATIONS AND PREDICTIONS

The Lorentz–Lorenz equation (5.5) was used for predicting the density ρ , which is related to the refractive index *n*, by:

$$\rho = \frac{\left(\frac{n^2-1}{n^2+2}\right)\left(x_1 M_1 + x_2 M_2\right)}{\left(\frac{n_1^2-1}{n_1^2+2}\right)x_1\frac{M_1}{\rho_1} + x_2\left(\frac{n_2^2-1}{n_2^2+2}\right)\frac{M_2}{\rho_2}} \tag{5.5}$$

By using equation (5.6), *n* can be calculated from pure component density and refractive index data and from the experimental density of the mixture. The equation for *n* is given below:

$$n = \left(\frac{2\left[\left(\frac{n_1^2-1}{n_2^2-1}+\right)x_1\rho\frac{M_1}{M_1} + x_2\left(\frac{n_1^2-1}{n_2^2-1}+\right)\rho\frac{M_2}{M_2}\right] + \left[x_1 M_1 + x_2 M_2\right]}{\left[x_1 M_1 + x_2 M_2\right] - \left[\left(\frac{n_1^2-1}{n_2^2-1}+\right)x_1\rho\frac{M_1}{\rho_1} + x_2\left(\frac{n_1^2-1}{n_2^2-1}+\right)\rho\frac{M_2}{\rho_2}\right]} \right)^{1/2} \tag{5.6}$$

Table 5.10. lists the root mean square deviation, σ for excess molar volume, density and refractive index for the binary mixtures at *T* = (298.15, 303.15, 308.15, 313.15 and 318.15) K obtained by using the Lorentz-Lorenz equations.

Table 5.10 Root mean square deviation, σ, obtained from the Lorentz-Lorenz equation, for V_m^E, ρ and n for the binary mixtures at T = (298.15, 303.15, 308.15, 313.15 and 318.15) K.

	σ				
Properties	T/K				
	298.15	303.15	308.15	313.15	318.15
	{methanol (x_1) + furfural (x_2)}				
V_m^E/(cm^3·mol^{-1})	0.008	0.011	0.013	0.012	0.018
ρ/(g·cm^{-3})	0.00235	0.00226	0.00221	0.00219	0.00208
n	0.00194	0.00190	0.00189	0.00192	0.00189
	{[EMIM][OAc] (x_1) + furfural (x_2)}				
V_m^E/(cm^3·mol^{-1})	0.963	0.974	0.982	0.974	0.981
ρ/(g·cm^{-3})	-0.01008	-0.0101	-0.01011	-0.00998	-0.01000
n	0.0086	0.00884	0.00884	0.00871	0.00872
	{methanol (x_1) + furfuryl alcohol (x_2)}				
V_m^E/(cm^3·mol^{-1})	0.048	0.065	0.074	0.081	0.609
ρ/(g·cm^{-3})	0.00118	0.00089	0.00073	0.00060	-0.00890
n	0.00082	0.00067	0.00061	0.00058	0.00670
	{[EMIM][OAc] (x_1) + furfuryl alcohol(x_2)}				
V_m^E/(cm^3·mol^{-1})	0.228	0.233	0.234	0.230	0.233
ρ/(g·cm^{-3})	-0.00225	-0.00228	-0.00226	-0.00222	-0.00223
n	0.00149	0.00151	0.00149	0.00146	0.00148

Standard uncertainties u are $u(T)$ = ±0.01 K and the combined expanded uncertainty Uc in density and refractive index measurements were less than $U_c(\rho)$ = ± 5 x 10^{-5} g ·cm^{-3}, and $U_c(n)$= 5 x10^{-5} , respectively (0.95 level of confidence)

CHAPTER **6**

DISCUSSION

6.1. DENSITY

6.1.1. EFFECT OF TEMPERATURE ON DENSITY

The experimental density data, ρ, for the binary mixtures (methanol or [EMIM][OAc] + furfural or furfuryl alcohol) was measured at T = (298.15, 303.15, 308.15, 313.15 and 318.15) K over the entire mole fraction range and at different temperatures are listed in Tables 5.1-5.4. The density for all binary mixtures decreases slightly with an increase in temperature.

6.1.2. EFFECT OF COMPOSITION ON DENSITY

The measured densities for all binary mixtures against mole fraction, x_1 at several temperatures are plotted in Figure 6.1-6.4 below.

Methanol + furfural or furfuryl alcohol

The experimental density data for the binary systems {methanol (x_1) + furfural or furfuryl alcohol (x_2)} decreases with increasing mole fraction of methanol and increases with an increase in the concentration of furfural or furfuryl for both binary systems.

[EMIM][OAc] + furfural or furfuryl alcohol

In the binary mixtures {[EMIM][OAc] (x_1) + furfural (x_2)} at mole fractions between x_1= 0.05 to x_1= 0.55 and x_1= 0.05 to x_1= 0.2 for {[EMIM][OAc] (x_1) + furfuryl alcohol (x_2)} a sudden

increase in density is seen which thereafter decreases as the composition increases. These observations are consistent with the experimental measurements of Anantharaj and Banerjee (2012; 2011) which reported the experimental the density for the binary systems ([EMIM][OAc] + quinoline or thiophene or water) at (298.15 to 323.15) K, [EMIM][$EtSO_4$] + quinoline at (298.15 to 323.15) K and ([EMIM][SCN] + thiophene at (298.15 to 323.15) K. This is also consistent with the measurements of Quijada-Maldonado *et al.* (2012) which reported the densities of the binary mixture ([EMIMI][OAc] + water) at (298.15 to 323.15) K. This sudden increase in density at initial mole fraction is due to the fact that at individual concentration (higher dilution rate), the oxygen sites are stabilized by electron or partial charge transfer (Anantharaj and Banerjee 2012). Thus [EMIM][OAc] has strong attraction with furfural or furfuryl alcohol at low concentrations. These results show that the ratio of IL and aromatic/non aromatic structure of molecules is important for the effective removal of such compounds using [EMIM][OAc].

The ionic liquid, [EMIM][OAc] can interact with aromatic or nonaromatic structure compounds by (1) CH–π interaction, (2) π–π interaction, and (3) n–π interaction, where n = N, O, F, and S atoms are located on the aromatic/nonaromatic compound or ionic liquid structure (Anantharaj and Banerjee 2011).

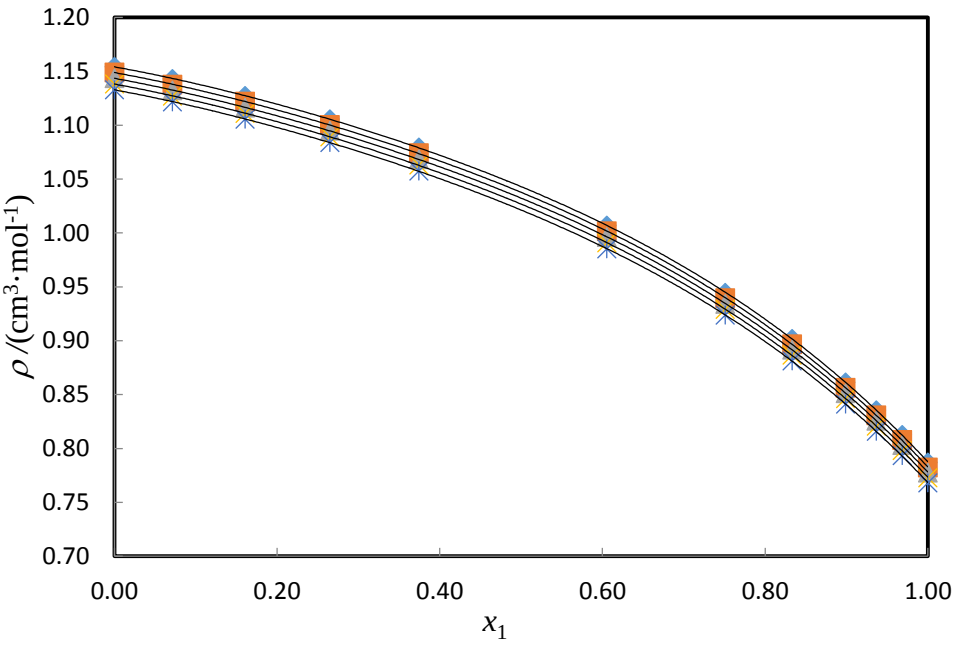

Figure 6.1 Experimental density, ρ, of the binary mixture {methanol (x_1) + furfural (x_2)} against mole fraction x_1 of methanol at 298.15 K;◊, T = 303.15 K;□ , T = 308.15 K;Δ , T = 313.15 K; × and , ∗, T = 318.15 K.

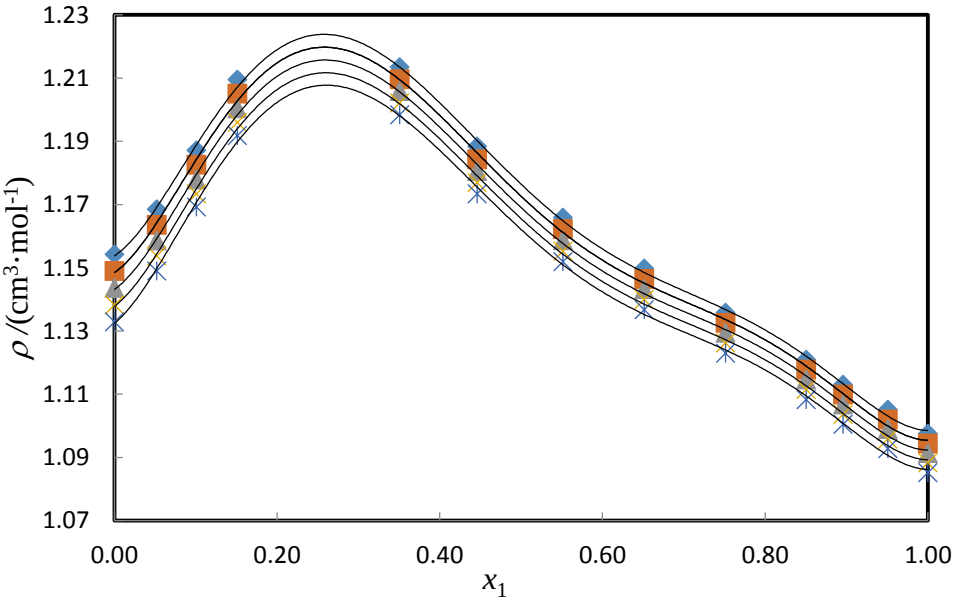

Figure 6.2 Experimental density, ρ , of the binary mixture {[EMIM][OAc] (x_1) + furfural (x_2)} against mole fraction x_1 of [EMIM][OAc] at 298.15 K;◊, T = 303.15 K;□ , T = 308.15 K;Δ , T = 313.15 K; × and , ∗, T = 318.15 K.

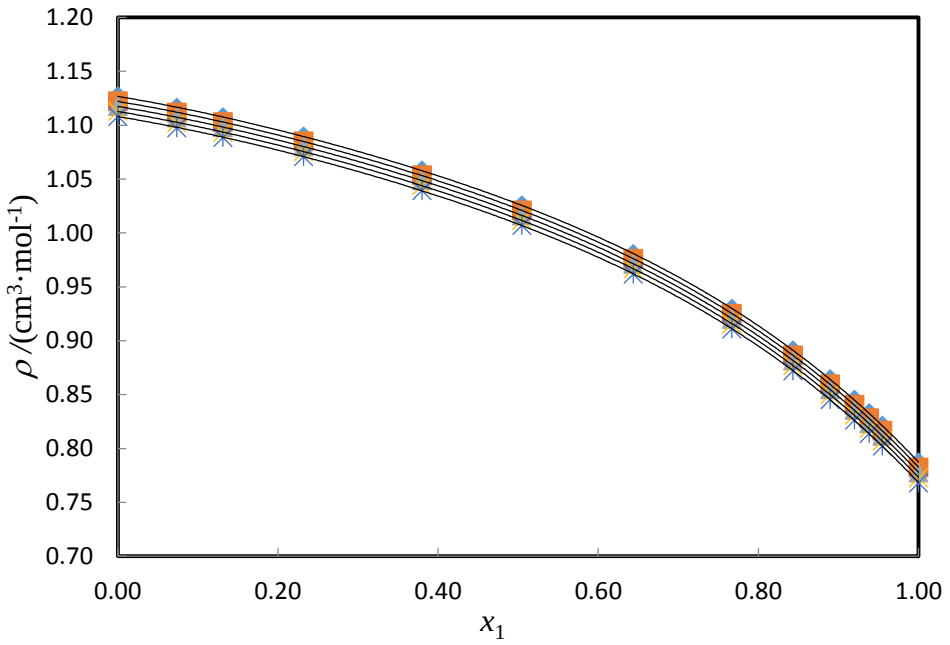

Figure 6.3 Experimental density, ρ, of the binary mixture {methanol (x_1) + furfuryl alcohol (x_2)} against mole fraction x_1 of methanol at 298.15 K;◊, T = 303.15 K;□ , T = 308.15 K;Δ , T = 313.15 K; × and , ∗, T = 318.15 K.

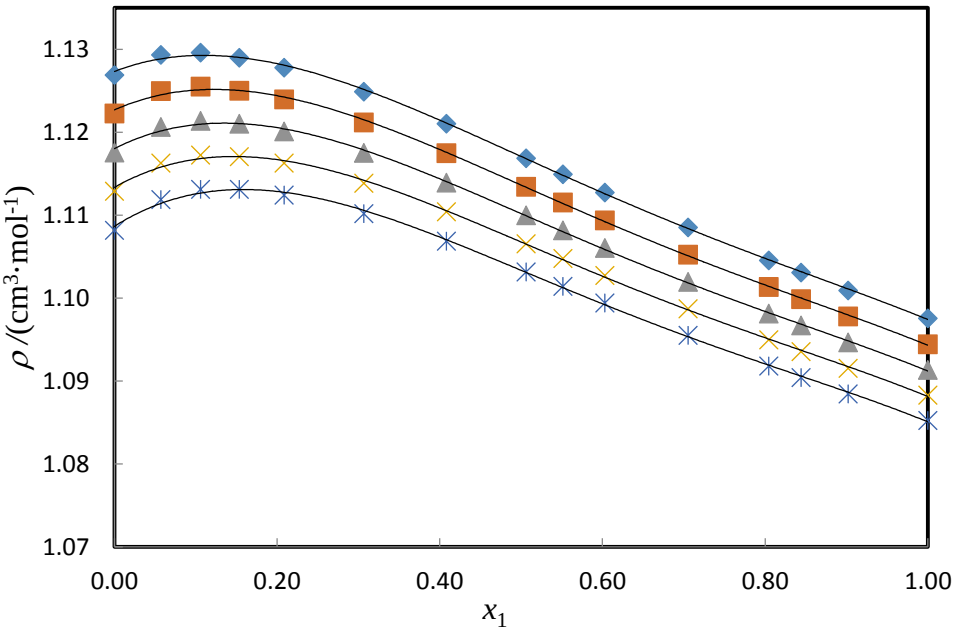

Figure 6.4 Experimental density, ρ, of the binary mixture {[EMIM][OAc] (x_1) + furfuryl alcohol (x_2)} against mole fraction x_1 of [EMIM][OAc] at 298.15 K;◊, T = 303.15 K;□ , T = 308.15 K;Δ , T = 313.15 K; × and , ∗, T = 318.15 K.

6.1.3. PREDICTION OF DENSITY BY LORENTZ-LORENZ (L-L) APPROXIMATION

The Lorentz–Lorenz equation was used for predicting the density, which is related to the refractive index *n*, by:

$$\rho = \frac{\left(\frac{n^2-1}{n^2+2}\right)\left(x_1 M_1 + x_2 M_2\right)}{\left(\frac{n_1^2-1}{n_1^2+2}\right)x_1\frac{M_1}{\rho_1} + \mathrm{x}_2\left(\frac{n_2^2-1}{n_2^2+2}\right)\frac{M_2}{\rho_2}}$$

The density values obtained/predicted for the Lorentz-Lorentz equation are given in Table 5.10. The Lorentz–Lorentz equation gives a better correlation for the density for the system (methanol + furfuryl alcohol) and a poor correlation for the binary system ([EMIM][OAC]+ furfural).

6.2. EXCESS MOLAR VOLUME

The excess molar volume, V_m^E, depends mainly on two factors (i) variation in intermolecular forces between two components in contact and (ii) variation in molecular packing as a consequence of differences in size and shape of molecules (Anouti 2010). The excess molar volume, V_m^E, for all systems studied in this work are negative. According to the literature, the excess molar volumes are the result of several opposing effects. It is known that interactions between like molecules lead to increased V_m^E values, while negative contributions to V_m^E arise from interactions between unlike molecules such as ion-dipole and hydrogen bonding, or structural effects such as packing (Govinda et al. 2011;Kurnia et al. 2012; Jacquemin et al. 2011; Chen 2014). Therefore, if the interactions or packing efficiency between unlike molecules in the binary system is higher than those between like molecules, V_m^E values will be negative, i.e. there is stronger attraction/ intermolecular interaction between the unlike molecules.

Excess parameters associated with a liquid mixture are a quantitative measure of deviation in the behavior of the liquid mixture from ideality. These functions are found to be sensitive towards the intermolecular forces and also on the difference in size and shape of the molecules. Excess volumes of liquid mixtures reflect the result of different contributions arising from structural changes undergone by the pure cosolvent (Shah *et al.* 2013).

The temperature effect on excess molar volumes, V_m^E, of the mixtures is very important, which can be used to investigate the microstructures of the system. In general, specific interactions in mixtures, typically hydrogen bonding, decreases as the temperature increases, while the dependence on temperature of the non-specific interactions is smaller and can usually be neglected (Qian 2012; Anouti 2010). Therefore, as the temperature increases, the V_m^E

values of the mixtures will be less negative due to reduced hydrogen bonding in the mixtures (Anouti 2010). In the second place, the kinetic energy of two components also increases with the temperature increasing, which leads to reduced interactions of the pure components and results in much greater packing efficiency between the two components, so contraction in volume increases, and $V_{\mathrm{m}}^{\mathrm{E}}$ values will be more negative (Zhong, 2007). In other words, with the increase of temperature, hydrogen bonding interaction in the mixtures weakens between two components and the packing efficiency strengthens. Therefore, the variation of $V_{\mathrm{m}}^{\mathrm{E}}$ values with temperature is a result of the competition between the hydrogen bonding interaction and packing efficiency in all the binary mixtures with temperature, it may be deduced that the hydrogen bonding interactions are more dominated than the packing efficiency, which lead to the $V_{\mathrm{m}}^{\mathrm{E}}$ values of the system becoming less negative with increasing temperature (Jacquemin 2011; Chen 2014).

In the pure state, the molecules of furfural are associated through dipole-dipole interactions (Shapiroan 1971; Kulnevicahnd *et al.* 1972). Also, the unusually higher viscosity value of furfuryl alcohol (4.63 cPs at T = 298.15 K) is indicative of the fact that the molecules of furfuryl alcohol, like aliphatic alcohols, are self-associated through hydrogen bonding in the pure state. The addition of a liquid to furfural (1.49 cPs) or furfuryl alcohol would, therefore, tend to break the molecular aggregates in pure furfural or furfuryl alcohol (Naorem and Suri 1989). The negative $V_{\mathrm{m}}^{\mathrm{E}}$ values for the binary system suggest that the unlike dipolar interactions are stronger and predominant over the structure breaking effects in the mixtures (Radojkovic *et al.* 1977; Homer *et al.* 1973; Grolier *et al.* 1975).

6.2.1. METHANOL (x_1) OR [EMIM][OAc] (x_1) + FURFURAL (x_2)

Figure 5.1 shows that the excess molar volume for the binary mixture {methanol (x_1) + furfural (x_2)} are negative throughout the temperature and composition range, which indicates that a more efficient packing and/or attractive interaction occurred between methanol and furfural. According to literature (Naorem *et al.* 1989), the negative excess volume indicates that the volumetric effects arising from the unlike interactions between furfural and methanol supersedes the positive contribution to V_m^E the latter due to the structure breaking of the polymer aggregates of methanol. There is hydrogen bonding between the hydroxyl group of the alcohol and the hydrogen acceptor oxygen of furfural but the packing effect dominates resulting in negative V_m^E values (Naorem *et al.* 1989). The V_m^E first shows a small decrease with temperature from (T = 298 to 303) K and then a small increase with temperature at (T =308 to 318) K. The $V^E_{m.min}$ occurred at x_1 = 0.6054 at all temperatures. Our $V^E_{m.min}$ value for the binary mixture {methanol (x_1) + furfural (x_2)} at T = 308.15 K is smaller than that reported by Naorem *et al.* (1989), the difference being ± 0.358 $cm^3 \cdot mol^{-1}$. Possible reasons being that in this work, (i) an Anton Paar DSA 5000 M digital vibrating tube densimeter was used, which gives higher accuracy whereas Naorem *et al.* (1989) used a vibrating tube flow densimeter (Model DMA 601602 Anton Paar, Austria), (ii) the period of oscillation is used to calculate the density and (iii) a water bath was used to control the temperature for the Naorem *et al.* (1989). The $V^E_{m.min}$ obtained from the literature for the binary mixture (methanol + furfural) at T = 308.15 K is ± -0.21$cm^3 \cdot mol^{-1}$. In this work it was -0.568 $cm^3 \cdot mol^{-1}$ at T = 308.15 K. The graph of excess molar volume versus mole fraction for the binary system (methanol + furfural) by Naorem *et al.* (1989) is shown in Figure 6.1.

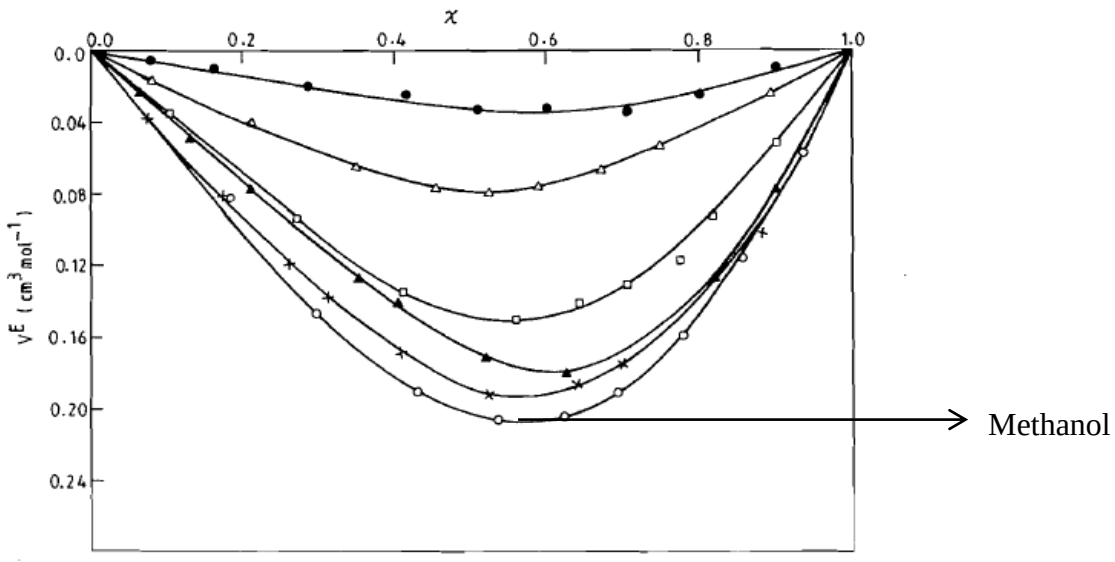

Figure 6.5 Excess molar volume, V_m^E, at 308.15K for the binary mixtures of furfural with (O) methanol, (×) ethanol, (▲) 1-propanol, (Δ,) 2-propanol, (□) 1-butanol, and (●) 2-butanol. (Naorem *et al.* 1989)

The excess molar volume for the binary mixture {[EMIM][OAc] (x_1) + furfural (x_2)} is shown in Figure 5.2. The negative excess molar volumes indicated that a more efficient packing and/or attractive interaction occurred when the IL and furfural were mixed. Figure 5.2 shows asymmetrical curves for the excess molar volume, which are quite common in mixtures containing two components with a large molar volume difference, as is indeed the case in this work. $V^E_{m.min}$ is skewed to low mole fractions of the alcohol meaning that the greatest intermolecular interaction occurred at low mole fractions of methanol, probably, due to better packing effects.

6.2.2. METHANOL (x_1) OR [EMIM][OAc] (x_1) + FURFURYL ALCOHOL (x_2)

The excess molar volumes for both these binary systems are negative over the entire composition range which indicates that a more efficient packing and /or attractive interaction occurred when the ionic liquid or, methanol and furfuryl alcohol were mixed.

Figure 5.3 shows the excess molar volume for the binary system (methanol + furfuryl alcohol). The curve is slightly skewed towards the furfural rich region, since methanol has a smaller molar volume. The excess molar volumes become more negative as the temperature increases because the kinetic energy of molecules also increases with temperature, which leads to a greater interaction of the molecules (Zhong and Wang 2007).

Figure. 5.4 shows, the values of excess molar volume for the mixtures ([EMIM][OAc] + furfuryl alcohol) which are more negative than those for the mixtures of (methanol + furfuryl alcohol), due to the size of the ionic liquid. This fact suggests that the chemical structure of the anion plays an important role on the value of the excess properties, and therefore on the thermodynamic behaviour of the studied systems (González *et al.* 2012).

For the binary system ([EMIM][OAc] + furfuryl alcohol), the obtained curve is asymmetric, with the minima in the alcohol rich-region. This can be attributed partly to the greater difference in the molar volume of the ionic liquid and the alcohol, since furfuryl alcohol has a smaller molar volume, changes in V_m^E is more pronounced and also due to the specific interactions between highly associated (H-bonding) molecules of the alcohol and the IL ion $[OAc]^-$ (Bhujrajh and Deenadayalu 2006; Abareshi *et al.* 2009). Furthermore, it is known that in several binary mixtures containing ionic liquids the locus of maxima/minima in V_m^E against composition is also away from the equimolar composition (Anouti *et al.* 2010).

6.3. ISENTROPIC COMPRESSIBILITY

The results of the speed of sound, *u*, and isentropic compressibility, κ_s, for the binary systems (methanol, or [EMIM][OAc] + furfural or furfuryl alcohol) at various temperatures are presented in Tables 5.1- 5.4.

The speed of sound of the binary mixtures decrease with an increase in temperature for all the systems studied and increases with increasing concentration of furfural or furfuryl alcohol for the binary systems (methanol + furfural or furfuryl alcohol) and decreases with concentration of furfural or furfuryl alcohol for the binary systems ([EMIM][OAc] + furfural or furfuryl alcohol)

The κ_s value increases with an increase in temperature for all systems and decreases with increasing concentration of furfural or furfuryl alcohol for all binary systems except ([EMIM][OAc] + furfuryl alcohol) system due to an increase in thermal agitation. The isentropic compressibility, κ_s, values increases with an increase in temperature for the binary systems due to an increase in thermal agitation, making the solution more compressible (Singh *et al*. 2013). The isentropic compressibility is an indication of the compressibility of the mixture and the positive values indicate that the mixture is compressible. The κ_s values have been plotted in Figures 5.5 to 5.8.

6.4. DEVIATION IN REFRACTIVE INDEX

The refractive index, *n*, can be used as a measure of the electronic polarizability of a molecule and can provide useful information when studying the interaction forces between molecules or their behavior in solution, and the refractive index deviations, Δ*n*, can be physically interpretable as the deviation of the reduced free volume, which are negatively correlated to V_m^E values (Anouti *et al*. 2010).

The results for deviation in refractive index, Δn, for the binary systems {methanol (x_1), or [EMIM][OAc] + furfural or furfuryl alcohol (x_2)} at T = (298.15, 303.15, 308.15, 313.15 and 318.15) K are given in Tables 5.5 -5.8 and plotted in Figures 5.9- 5.12. For the {methanol (x_1), or [EMIM][OAc] + furfural (x_2)} binary systems, the refractive index decreases with an increase in the temperature and increases with the concentration of furfural for both systems. The refractive index decreases with an increase in the temperature and increase with the concentration of furfuryl alcohol for the (methanol or [EMIM][OAc] + furfuryl alcohol) systems. Deetlefs *et al* (2006) and Brocos *et al.* (2003) reported that the larger the reduced molar free volume of the substance, the smaller would be its refractive index. So it could be suggested that in case of the ([EMIM][OAc] + furfuryl alcohol) system increasing concentration of the IL within solution would lead to more interactions and hence more aggregate formation. The Δn values are positive for the whole composition and temperature range and decreases slightly with increasing temperature. Refractive index for (methanol + furfural or furfuryl alcohol) and ([EMIM][OAc] + furfural) binary systems decreases linearly with increasing mole fraction. However, the ([EMIM][OAc] + furfuryl alcohol) binary system which shows an increasing trend with increasing mole fraction due to the increased strength of hydrogen bond. Among the four binary systems, the higher refractive index was observed for the binary system ([EMIM][OAc] + furfural) which indicates an increased interaction with [EMIM][OAc].

6.5. CORRELATIONS AND PREDICTIONS

Table 5.9. gives the correlation parameters for the Redlich-Kister smoothing polynomial. The Redlich-Kister correlation for the V_m^E data for the ([EMIM][OAc] + furfural) binary mixture gave the most error. The Redlich-Kister polynomial fit gave the least error for the

([EMIM][OAc] + furfuryl alcohol) binary system. The Redlich-Kister polynomial fit for the Δn values give the best fit for the ([EMIM][OAc] + furfuryl alcohol) binary mixture.

From Table 5.10. the Lorentz-Lorenz correlation of the V_m^E data gave a very poor correlation of the V_m^E data gave a very poor correlation of the V_m^E data, the best correlation obtained for the (methanol + furfural) binary system, and the worst correlation for the ([EMIM][OAc] + furfuryl alcohol) binary system. This indicates that the Lorentz-Lorenz equation does not correlate V_m^E data very well.

The prediction of density, ρ, from the Lorentz-Lorenz equation was best for (methanol + furfural) binary systems. The Lorentz-Lorenz prediction of *n* was better than that for the ρ.

The system ([EMIM][OAc] + furfuryl alcohol) gave the best prediction of n for the Lorentz-Lorenz equation.

CHAPTER **7**

CONCLUSION

The thermophysical properties, which include density, speed of sound and refractive index were measured as a function of temperature and composition for the binary mixtures {methanol or [EMIM][OAc] + furfural} and {methanol or [EMIM][OAc] + furfuryl alcohol}. The results were discussed in terms of intermolecular interactions between the components of the binary mixtures. The density and speed of sound decreases slightly with increasing temperature for all binary systems and increases with increasing concentration of furfural or furfuryl alcohol. The excess molar volume were calculated from the density data. The isentropic compressibility and deviation in refractive index values were found to be both positive for the whole composition and temperature range and decreases slightly with increasing temperature. The calculated values of excess molar volumes and change of refractive index on mixing were compared with the results obtained by applying the Lorentz- Lorentz equation to correlate excess molar volume. The Redlich–Kister fitting smoothing polynomial was used to obtain the fitting parameters of the binary systems together with the standard deviations. The Lorentz–Lorenz approximation predicted the refractive index from density more accurately than the prediction of density from refractive index.

REFERENCES

Abareshi M., Goharshadi E. K., Zebarjad S. M., J. Mol. Liq. 149, **2009**, 66–73.

Alonso D. M., Bond J. Q., Dumesic J. A., Green Chem 12, **2010**, 1493–1513.

Alvarez V. H., Mattedi S., Martin-Pastor M., Aznar M., Iglesias M., J. Chem. Thermodyn. 43, **2011**, 997–1010.

Anantharaj R., Banerjee T., Int. J. Chem, 2011, **2011**, 1-13.

Anantharaj R., Banerjee T., J. Ind. Eng. Chem. 18, **2012**, 331–343.

Anantharaj R., Banerjee T., J. Thermodyn. 2011, **2011**, 1-14.

Anastas P. T., Warner J. C., Green Chem.: Theory and Practice, Oxford University Press, New York, **1998**.

Anouti M., Caillon-Caravanier M., Dridi Y., Galiano H., Lemordant D., J. Phys. Chem. B 112, **2008**, 13335–13343.

Anouti M., Vigeant A., Jacquemin J., Brigouleix C., Lemordant D., J. Chem. Thermodyn. 42, **2010**, 834–845.

Armand M., Endres F., MacFarlane D. R., Ohno H., Scrosati B., Nat. Mater. 8, 2009, 621-629.

Armstrong D.W., He L.F., Liu Y.S., Anal. Chem. 71, **1999**, 3873.

Azevedo R., Szydlowski J., Pires P.F., Esperança J.M.S.S., Guedes H.J.R., Rebelo L.P.N. , J. Chem. Thermodyn. 36, **2004**, 211-222.

Bahadur I., Naidoo P., Singh S., Ramjugernath D., Deenadayalu N., J. Chem. Thermodyn. 78, **2014**, 7–15.

Battino R., Chem. Revs. 71, **1971**, 5.

Bendiaf L., Bahadur I., Negadi A., Naidoo P., Ramjugernath D., Negadi L., Thermochim. Acta 599, **2015**, 13–22.

Bendiaf L., Negadi A., Daouadji Z., Negadi M. L., J. Chem. Thermodyn. 91, **2013**, 245–256.

Bhujrajh P., Deenadayalu N., J. Chem. Thermodyn. 38, **2006**, 278-282.

Bottomly G.A., Scott R.L., J. Chem. Thermodyn. 6 (10), **1974**, 973-981.

Bozell J. J., Petersen G. R., Green Chem. 12, **2010**, 539 -554.

Brennecke, J. F.; Maginn, E. J., AIChE J. 47 (11), **2001**, 2384-2389.

Cai C. M., Zhang T., Kumara R., Wymana C. E., J. Chem. Technol. Biotechnol. 89, **2014**, 2–10.

Chen J., Chen L., Lu Y., Xu Y., J. Mol. Liq. 197, **2014**, 374–380.

Cunha D., Coutinho L., Daridon J. A. P., Reis J. L., Márcio R. A., Paredes L. L, J. Chem. Eng. Data 58, **2013**, 2925−2931.

de Almeida B. F., Waldrigui T. M., de C. Alves T., de Oliveira L. H., Aznar M., Fluid Phase Equilib. 334, **2012**, 97-105.

De Jong W., Marcotullio G., Int. J. Chem. React. Eng. 8, **2010**, Article A69, 3-5.

Debbie S. S., Analyst, 136, 2011, 4871.

Demirbas A., Energy Conversion and Management 49, **2008**, 2106–2116.

Demirbas A., Energy Sources, Part A, 31, **2009**, 573–1582.

Dikio E. D., Nelana S. M., Isabirye D. A., Ebenso E. E., Int. J. Electrochem. Sci. 7, **2012**, 11101 – 11122.

Doherty T. V., Mora-Pale M., Foley S. E., Linhardt R. J., Dordick J. S., Green Chem. 12, **2010,** 1967–1975.

Dunlop, A. P., Peters, F. N., Reinhold Publishing Corporation, New York (USA), **1953**.

Dutta S., Pal S., Biomass and bioenergy 62, **2014**, 182-197.

Fang Z., Smith R. L., Qi X., Biofuels and Biorefineries, Springer Science, New York, NY, USA, **2014**.

Ficke L. E., Degree of Doctor of Philosophy (thesis), Notre Dame, Indiana, **2010**.

FitzPatrick M. A., Masters of Applied Science (thesis), Queen's University, Canada, **2011.**

Fortin T. J., Laesecke A., Freund M., Outcalt S., J. Chem. Thermodyn. 57, **2013**, 276–285.

Francisco M., van den Bruinhorst A., Kroon M. C., Green Chem. 14, **2012**, 2153.

Franks F., Smith H. T., Faraday Soc. 63, **1967**, 2586-2598.

Fredlake C.P., Crosthwaite J. M., Hert D.G., Sudhir N. V., Aki K., Brennecke J. F., J. Chem. Eng. Data 49, **2004**, 954-964.

Fröba A. P., Rausch M. H., Krzeminski K., Assenbaum D., Wasserscheid P., Leipertz A., Int. J. Thermophys. 31, **2010**, 2059–2077.

Gabriel S., Weiner J., European Journal of Inorganic Chemistry 21 (2), **1888**, 2669–2679.

García-Mardones M., Barrós A., Bandrés I., Artigas H., C. Lafuente, J. Chem. Thermodyn. 54, **2012**, 17–24.

García-Mardones M., Cea P., Carmen López M. C., Lafuente, Thermochim. Acta 572, **2013**, 39 – 44.

Gardezi S. A., Joseph B., Prado F., Barbosa A., Biomass and Bioenergy 59, **2013,** 168-186.

Gathergood N., Garcia M. T., Scammells P. J., Green Chem. 8, **2006**, 156– 160.

Gonza´lez B., Dominguez A., Tojo J., J. Chem. Eng. Data 49, **2004**, 1590-1596.

González B., González E. J., J. Chem. Thermodyn. 68, **2014**, 109–116.

González E. J., Calvara N., Fernández P., Domínguez A., Macedo E. A., Procedia Eng. 42, **2012**, 1383 – 1389.

Govinda V., Attri P., Venkatesu P., Venkateswarlu P., J. Mol. Liq. 164, **2011**, 218–225.

Gravitis J., Vedernikov N., Zandersons J., Kokorevics A., J. Am. Chem. Soc. , **2001**, 110–122.

Grolier J. P. E., Benson G. C., Picker P., J. Chem. Thermodyn. 7, **1975**, 89-95.

Gunny A. A., Arbain D., Adv. Mater. Res. 701, **2013**, 399 – 402.

Han, D., Row, K., Molecules 15, 2**010**, 12405-2426.

Handa Y. P., Benson G. C., Fluid Phase Equilib. 3 (2-3), **1979**, 185-249.

Handa Y.P., Benson G.C., Fluid Phase Equilib. 3, **1976**, 185.

He L. J., Zhang W.Z., Zhao L., Liu X., Jiang S.X., J. Chromatogr. A 1007, **2003**, 39–45.

Holbrey J. D., Seddon K. R., Clean Products and Processes 1, **1999**, 223-236.

Holm J., Lassi U., InTech publishers, Finland, **2011**, 551.

Homer J., Cooke M. C., J. Chem. Sou. Farad. Trans. 69, **1973**, 1990-1994.

http://www.westprochem.com/page0008.htm.

Huber G.W., Iborra S., Corma A., Chem. Rev 106, **2006**, 4044 – 4098.

Iglesias M., Orge B., Tojo J., Fluid Phase Equilib. 126, **1996**, 203-223.

Iglesias M., Pineiro M. M., Marino G., Orge B., Dominguez M., Tojo J., Fluid Phase Equilib. 154, **1999**. 123–138.

Iglesias-Otero M.A., Troncoso J., Carballo E., Romanı´ L., J. Chem. Thermodyn. 40, **2008**, 949–956.

Jacquemin J., Anouti M., Lemordant D., J. Chem. Thermodyn. 56, **2011**, 556–564.

Keyes D.B., Hildebrand J.H., J. Am. Chem. Soc., 39 (10), **1917**, 2126–2137.

Khupse N.D., Kumar A., Ind. J. Chem. 49A, **2010**, 635-648.

Kim T., Assary R. S., Marshall C. L., Gosztola D. J., Curtiss L. A., Stair P. C., Chem. Cat. Chem. 3, **2011**, 1451 – 1458

Kottke R. H., Kirk-Othmer Encyclopedia of Chemical Technology, John Wiley and Sons, **2000**.

Kulnevich V.G., Shapiro Y. M., Khim. Geterots. Soedinenii 12, **1972**, 1594.

Kumaran M.K., McGlashan M.L., J. Chem. Thermodyn. 9 (3), **1977**, 259-267.

Kurnia K. A., Taib M. M., Mutalib M. I., Murugesan T., J. Mol. Liq. 159, **2012**, 211–219.

Kurnia K.A., Harris F., Wilfred C.D., Mutaliv M.I., Murugesan T., J. Chem. Thermodyn. 41, **2009**, 1069–1073.

Lange J. P., Weinheim: Wiley-VCH; **2007**, 21–51.

Li H., Zhang S., Luo H., Mater. Lett. 58, **2004**, 2741–2746.

Lomba B., Giner M., Lopez C., Aldea L., Lafuente C., J. Chem. Eng. Data 59, **2014**, 329-338.

Lomba L., Giner B., Bandres I., Lafuente C., Pino M. R., Green Chem. 13, **2011**, 2062–2070.

Lomba L., Giner B., Bandres I., Lafuente C., Pino M. R., Electronic supplementary material (ESI) for green chemistry, Green Chem. **2011**, www.rsc.org.

Lomba L., Giner B., Zuriaga E., Moya J., Lafuente C., J. Chem. Thermodyn. 66, **2013**, 131 – 136.

Malek N. I., Singh A., Surati R., Ijardar S.P., J. Chem. Thermodyn. 74, **2014**, 103–118.

Malinowski A., Wardzińska D., Chemik 66 (9), **2012**, 982 -990.

Mamman A. S., Lee J., Kim Y., Hwang I., Park N., Hwang Y. K., Hwang J., Biofuels, Bioproducts and Biorefining 2 , **2008**, 438-454.

Mandalika, A. S. Master of Science (thesis), University of Wisconsin-Madison, **2012.** McKillip W. J., Collin G., Hoke H., Zeitsch K.J., Ullmann's Encyclopedia of Industrial Chemistry, 6th edition, Weinheim, Germany, Wiley-VCH, **2001**.

McKendry P., Bioresource Technology 83, **2002**, 37–46.

Mercer-Chalmers J. D., Degree of Doctor of Philosophy (thesis), Rhodes University, **1992**.

Mohammed A. K., Hussain H. K., Sadiq R. J., Iraqi J. Chem. Pet. Eng. 8, **2007**, 1-12.

Mythri J., Anusha B.S., Reddy M.S., J. Chem. Pharm. Sci. 2014, 80 – 82.

Nagaraja B.M., Padmasri A.H., David Raju B., Rama Rao K.S., J. Mol. Catal. A: Chem. 265, **2007,** 90–97.

Naorem H., Kishore N., Suri S. K., Can. J. Chem. 67, **1989**, 648-650.

Naorem H., Suri S. K., Can. J. Chem. 67, **1989**,1672-1675.

Naorem H., Suri S.K., J. Sol. Chem. 22, **1993**, 183-184.

Narasimhan P. T., J. Indian Inst. Sci. **1954**, 30-34.

Nevines J.A., PhD thesis, UKZN, Durban, **1997**, 78-80.

Orge B., Iglesias M., Rodriguez A., Canosa J. M., Tojo J., Fluid Phase Equilib. 133, **1997**, 213-227.

Orge B., Rodriguez A., Canosa J. M., Marino G., Iglesias M., Tojo J., J. Chem. Eng. Data 44, **1999**, 1041-1047.

Pandey S., Analytica Chimica Acta 556 (1), **2006**, 38-45.

Park M. J., Choi I., Hong J., Kim O., J. Appl. Polym. Sci. 129 (5), **2013**, 2363-2376.

Patil P. P., Patil S. R., Borse A. U., Hundiwale D. G., Rasayan J. Chem. 4 (3), **2011**, 599-604.

Pereira S.M., Rivas M.A., Legido J.L., Iglesias T.P., J. Chem. Thermodyn., 35, **2003**, 383 – 391.

Pieraccini D., Chiappe C., Intorre L., Pretti C., Thermodynamics, Solubility and Environmental Issues, Elsevier, **2007**, 262.

Qian W., Xu Y., Zhu H., Yu C., J. Chem. Thermodyn. 49, **2012**, 87–94.

Quijada-Maldonado E.,van der Boogaart S., Lijbers J.H., Meindersma G.W., de Haan A. B., J. Chem. Thermodyn. 51, **2012**, 51–58.

Radojkovic N., Tasic A., Grojdanic D., Djordjevic B., Malic D., J. Chem. Thermodyn. 9, **1977**, 349-356.

Redhi G.G., PhD thesis, UKZN, Durban, **2003**, 6-16.

Redlich, O., Kister. A.T., Ind. Eng. Chem. 40, **1984**, 345-348.

Requejo P. F., González E. J., Macedo E. A., Domínguez A., J. Chem. Thermodyn. 74, **2014**, 193–200.

Rodriguez H., Williams M., Wilkes, J. S., Rogers R. D., Green Chem. 10 (5), **2008**, 501-507.

Rogers R. D., Seddon K. R., Volkov S., Kluwer Academic Publishers: The Netherlands, **2002**.

Romero A., Santos A., Tojo J., Rodriguez A., J. Hazardous Materials 151, **2008,** 268–273.

Saba H., Zhang Y., Wang H., Adv. Mater. Res. 937, **2014**, 99-104.

Sattarib M., Gharagheizia F., Ilani-Kashkoulia P., Mohammadic A. H., Ramjugernath D., Fluid Phase Equilib. 367, **2014**, 188–193.

Shah M. R., Anantharaj R., Banerjee T., Yadav G. D., J. Chem. Thermodyn. 62, **2013**, 142–150.

Shana'a M., Canfield F., Transactions of the Faraday Soc. **1968**, 2281-2286.

Shapiro Y. M., Kulnevich V. G., Zh. Fiz. Khim. 45, **1971**, 981.

Sheldo R.A., Green Chem. 7, **2005**, 267–278.

Shittu A. A., Master of Science Degree (thesis), **2010**.

Shittu A. A., MSc (Eng) thesis, University of Toledo**, 2010**, 7-9.

Singh S., Aznar M., Deenadayalu N., J. Chem. Thermodyn. 57, **2013**, 238–247.

Singh S., MTech thesis, Durban University of Technology, **2013**, 87-89.

Singh V. V., Boopathi M., Ganesan K., Singh B., Vijayaraghavan R., Electroanalysis 22 (12), **2010**, 1357-1363.

Singh V. V., Nigam A. K., Batra A., Boopathi M., Singh B., Vijayaraghavan R., Int. J. Electrochem., 2012, **2012**, 1-19.

Swatloski R. P., Spear S. K., Holbrey J. D, Rogers R. D., J. Am. Chem. Soc. 124, **2002**,4974 – 4975.

Tai W., Lee H., Lee M., Fluid Phase Equilib. 384, **2014**, 134-142.

Tsuda T., Hussey C. L., Electrochem. Soc. Interface, Spring, 2007, 42 - 49.

Vedernikovs N., Kampars V., Puke M., Kruma I., Sci. J. Riga. Technic. Univ. 22, **2010**, 68–73.

Walden P, Wikipedia, Bull. Acad. Sci. St. Petersburg 8, **1914**, 405- 422.

Wasserscheid P., Welton T., Ionic Liquids in Synthesis. Wiley-VCH: Weinheim, **2003**.

Welton T., Chem. Rev. 99, **1999**, 2071–2283.

Westpro, Huaxia furfural technology,**2004**.

Wettstein S. G., Alonso D. M., Gurbuz E. I., Dumesic J.A., Current Opinion in Chemical Engineering 1, **2012**, 218-224.

Wilkes J.S., Levisky J.A., Wilson R.A., Hussey C.L., Inorg, 21 (3), **1982**, 1263–1264.

Wilkes J.S., Zaworotko M.J., J. Chem. Soc., Chem. Commun. **1992**, 965-967.

Wojcik, B. H., Industrial and Engineering Chemistry 40 (2) **1948**, 210-216.

Wood S.E., Brusie J.P, J. Am. Chem. Soc. 65, **1943**, 1891.

Yan K., Wu G., Lafleu T., Jarvis C., Renewable and Sustainable Energy Reviews 38, **2014**, 663–676.

Yan K., Wu X., An X., Xie X. M., Chem. Eng. Commun. 201, **2014**, 456 – 65.

Yang C., Xu W., Ma P., J. Chem. Eng. Data 49, **2004**, 1794-1801.

Yuan X. L., Zhang S.Z., Liu J., Lu X., Fluid Phase Equilib. 257, **2007**, 195–200.

Zafarani-Moattar M. T., Sadeghi R., Sarmad S., J. Chem. Thermodyn. 38, **2006**, 257– 263.

Zaitseva A., Laavi H., Pokki J., Uusi-Kyyny P., Alopaeus V., Fluid Phase Equilib. 372, **2014**, 85–99.

Zeitsch K. J., the Chemistry and Technology of Furfural and Its Many By-Products Amsterdam: Elsevier, **2000**, 374.

Zaoui-Djelloul-Daouadji M., Bendiaf L., Bahadur I., Negadi A., Ramjugernath D., Ebenso E. E., Negadi L., Thermochim. Acta **2015**, accepted.

Zhao H., Chem. Eng. Comm. 193 (12), **2006**, 1660-1677.

Zhao H., Holladay J.E., Brown H., Zhang Z.C., Science 316, **2007**, 597-600.

Zhong Y., Wang H., Diao K., J. Chem. Thermodyn. 39, **2007**, 291–296.

APPENDICES

Articles submitted for publication:

1. Mbalenhle Nduli, Nirmala Deenadayalu, Thermophysical properties of the binary mixtures (methanol or 1-ethyl-3-methylimidazolium acetate + furfural or furfuryl alcohol) at T = (298.15, 303.15, 308.15, 313.15 and 318.15) K: *In preparation*